THE UNIVERSITY OF QUEENSLAND

Bachelor of Engineering Thesis

Flutter: History, Theory and Simulations

Student Name: William Thomasson

Course Code: MECH4500

Supervisor: Dr. Alex Klimenko

Submission date: 28 October 2016

A thesis submitted in partial fulfilment of the requirements of the Bachelor of Engineering degree in Mechanical and Aerospace Engineering

Acknowledgements

To Dr. Alex Klimenko, thank you for the opportunity to complete this thesis. Flutter has proven to be a very interesting topic and so I am grateful to have been able to complete this work.

Due to the multi-faceted nature of flutter, this thesis has been the epitome of a capstone project. It has required knowledge from a broad range of courses undertaken during my time at UQ. As such, I would like to thank all of the lecturers, tutors and staff that have made been involved in my undergraduate studies.

Abstract

The nature of wing and bridge flutter is investigated in this study. Through comparisons, it is intended to gain an understanding of the cross disciplined nature of flutter. In order for this to be achieved the historical development and pertinent theories are initially analysed. From here, numerical modelling and computational fluid dynamics simulations are engaged to provide a quantitative aspect to the investigation.

From the historical review, it was revealed that flutter has primarily manifested itself in various aircraft lifting structures. Subsequently, much of the early flutter theory was centred around developing analytical solutions for an oscillation aerofoil. However, the collapse of the Tacoma Narrows Bridge in 1940 cast a new light on flutter and rendered it as an integral design consideration for that of long span suspension bridges. This also led to a surge in the work concerned with the development of theory for the prediction of the bridge critical flutter speed.

An exploration of the theory first involved comparing the mechanism of instability for four types of flutter. These included classical wing flutter, torsional bridge flutter, classical bridge flutter and wing stall flutter. The two classical forms involve modal coupling whereby the motion of the structure contribute to the self-excited forces causing flutter. Conversely, torsional bridge flutter and stall flutter are a consequence of flow separation and vortex shedding that is influenced by the oscillatory motion of the respective structures.

The unsteady aerodynamic models are then presented for the wing and bridge flutter cases. Due to the premise of potential flow theory upon which the wing model is based, it is deduced that its application to the bridge flutter problem is inappropriate. Rather, the complex nature of the fluid-structure interaction that is facilitated by both forms of bridge flutter necessitates a model that is semi-empirical.

Respective aerofoil and bridge flutter models are developed through the consolidation of the structural and aforementioned aerodynamic sub-models. This allowed for a numerical investigation to proceed where the critical speed for the different types of flutter is ascertained. Following this, a parametric study was completed in which the influence of various parameters on the flutter boundaries was ascertained. Finally, computational fluid dynamics simulations were generated to illustrate the nature of the fluid-structure interaction that is necessary for the different types of flutter.

Nomenclature

Symbol	Definition	Units
A	Response Amplitude	$[m]$
B	Bridge Deck Width	$[m]$
C	Damping Coefficient	$[kgs^{-1}]$
$C(k)$	Theodorsen's Function	-
$F(k)$	Real Part of Theodorsen's Function	-
$G(k)$	Imag. Part of Theodorsen's Function	-
K	Structural Stiffness	$[Nm^{-1}]$
L	Aerodynamic Lift	$[N]$
M	Aerodynamic Moment	$[N\ m]$
St	Strouhal Number	-
T	Kinetic Energy	$[J]$
U	Free-stream Velocity	$[ms^{-1}]$
V	Potential Energy	$[J]$
a	Non-dimensional Position of Elastic Axis	-
b	Half Chord Length	$[m]$
c	Chord Length	$[m]$
μ	Mass-to-Air Ratio	-
ξ	Damping Ratio	-
ρ	Free-Stream Density	$[kg/m^3]$
σ	Natural Frequency Ratio	-
s	Non-Dimensional Time	-
t	Dimensional Dime	$[s]$
f	Vortex Shedding Frequency	$[Hz]$
k	Reduced Frequency	-
m	Structural Mass	$[kg]$
r	Radius of Gyration	-
$\phi(s)$	Wagner's Function	-
A_i^*	Bridge Flutter Derivative	-
$H_i^{(2)}$	Hankel Functions	-
H_i^*	Bridge Flutter Derivative	-
I_α	Mass Moment of Inertia	$[kgm^2]$

Q_i	External/Dissipative Forces	$[N]$
S_α	Static Mass Unbalance	-
q_i	Generalised Coordinate	-
$\vec{r}$	Particle Displacement	-
x_α	Distance from Elastic Axis to Centre of Mass	-
ω_F	Flutter Frequency	$[rad/s]$
ω_n	Natural Frequency	$[rad/s]$
h	Vertical Displacement	$[m]$
$\mathcal{L}$	Lagrangian	-
Γ	Circulation Strength	-
w	Down-Wash Velocity	$[ms^1]$
α	Angle of Attack	$[rad]$

Table of Contents

List of Figures

List of Tables

1 Introduction

1.1 Background

The innovation of flight in the early 20th century was a significant milestone in the progression of the capability of mankind. A rapid development of flight vehicles has ensued which is exemplified by the achievement of inter-continental travel, access to space and, more recently, re-usable launch systems and the ability of unmanned aerial vehicles. However, this development has not occurred without issues. The risks associated with flight has prompted the establishment of new areas of engineering that are concerned with the research and understanding of the requirements of flight vehicles.

One such issue is that of the potentially devastating phenomenon known as flutter, which has persistently plagued aircraft since their inception. Flutter is a constituent of a branch of research known as aeroelasticity which is concerned with the coupling of structural, aerodynamic and inertial forces that a structure is subjected to in fluid flow. Essentially, any elastic body immersed in a fluid flow is at risk of incurring flutter. However, for several decades following the first successful flight, it was perceived as an issue that garnered the attention exclusively of aeronautical engineers.

The collapse of the Tacoma Narrows Bridge in 1940 challenged this perception and cast a new light on the understanding of flutter and aeroelasticity in general. This particular incident captivated prominent aeroelasticians, aeronautical engineers and civil engineers alike. In doing so, the incident has undoubtedly become the most documented real world example of flutter. As a result, the cross-discipline nature of flutter became more prominent, with this phenomenon nowadays prevalent in areas of aerospace, mechanical and civil engineering. In this instance, it must be noted that cross-disciplined refers to the ability for flutter to occur in contexts such as aircraft structures, long span suspension bridges and various forms of turbomachinery.

1.2 Thesis Goal

Despite this stated prominence of flutter in a variety of applications, the studies that are explicitly concerned with the cross-disciplined nature of flutter are few and far between.

The overall aim of this thesis is contribute to the study of flutter by providing an insight into the extent of the cross-disciplined nature of the phenomenon via an explicit qualitative and quantitative analysis of flutter in different contexts.

1.3 Thesis Objectives

The previously stated thesis aim is intended to be achieved via the accomplishment of a number of objectives. These are listed here:

1. Examine the major flutter incidents over the last century and observe how these have enabled the understanding of flutter to develop.
2. Compare the prominent theory pertaining to wing and bridge flutter. In doing so, identify the limitations associated with cross-discipline application of this theory.
3. Formulate and compare numerical models for an assortment of flutter cases.
4. Conduct a preliminary flutter boundary analysis for various types of flutter.
5. Perform a parametric study and computational fluid dynamics (CFD) simulations for further quantitative comparisons.

1.4 Thesis Structure

The structure of this thesis is such that it achieves each of the aforementioned outcomes while progressing in a logical manner. A brief breakdown of the structure is as follows:

Chapter 2 – History of Flutter

Featured in this chapter is a timeline of sorts outlining the significant incidents of flutter. Also included is the development of the understanding of flutter and how this has allowed relevant theory to progress.

Chapter 3 – Literature Review

A review of the prominent literature in the study of flutter will be presented in this chapter. The literature review intentionally proceeds the history chapter so that the prevalent work is identified in the latter.

Chapter 4 – Fundamental Theoretical Concepts

The theory component of this study is comprised of two parts, the first of which is concerned with the underlying principles of structural dynamics, fluid mechanics and aerodynamics. An understanding of these will be beneficial for the discussion of flutter specific theory.

Chapter 5 – Flutter Specific Theory

The different theories pertaining to the flutter of wings and bridges is presented here. Particular attention is placed on any similarities that exist between the theory surrounding flutter in aerospace and civil engineering.

Chapter 6 – Model Development

This chapter will concentrate on deriving the relevant equations of motion for flutter of the different structures and consolidating them with appropriate aerodynamic models. The difference in the models for wing and bridge flutter will be alluded to here.

Chapter 7 – Simulations

Presented in this chapter is an overview of the of the flutter analysis and simulations that will be carried out in this study. The solution methods for flutter boundary prediction will be described here along with validation of these methods.

Chapter 8 – Results and Discussion

The results obtained from the numerical analysis and simulations will be presented here allowing for an interpretation of these results to ensue. Additionally, a discussion of the results will feature with emphasis placed on any observable relationships between the results.

Chapter 9 – Conclusion

The concluding chapter will comprise of a summary of the thesis and an evaluation of the effectiveness of the study. Additionally, further work that could be done regarding the work of this thesis is also included.

2 History of Flutter

Like so many engineering problems, the understanding of flutter and how it has been dealt with has progressed markedly over the years. A historical overview of flutter will contribute significantly to an understanding of how it has come to be a prominent design consideration in various engineering disciplines. In this chapter, the major flutter events will be investigated to determine the effect they have had, from an engineering perspective, on the development of relevant theory and countermeasures. It is also hoped that the historical overview will identify fundamental concepts and key players in the field of aeroelasticity that will cater for a comprehensive review of relevant literature.

2.1 Pre 1920: World War I

The advent of World War I saw the first large scale use of aircraft in a major conflict. With the successful application of aircraft and, subsequently, the aviation industry, still in its infancy, a multitude of problems inundated the pioneers of flight. One such problem was flutter, or more generally, various aeroelastic instabilities.

The first documented flutter incident occurred during the flight of a Handley Page O/400 bi-plane in 1916. British engineer Frederick William Lanchester was tasked with investigating the cause of violent oscillations of the fuselage and tail of this aircraft. It was deemed that the oscillations were a result of the coupling between the torsional mode of the fuselage and the rotation mode of the rear elevators [1]. Recognising this, Lanchester was able to make two assertions:

1. The oscillations were self-excited as opposed to vibrational resonance
2. Increasing the torsional stiffness of the elevators would successfully eliminate the oscillations [2].

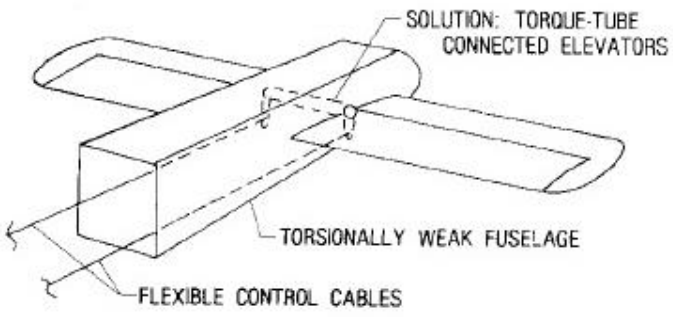

Figure 1: Lanchester's solution to the first documented flutter incident [2]

Leonard Bairstow conducted an analytical investigation with the intention of verifying Lanchester's theory. This culminated in the publishment of a paper containing the first theoretical analysis of flutter. In this paper, the equations of motion corresponding to two degrees of freedom were introduced as were the aerodynamic coefficients necessary for stability analysis. The significance of this is quite profound, with a similar process that was implemented in Bairstow's study still relevant today.

In 1917, another incident of tail flutter occurred during the operation of a de Havilland DH-9, seen here in Figure 2, which resulted in multiple fatalities. A remedy similar to that implemented by Lanchester in 1916 was deemed to be again necessary in this instance. These early flutter incidences emphasised the importance of a torsionally stiff connection between the elevators for flight vehicles [2]. Additionally, it identified the pertinence that the stiffness of a structure had in preventing the onset of flutter.

Figure 2: The de Havilland DH-9

A third incident, that has since been attributed to wing flutter, occurred in 1919 in Italy. During the flight of a Caprioni Ca.48, it was reported that witnesses observed the flutter of the wings and eventual failure [3]. There is minimal record of this incident despite it resulting in many fatalities. This tragedy, and those others discussed, brought to the fore the issue of flutter and emphasised the real threat that faced aircraft and their operators and passengers.

2.2 1920 – 1930: Developments in Flutter Theory

In examining the historical progression of flutter, it can be seen that from about 1920 onwards there occurred a substantial uptake in work regarding the unsteady aerodynamics associated with an oscillating wing. This was potentially due to the recognition of the threat that flutter posed to the success of the aviation industry, which was still only new, and the need to consider the unsteady effects facilitated by an oscillating body immersed in fluid. Despite this intensification in flutter-related work, it continued to hinder aircraft around the world.

The van Berkel W.B. monoplane was a reconnaissance seaplane that fell victim of aileron flutter shortly after World War I. Albert Gillis von Baumhauer and C Koning, two Dutch aviation pioneers, carried out an experimental and theoretical investigation that attempted to understand the root cause of the failure. It was deemed that the vertical bending of the wing coupled with the twisting motion of the ailerons and led to initiation of self-excited motion. This type of control surface flutter was prevalent during this period thus a remedy was crucial in order for the development of safe flight.

Baumhaurer and Koning discovered a solution to this problem which involved a mass balance of the aileron. This was the first recognition of the need for the interaction of two modes of motion to facilitate flutter. Subsequently, the pertinence that decoupling interacting modes could have on eliminating flutter became obvious [2]. Additionally, the methodology for this particular investigation depicted elements that are consistent with modern aeroelastic analysis techniques.

Despite the pioneering nature of the work of these two engineers, the issue of flutter continued to plague the aviation industry throughout the 1920's and 1930's. This prompted a considerable amount of work to be conducted in bolstering the capability of theoretical prediction of flutter. Over this decade individuals such as Birnbaum, Wagner and Kussner advanced the understanding of the aerodynamic forces prevalent to the flutter phenomenon.

Evidence of flutter occurrence in the United States was recorded in 1927 when work was proceeding to identify the cause of tailplane flutter of a MO-1 aircraft. The analysis technique that was adopted resembled that of Baumhaurer and Koning in the Netherlands. The initiation of flutter in this case was attributed to the coupling between the bending and torsion modes of vibration of the tailplane. Countermeasures such as an increased torsional stiffness were recommended to eliminate the threat [2].

2.3 1930 – 1940: Developments in Flutter Testing

The years between 1930 and 1940 was a tumultuous time for aeroelasticians given the rapid rate in development of not only flutter theory but also flight testing techniques. During this time, Theodorsen was prominent in formulating his two-dimensional flutter theory accounting for unsteady aerodynamics which continues to be extensively utilised today. While ground-breaking work was being conducted regarding analytical models of flutter, perhaps more significantly was the evolution of flight flutter testing techniques that was occurring.

The German von Schlippe is recognised as the first to perform in-flight flutter testing when he utilised resonance testing techniques during operation in 1935. Prior to this it was common practice for the aircraft to dive in order to reach its maximum velocity and hope that flutter did not occur [2]. Von Schlippe understood that the desire for planes to reach higher velocities would consequently render them more susceptible to flutter. His testing technique was based upon exciting the structure during flight and recording the amplitude of the response against airspeed. As the aircraft approached its flutter speed the response amplitude would rapidly increase offering an indication of the onset of flutter [1].

A rising amplitude would indicate a reduction in structural damping and the initiation of flutter. This practice proved to be effective until in 1938, while undergoing resonance testing, a Junkers JU90 experienced unexpected flutter and crashed. This flutter event was significant in that it resulted in the modification of flutter techniques to ensure that it was done safely. These modifications involved advancements of testing equipment and instrumentation in conjunction with a better conceptual understanding of flutter.

Despite the advancements being made in both theoretical and experimental techniques, the occurrence of flutter incidences did not appear to become less frequent. Numerous flutter experiences were reported in both the United States and Britain which again led to an intensified effort in obtaining an effective means of flutter prevention. Additionally, the capabilities of aircraft and aerospace were advancing at an alarming rate which had the consequence of bringing new forms of flutter to the fore.

2.4 1940 – 1950: The Changing Face of Flutter

Up until 1940, aeroelastic effects, especially that of flutter, were considered to be prevalent only in an aeronautical context. Previous flutter incidents reinforced this belief, with flutter being a destructive phenomenon in an era where flight vehicles were becoming more capable. However, the collapse of the Tacoma Narrows Bridge in 1940 was an initial indication of the cross-discipline nature of the flutter problem. It was the first recorded flutter event outside of an aeronautical setting and has likely become the most renowned association with flutter. Initially, there was a substantial amount of speculation regarding the exact reason for the collapse of the bridge with many investigations conducted into identifying the means of failure.

It was a common occurrence for Tacoma Narrows Bridge to display vertical modes of bending in the form of undulations, as seen in Figure 3, for which it became known as ‘Galloping Gertie’. This mode of bending was believed to have been of little consequence to the eventual failure of the bridge [4]. It is reported that on the morning of the collapse, a cable located at

mid-span failed and allowed a torsional mode of oscillation to dominate as depicted in Figure 4. At this point, torsional flutter, also referred to as single-degree-of-freedom flutter, became prominent and led to the eventual failure of the bridge.

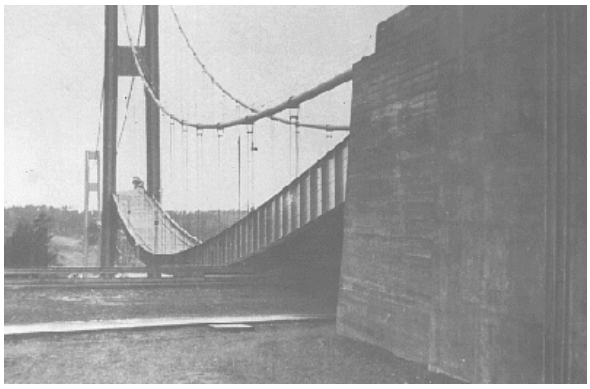

Figure 3: The undulations of the Tacoma Narrows Bridge

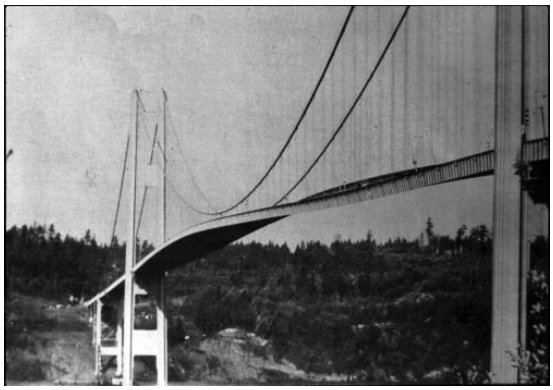

Figure 4: The torsional bending mode of the Tacoma Narrows Bridge

Many of the original investigations of the collapse lay blame to externally forced mechanical resonance. This was a popular opinion for many years and illustrated the belief that flutter was only confined to instances in an aviation setting. Up until that point, it was unfathomable that a structure on the scale of a bridge was susceptible to aeroelastic problems similar to plane wings and tail-fins. However, the design of the Tacoma Narrows Bridge was such that it was in inherent danger of experiencing aeroelastic effects.

The principal cause of the bridge's vulnerability to flutter was its flexibility that was derived from its overall lightweight design and its high width to length ratio. The failure of the Tacoma Narrows Bridge was an illustration of the lack of understanding of aerodynamic forces during the design phase of suspension bridges. The incident and ensuing investigations emphasized the need for consideration of fluid-structure interaction in bridge design and prevalence of the flutter problem in civil engineering.

While the incident of the Tacoma Narrows Bridge established flutter as a problem in a civil engineering context, aircraft structures continued to be prone to the instability. The World War II era saw the initiation of many developments in aviation technology and aircraft capabilities as countries vied for air superiority. As a consequence of the invention and use of the jet engine, aircraft were soon able to reach transonic and supersonic speeds. In addition to this, the desirability of planes to be constructed from metal, as opposed to the traditional option of mostly timber, entailed the introduction of many new flutter effects. This ensured that the research, both theoretical and experimental, continued with vigour by many groups and individuals around the world.

One incident that illustrated the new problems involving flutter occurred during the high speed operation of a P-80 aircraft in 1944. The P-80, seen here in Figure 5, exemplified the direction that aircraft construction was taking with its metal frame powered by jet engines making it one of the fastest planes at the time of its inception. The flutter effect that was witnessed during the operation of the P-80 involved the oscillations of the ailerons which was referred to as 'aileron buzz'. These oscillations were characterised as being single-degree-of-freedom that were attributed to the coupling of the rotation of the control surfaces and the 'chord-wise motion of shockwaves on the wing' [2].

Figure 5: The Lockheed P-80 Shooting Star

Thus, the issue facing aeroelasticians became one that revolved around eliminating control surface flutter in the transonic flow regime. Members of the National Advisory Committee for Aeronautics (NACA) Ames Research Centre set about doing just this with analysis of 'aileron buzz' becoming a prevalent area of work during the 1940's. It was a common belief by those conducting the research that aileron flutter at very high speeds would eventually induce entire wing flutter if preventative measures were not taken [5]. Initial wind tunnel tests revealed that the method of mass balances, which had been successful in previous flutter problems, was ineffective in nullifying aileron flutter. However, eventual solutions were discovered in the form of increasing the stiffness of control surfaces, modifying profile shapes and, probably most revolutionary, the incorporation of dampening systems [6].

2.5 1950 – 1970: Flutter at the Speed of Sound

Supersonic flight also began to demand the attention of aeroelasticians as it gradually became more common for aircraft to be travel at, or beyond, the sound barrier. As was the case with transonic flight, the operation of aircraft in the supersonic flow regime presented new difficulties pertaining to aeroelasticity. The dangerous nature of flight at such high speeds made it imperative that these aeroelastic effects were fully understood and designed against. The destructiveness of the flutter problem in supersonic flight would soon become apparent.

During a test flight in the 1950's, a fighter plane crashed due to the failure of a hydraulic line. This hydraulic line was fixed to a panel that had experienced flutter while travelling a speeds faster than that of sound. This was one of the first documented incidents of what would become known as panel flutter, an aeroelastic phenomenon that was only capable of occurring at supersonic speeds. This type of flutter involved the formation of ripples that travelled along the skins covering the aircraft. The movement of the skins in this manner was a gradual hindrance to the structural integrity of the coverings that would lead to eventual fatigue failure [1].

Panel flutter also played significant role during the development of access to space vehicles during this period. Given the unprecedented and extreme speeds that the early rocket systems would eventually achieve, the problem of panel flutter presented itself as an inherent problem. One such example was the Saturn V rocket which was purported to have displayed a susceptibility to panel flutter. It was even reported that panel flutter had been witnessed as early as World War II, with it blames for the destruction of numerous V2 rockets.

The carriage of stores on the wings was also known to induce aeroelastic instability for some aircraft during this period. Limit cycle oscillation (LCO) was a phenomenon associated with wings that possessed these external stores that experienced flutter. These oscillations were characterised by aerodynamic or structural nonlinearities and were mainly seen in military-type aircraft. Incidences of LCO are documented to have occurred during the operation of the F-16, F-18 and F-111 [1]. The study of LCO is an area of aeroelasticity that has been carried out extensively given the nature of operation during which the phenomenon is likely to occur. These oscillations have been known to impede most significantly on the plane's handling quality and weapon aiming capability [7]. The extent of the problem posed by LCO is illustrated by the fact that it continues to plague modern aircraft that possess external store configurations.

2.6 1970 and Beyond: Present Day Flutter

Gradually, prediction methods were able to accurately identify the flutter boundary for an aircraft during the design phase. This has resulted in fewer catastrophic flutter events in the last few decades. Despite this however, flutter continues to pose a problem in a range of applications. While technological advances have been beneficial in some circumstances for flutter prevention, it has proven to facilitate it in others.

The presence of flutter in turbomachinery provides a further illustration of the prevalence of flutter in a range of engineering applications. As the application of various turbomachines has become more common, the aeroelastic effects associated with fan blades operating at high angles of attack has become a major topic of research. The type of flutter that is prominent is

that of stall flutter which is characterised by a single mode of vibration. Since the late 1980's to present, stall flutter has been analysed extensively as, just like flutter of aircraft and bridge structures, it has the potential to be detrimental to the function and efficiency of turbomachinery.

The most recent, well documented aeronautical flutter incident involved a United States Air Force F-117 Stealth Fighter in 1997. Investigations into this incident revealed that a number of fasteners had come loose on the one of the elevons which consequently reduced the stiffness of the structure. This, in turn, accommodated the onset of flutter and the ultimate demise of the aircraft. This incident served as a reminder that even though the developments that had been made in preventing flutter over the decades, there was still the potential for it to arise.

Despite the collapse of the Tacoma Narrows Bridge occurring many years before, there continued to be a substantial amount of interest in analysing the mechanisms of failure. Civil engineers with expertise in wind loading on structures went about discrediting the theory that the collapse of the bridge was instigated by resonance. A significant amount of work, both theoretical and experimental, has been conducted over the years that suggests that failure was a result of flutter.

The traditional means of flutter prevention such as mass balancing and structure stiffening are still common practise. However, given the inefficient nature of these techniques, flutter continues to be a problem for aircraft today [8]. Many projects in recent years exemplify the prevalence that flutter continues to have in current engineering applications. The Perlan II project is one such example. This project consists of the flight of a glider in the upper echelons of the atmosphere for research purposes. The design of the glider and the conditions at which it is intended to operate render it susceptible to flutter.

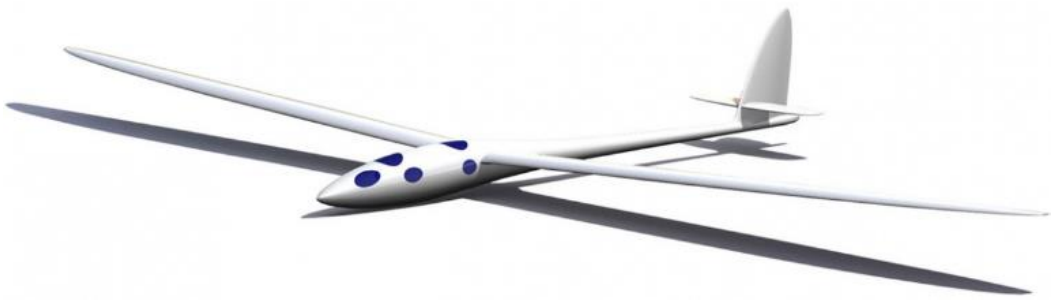

Figure 6: The Perlan II glider

Hence, the design process placed particular emphasis on ensuring that the glider was flutter-safe. The glider had a design criterion that required it to extremely strong and light but stiff

enough to prevent flutter [9]. This illustrates how Lancaster's early remedy of stiffening is still relevant in far more advanced aerospace vehicles today.

A somewhat culmination of the flutter research from the past century comes in the form of the field of research that is aeroservoelasticity. This is a synthesis of traditional aeroelasticity research with the study of control theory. The development of computational techniques has provided the capability for this branch of aeroelasticity to thrive. Aeroservoelasticity deals with the generation of computational models of structures in an effort to implement relevant control theory to lessen the susceptibility to aeroelastic effects. While being predominantly applied to aerospace applications, there have been instances of aeroservoelasticity studies concerning bridges.

2.7 History Summary

The prominent flutter events that have been outlined indicate that it is a problem that is largely problematic in an aviation setting. From the early years of flight, mitigation of instability due to flutter has been a primary design consideration. As aircraft developed over the years, the flutter problem continued to plague engineers. Gradual technological advancements allowed for experimental investigations that enabled a more thorough theoretical understanding of flutter.

Accompanying the progression of the understanding of flutter was the knowledge of its effects in applications other than aviation. The collapse of the Tacoma Narrows Bridge is indicative of this fact. Despite being significantly larger in size and being comprised of vastly different materials, a structure like the bridge at Tacoma Narrows was privy to the same aeroelastic concerns as a wing or tail fin on a plane.

3 Literature Review

The examination of the flutter history allows for a suitable transition to review the literature relevant to this particular study. As identified in the previous chapter, there have been a number of people whose work has been fundamental to the study of flutter. It is this work that will form the basis of the following literature review.

3.1 Aeroelasticity

As alluded to in the introduction, flutter is a phenomenon attributed to the branch of engineering known as aeroelasticity which is an encapsulation of the structural, aerodynamic and inertial forces acting on a body immersed in fluid flow. Collar [15] offered a convenient explanation of aeroelasticity when describing it as 'the study of the mutual interaction that takes place within the triangle of the inertial, elastic and aerodynamic forces acting on a structure exposed to an airstream'. Figure 7 below depicts the triangle that is being referenced, which is now commonly known as 'Collar's Aeroelastic Triangle'.

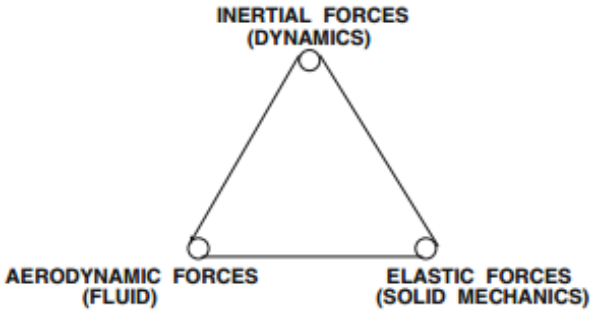

Figure 7:Collars Aeroelastic Triangle [15]

Aeroelastic effects are typically classified as either static, where only the aerodynamic and elastic forces are considered, or dynamic, where inertial forces are also involved. Flutter, along with buffeting, are the prime examples of dynamic aeroelasticity. From Collar's definition of aeroelasticity, it is evident how a wing during air travel and a bridge exposed to wind loading are examples of the types of structures susceptible to aeroelastic effects.

3.2 Wing Flutter Literature

There exist copious amounts of literature regarding the study of wing flutter that range from texts for educational purpose to pioneering research papers. This section will endeavour to survey the literature concerned with the fundamental aspects of wing flutter.

3.2.1 Aerodynamic Models

Within literature, the modelling of flutter is performed through the use of either steady or unsteady aerodynamic forces. There is a trade-off between complexity in application and accuracy of results when opting for quasi-steady or unsteady aerodynamics. During the 1920s considerable work was conducted to investigate flutter that utilised both quasi-steady and unsteady aerodynamics [2]. Dowell [17] offers a solid explanation of some of the steady-flow approximations for the aerodynamic modelling and details the approach taken for their implementation. The models presented here include those of quasi-steady approximation and strip-theory approximation. Both utilise assumptions that allow for a simplified process in evaluating the aerodynamic forces.

The strip-theory, referred to also as blade element theory, involves the division of the wing into chord-wise segments with width dy. Thus, this approximation is a three dimensional one that requires knowledge of both the section model and the span-wise coordinates of the wing which are depicted below in Figure 8.

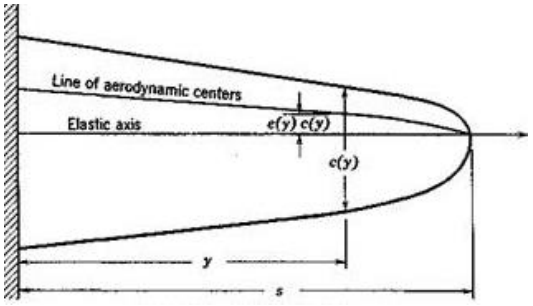

Figure 8: Cantilever wing [16]

According to the strip-theory approximation, the aerodynamic lift and moment in each specific segment is dependent only on the angle of attack in that segment and is independent of the angle of attack of any other segments. The aerodynamic forces and moments are then determined on each individual portion given the local free stream velocity. Using the coordinates from Figure 8, the lift and moment per segment is calculated through the use of the relevant equations.

The quasi-steady approximation can take many forms and Dowell [17] recommends that care should be taken when implementing this technique. Haddadpour and Firouz-Abadi [18] presented a quasi-steady approximation that incorporated an unsteady angle of attack into the aerodynamic lift and moment for steady motion. The quasi-steady approach offers a simple approximation capable of preliminary aerodynamic calculations. However, there is the potential for misinformed understanding of the flutter boundaries given the nature of the approximation. The work of Haddadpour and Firouz-Abadi [18] centred largely around how the aerodynamic

loading that is applied to the model impacts the resulting flutter boundary. It was concluded that the aerodynamic forces resulting from the quasi-steady assumption caused a divergence from the actual flutter boundaries.

Unlike the strip theory approximation, the quasi-steady approximation is concerned only with the two dimensional wing model. It is one that is commonly used in the analysis of wing flutter for its simplistic approach. In essence, the underlying principle of the quasi-steady approximation is that the history of prior motion and the effect of the wake is disregarded. Hence, it can be understood that this method approximates the aerodynamic forces by assuming that they are a dependent only on the instantaneous motion of the structure. This is rectified by implementing unsteady aerodynamics in order to obtain a more accurate prediction of the lift and moment exerted on the wing.

Birnbaum [19] was one of the first to give significant consideration to the effects of unsteady flow in 1923 when he published a paper concerning the classical vortex theory of two dimensional steady flow of thin aerofoils [2]. The approach incorporated a harmonically oscillating aerofoil in uniform motion. Included in this paper is the development of an integral equation that expresses the pressure on the aerofoil in terms of the normal velocity at the aerofoil surface. In his work, Birnbaum introduced the dimensionless property that is the reduced frequency.

In 1925, Wagner [20] extended the previous work of Birnbaum with his own approach concerning the harmonically oscillating aerofoil. The essence of Wagner's work was the effect on lift and the growth of vorticity in the wake as a result of a change in angle of attack. His work yielded an integral equation that related the lift force to the growth of vorticity in the wake which was denoted as Wagner's function. Further work was completed by Glauert in 1929 that carried on the work by Wagner and established integral expressions for the lift and moment of an aerofoil undergoing steady angular oscillations [2].

A culmination of the previous work regarding unsteady aerodynamic theory occurred in 1934 with the development of Theodorsen's simple, exact theory for two-dimensional flutter. Theodorsen [21] postulated that the circulatory and non-circulatory effects contributed to the unsteady aerodynamic forces acting upon a thin aerofoil. The theory that was proposed featured a term called Theodorsen's Function which was used to account for unsteady effects.

Of particular importance in this function is k, which is the reduced frequency of the circulatory flow. Fung [22] presents a table featuring the components and related quantities necessary for

the calculation of the Theodorsen function. Additionally, expressions for Theodorsen's Function in terms of reduced frequency have been formulated that are capable of yielding approximate solutions. The simple, exact theory of Theodorsen provided a deeper understanding of various elements of flutter and was supported through experimental observations. Many works regarding the analysis of flutter have since employed Theodorsen's theory successfully giving an indication of its value.

The topic of stall flutter is covered [17] and [22] in which qualitative explanations are provided. Similarly, several published reports seek to investigate stall flutter particularly in the context of turbomachinery [17]. These studies provide a clear insight into dynamic stall models necessitated by stall flutter. The Beddoes-Leishman model [24] is one such example of a dynamic stall model that has been commonly implemented for numerical investigations. A comprehensive analysis of a range of dynamic stall models is provided by [25]. This study aims to identify the differences between the various models and proposes advantages and disadvantages of each.

3.3 Bridge Flutter Literature

The research conducted into aeroelasticity in the field of civil engineering has become just as extensive as that for aeronautical engineering. An understanding of the fluid-structure interaction pertaining to suspension bridges is fundamental during the design process. The prominence of the flutter incident concerning regarding the Tacoma Narrows Bridge in the discussion of bridge flutter renders it a suitable topic for review.

3.3.1 Tacoma Narrows Bridge

The speculation and theories surrounding the collapse of the Tacoma Narrows Bridge in 1940 is widespread. Flutter has become the primary explanation with the belief that aeroelastic oscillations induced by aerodynamic forces ultimately contributed to structural failure. Just as there are many reasons as to why the bridge could have collapsed, the literature in regards to the incident is comprehensive.

Fung [22] recognised in his text the role that flutter plays in both aerospace and civil engineering. In his work, he makes reference to the collapse of the Tacoma Narrows Bridge, attributing it to the structure being subject to stall flutter. However, the discussion of bridge flutter in this instance is somewhat flawed as it applies aerofoil flutter theory to the flutter analysis of a bridge.

The work of Billah and Scanlan [4] aimed at settling the confusion that surrounded the explanation of the Tacoma Narrows Bridge collapse. It has become generally accepted from an engineering viewpoint that the collapse was a result of an 'aerodynamically induced condition of self-excitation or negative damping in the torsional degree of freedom' [27]. The way in which the bridge was designed rendered the flow of air incapable of passing through the structure forcing it instead to travel above and below.

Zhan and Fang [28] developed a numerical simulation using computational fluid dynamics that was capable of performing flutter stability studies for the Tacoma Narrows case. The simulation was successful in producing the critical flutter velocity and the mode shapes. It was concluded that torsional flutter was clearly evident in the Tacoma Narrows model above a specific wind speed. The Tacoma Narrows incident is the most prolific case of aeroelastic effects relating to suspension bridges, rendering it the motivating example for this thesis.

3.3.2 Aerodynamic Models

von Karman and Dunn's experimental work [28] on the aerodynamic interaction with the H-shaped section revealed several self-induced motions that were of interest to the initiation of bridge flutter. These included vertical, torsional and vertical-torsional. When the model undergoes torsional motion, and α changes, the vortices that are shed into the structures wake influences the motion further. The torsional mode is of the most relevance to suspension bridges because the resulting destabilising aerodynamic force increases when the critical speed is exceeded [22]. This torsional oscillation has since been identified as a fundamental mechanism of bridge flutter.

The aerodynamic instabilities, which include vortex shedding, galloping, torsional divergence, flutter and buffering, that are associated with the H-shaped section were detailed by Scanlan and Simiu [26]. In their text, single degree of flutter is recognized as a being prevalent for bluff bodies that are subject to separated flow. This single degree of freedom is translated as torsional instability which is the mechanism of flutter that the Tacoma Narrows Bridge failure was attributed to.

In their analysis of this single degree of freedom flutter, Scanlan and Simiu [26] reference Theodorsen's theory, which was introduced in the wing flutter literature, as being beneficial to account for the circulatory flow of the aerodynamic lift and moment. There are limitations in the application of this theory in that the necessary aerodynamic coefficients are not capable of being derived from first principles for bluff bodies.

Scanlan and Tomko [29] were pioneers in the analysis of bridge flutter in their recognition of the fact that the use of aerofoil theory was inappropriate. The work conducted by these two was successful in yielding empirical values from wind tunnel testing. With the aid of the empirical data obtained from these tests, the aerodynamic forces associated with bridge flutter were able to be formulated.

In their discussion of bridge flutter, Salvam and Govindaswamy [30] proposed two methods for the calculation of the critical wind speed. The first of these was the free oscillation procedure which involves the application of an initial disturbance to the model and then allowing it to oscillate freely. Having determined the lift and moment forces, the equations of motion can be solved, thus yielding the heave displacement and pitch angle for a variety of moments in time. This allows for the pitch angle to be plotted against time from which the flutter condition and corresponding critical wind speed can be acquired. The second technique capable of producing the critical wind speed is the forced oscillation technique where a forcing sinusoidal function of known frequency and amplitude is applied to the structure. The resulting lift and moments are measured and used to compute the aerodynamic coefficients that were introduced by Scanlan and Simiu. Finally, the critical velocity can be solved having employed the previously calculated parameters.

3.4 Literature Review Summary

The review of the pertinent literature has revealed a significant amount of work on flutter over the last century. The pioneering work of researchers regarding both wing and bridge flutter has resulted in the development of an advanced understanding of an engineering phenomenon that is widespread. Similarly, the works that have been reviewed regarded either wing flutter or suspension bridge flutter. There has been very little research conducted into the comparison of flutter of these two structures, the result of which is a lack of understanding an appreciation for the cross-discipline nature of phenomenon.

4 Fundamental Theoretical Concepts

Due to the complexities and multi-faceted nature of flutter it is a worthwhile endeavour to fragment the theory component of this thesis. This has been accomplished through first presenting the underlying principles of which general aeroelasticity is comprised before delving into the flutter-specific theory. In doing so it is desired to begin to recognise, from a conceptual perspective, the similarities and differences between flutter in various applications. The following two chapters will include the information that will enable this to be realised.

The first of these chapters has been structured in a way that the fundamentals of structural mechanics, structural dynamics and aerodynamics are all presented and explored. This is intended to provide the necessary background to appreciate and understand the various types of flutter when they are introduced. Similarly, the underlying concepts presented here will also provide a foundation for the development of the flutter models.

4.1 Mass-Spring-Damper Analogy

The simple mass-spring-damper system offers an effective analogy to the dynamical systems that will be dealt with in the proceeding flutter analysis. Such a system is presented in Figure 9 below.

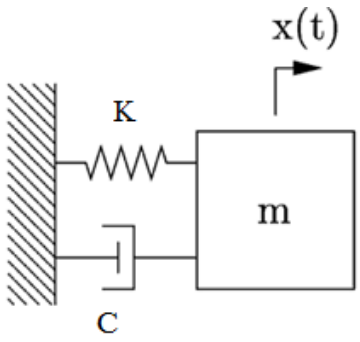

Figure 9: A spring-mass-damper system

Here K is the spring stiffness, C is the damping coefficient and m is the mass of the system. x is a Cartesian coordinate representing the displacement of the system and deemed to be positive when moving to the right. The dashpot of damping coefficient C is used to indicate the structural damping present in the system while the spring serves a similar purpose for the structural stiffness.

Hooke's Law is a fundamental principle in the study of structural mechanics and, more specifically, the area of elasticity. This law states that the strain experienced by an elastic body

is linearly proportional to the stress applied to the body when in the range of the elastic limit. Mathematically, Hooke's Law is described as:

$$F = Kx \tag{1}$$

Here, the spring stiffness introduced previously is clearly depicted. The significance of the use of Hooke's Law will become evident when the methods used for describing the motion of a system are introduced.

As will also be discovered in the following work, the equations of motion used to describe the aeroelastic behaviour of both an aerofoil and bridge deck include two forms of damping. The first of these is structural damping which is an embodiment of the restoring force that is proportional to the velocity of a dynamical body. Within the equations of motion, the damping component is often interchangeable with the non-dimensional damping ratio. The second instance of damping in the aeroelastic equations of motion is that of aerodynamic damping. This restoring force in this case is contributed to the system through interaction with the air flow and the subsequent aerodynamics.

4.2 Structural Dynamics

It is the role of structural dynamics to explain the motion of a dynamical system, like the aforementioned mass-spring-damper. This is achieved by considering various properties of the structure and formulating corresponding equations of motion. The following sections aim at providing a background on the two primary approaches used to derive these equations of motion.

4.2.1 Newtonian Mechanics

There are a number of mathematical principles that are fundamental when dealing with the structural dynamics of a system. Two approaches are commonly implemented for the acquisition of the equations of motion of an elastic body. The first of these to be examined involves the well-known Newtonian mechanics where an inertia and mass balance is conducted.

It is a common practice to employ Newton's Second Law of Motion when describing the dynamical action of a system possessing a minimal number of degrees of freedom. In mathematical terms, this Law is expressed as

$$\sum F = m\ddot{x} \tag{2}$$

Where m is the mass of the body in question and $\ddot{x}$ is the corresponding acceleration. In an effort to develop an understanding of how this concept is employed in structural dynamics, the simple 1-DOF spring-mass-damper system will be used as an example.

Performing a preliminary force balance of the system, the equation of motion is deemed to be:

$$m\ddot{x} = -C\dot{x} - Kx \tag{3}$$

Note the inclusion of Hooke's Law in Equation (3). After rearranging and dividing through by the mass term, (3) becomes:

$$\ddot{x} + \frac{C}{m}\,\dot{x} + \frac{K}{m}\,x = 0 \tag{4}$$

At this point it is worth introducing the natural frequency and damping ratio of the system. The natural frequency and the damping ratio which are defined as the following:

$$\omega_n = \sqrt{\frac{K}{m}} \tag{5}$$

$$\xi = \frac{C}{2\sqrt{Km}} \tag{6}$$

Using these newly formulated relationships, the equation of motion in (4) becomes:

$$\ddot{x} + 2\xi\omega_n\dot{x} + \omega_n^2 x = 0 \tag{7}$$

This is an equation that is come across quite regularly in the study of structural dynamics. It is a simple, yet effective, method used to generate the equations of motion for a dynamical structure. An alternative method that is based upon the energy of moving body.

4.2.2 Lagrangian Mechanics

The equations of motion can also be derived from an energy perspective via Hamilton's Principle used in conjunction with Lagrange's Equation. Hamilton's Principle is a powerful one that has been used extensively in the study of structural mechanics. It is introduced in both [17] and [31] as an effective starting point to assist in the formulation the equations of motion for a systems subject to aeroelastic effects.

Given initial and final conditions, the motion of a system will be such that the difference between the kinetic and potential energy will average out to be a minimum relative to other dynamical paths [31]. Quantitatively, Hamilton's Principle can be expressed in the following manner:

$$\delta \int_{t_0}^{t_1} (T - V) dt = 0 \qquad (8)$$

Here, t_0 and t_1 are the times at the initial and final conditions respectively. T is the kinetic energy of the system, V is the potential energy and δ is representative of virtual displacement. Figure 10 below, has been included to offer a graphical explanation of Hamilton's Principle.

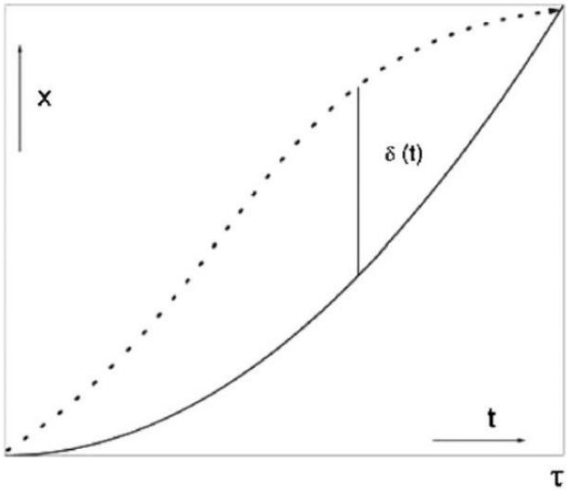

Figure 10: A graphical depiction of Hamilton's Principle

The solid line depicted in Figure 10 is representative of the actual motion of a system while the dashed line is the varied path. The two paths are separated by the virtual displacement $\delta(t)$. With this preliminary knowledge of Hamilton's Principle, it is an opportune time to introduce Lagrange's Equation.

The Lagrangian, denoted by $\mathcal{L}$, is described as being the difference between the kinetic and potential energies possessed by a system.

$$\mathcal{L} = T - V \qquad (9)$$

The relationship between Lagrange's Equation to Hamilton's Principle is immediately observed when comparing (9) and (8). In order to formulate Lagrange's Equation, it is necessary to introduce the concept of generalised coordinates. These are a set of coordinates are considered independent of other coordinates and are suitable in describing the motion of a system undergoing dynamical action [32]. The displacement of a single particle within the system can be written as:

$$\vec{r} = \vec{r}(q_i, q_{i+1}, \dots, t) \qquad (10)$$

Where q_i is the ith generalised coordinate [17]. These generalised coordinates are indicative of the number of degrees of freedom that a system possesses. Hence, the resulting kinetic and potential energy terms can be defined as:

$$T = T(\dot{q}_1, q_2, \dots, t) \quad (11)$$

$$V = V(\dot{q}_1, q_2, \dots, t) \quad (12)$$

With this knowledge, Lagrange's Equation is represented as:

$$\frac{d}{dt}\left(\frac{\partial T}{\partial \dot{q}_i}\right) - \frac{\partial T}{\partial q_i} + \frac{\partial V}{\partial q_i} = Q_i \quad (13)$$

Where Q_i is indicative of any external or dissipative forces. To illustrate the implementation of the energy method prescribed by Lagrangian Mechanics in ascertaining the equations of motion, the system depicted in Figure 9 will again be referred to. For this system, the kinetic and potential energies are required as well as the dissipative force of the system damping.

$$T = \frac{1}{2}m\dot{x}^2 \quad (14)$$

$$V = \frac{1}{2}kx^2 \quad (15)$$

$$Q_i = -c\dot{x} \quad (16)$$

Substituting (14), (15) and (16) into (13) the following expression is generated:

$$\frac{d}{dt}\left(\frac{\partial\left[\frac{1}{2}m\dot{x}^2\right]}{\partial \dot{q}_i}\right) - \frac{\partial\left[\frac{1}{2}m\dot{x}^2\right]}{\partial q_i} + \frac{\partial\left[\frac{1}{2}kx^2\right]}{\partial q_i} = -c\dot{x} \quad (17)$$

In this instance, the generalised coordinate, q_i, is the displacement of the system, x. Therefore, the expression in (17) becomes:

$$\frac{d}{dt}\left(\frac{\partial\left[\frac{1}{2}m\dot{x}^2\right]}{\partial \dot{x}}\right) - \frac{\partial\left[\frac{1}{2}m\dot{x}^2\right]}{\partial x} + \frac{\partial\left[\frac{1}{2}kx^2\right]}{\partial x} = -c\dot{x} \quad (18)$$

Performing the necessary derivations reduces the expression to:

$$m\ddot{x} + c\dot{x} + kx = 0 \quad (19)$$

Upon inspection it will be noted that this is identical to the equation of motion using the Newtonian approach outlined previously. The Newtonian and Lagrangian approaches have both been introduced because of the tendency in literature for both methods to be used to derive the equations of motion for a system experiencing flutter. While at first glance, the Newtonian approach is simpler, the Lagrangian method is advantageous in that it can be effectively employed for systems with multiple degrees of freedom. As such, it is commonly used in the derivation of the equations of motion in the flutter analysis process.

4.2.3 Modes of Vibration

An understanding of modes of vibration will serve well for later discussion of flutter. In simple beam mechanics the mode of vibration is a description of the manner in which a structure responds to some force input. Both a wing and bridge can be considered as beam structures, specifically that of a cantilever beam and a fixed-end beam respectively [33]. Consequently, these two structures exhibit modes of vibration that differ due to the boundary conditions that are they induce.

While in reality, a wing and bridge are continuous systems consisting of infinite modes of vibration, for the sake of this study they are treated as discrete system. The flutter analysis that will be conducted in this study is concerned with the first mode of bending and torsion of the different structures. Examples of these are shown in Figure 11.

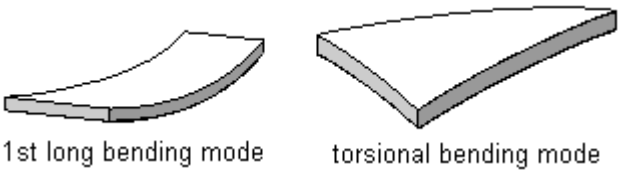

Figure 11: Simple representations of bending and torsion modes

Each of the modes of vibration dealt with here possess a specific natural frequency that is critical in the process implemented later. The natural frequency is a property of the system in question that defines the frequency at which oscillations will ensue. Thus, it follows that the natural frequency for the bending mode differs to the torsional natural frequency.

4.2.4 Simple Harmonic Motion

Another fundamental concept in structural dynamics and the study of vibrating systems that is applicable in the analysis of flutter is that of simple harmonic motion. Rao provides a concise explanation of this notion in stating that a system exhibits harmonic motion if it repeatedly oscillates at equal intervals of time [34]. The importance of the concept of simple harmonic motion to this study is due to the role it has at the flutter boundary. An analytical solution to the flutter instability problem is founded on the presumption that at the onset of flutter the structure is exhibiting simple harmonic motion [35]. The depiction of displacement over time in Figure 12 is a basic illustration of harmonic motion.

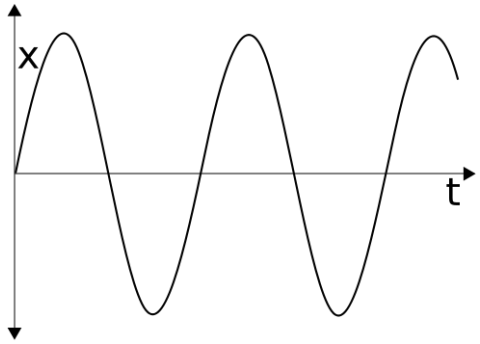

Figure 12: Time response of harmonic motion

The displacement portrayed in the graph can be described as a function of time by the following expression:

$$x = A \sin \omega_n t \quad (20)$$

Here, A is the amplitude of the response and ω_n is the natural frequency of the system whose displacement has been graphed. The first and second time derivatives of the displacement yield, respectively, the velocity and acceleration of the system.

$$\dot{x} = \omega_n A \cos \omega_n t \quad (21)$$

$$\dot{x} = \omega_n^2 A \sin \omega_n t = \omega_n^2 x \quad (22)$$

Equations (21) and (22) above suggest that the acceleration of the system is directly proportional to the displacement thus indicating that the system is indeed in harmonic motion. An alternate representation of the displacement of a system in harmonic motion is provided by complex number representation.

$$x = Ae^{i\omega_n t} \quad (23)$$

Harmonic motion is an idea of note as it is utilised in various analysis techniques of flutter. Thus, the notion of harmonic motion is an integral one to the structural component involved in the study of flutter.

4.3 Aerodynamics

The field of aerodynamics is one that is far reaching in a variety of engineering disciplines. Since first presenting itself as an of research of significance before the invention of aircraft, the theory of aerodynamics has developed substantially over the decades. Additionally, its prevalence to fields of engineering other than those of aeronautical and aerospace has been recognised. This has subsequently resulted in the progression of research into the aerodynamic impact on a variety of structures. An understanding of these aerodynamic forces is critical to the study of flutter which itself is largely dependent on the way in which these forces are modelled.

4.3.1 Potential Flow

Aerofoils are the predominant cross-sectional shapes of aircraft lifting and control surfaces. As such, the function of these aerofoils is to produce the lift necessary for the intended operational requirements. The shape of the aerofoil is critical in achieving lift when interacting with the free stream flow. An aerofoil is classified as a streamlined shape which is a result of its tapered design which is illustrated in Figure 13.

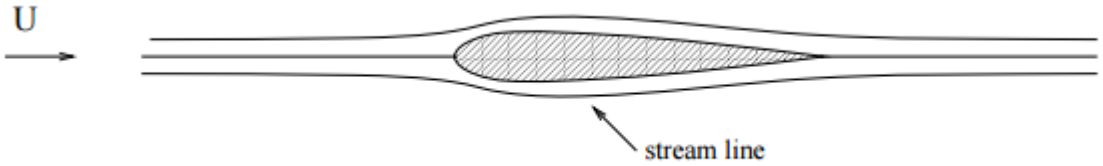

Figure 13: Streamlines over an aerofoil

Aerofoil aerodynamics is one of the few applications where the use of a field of aerodynamics known as potential flow theory is appropriate. As such, the theories that have been developed for wing flutter in the next chapter have been done so on the premise of potential flow. Essentially, potential flow theory makes two underlying assumptions [36]:

1. The flow over the aerofoil surface is inviscid
2. The flow over the aerofoil surface is irrotational

The flow-field solutions produced by potential flow theory are done so with the use of two governing equations:

$$\frac{du}{dx} + \frac{dv}{dy} = 0 \qquad (24)$$

$$\frac{dv}{dx} - \frac{du}{dy} = 0 \qquad (25)$$

From (24) and (25), u and v are used to represent the x- and y-velocity field respectively. Thus, in potential flow theory, the solution for a flow-field is valid if the equations above are fulfilled.

These assumptions allow for the use of two concepts in describing the flow interaction with an aerofoil. The Kutta-Joukowski Theorem is an aerodynamic principle that is used to determine the lift generated by an aerofoil. It was proposed that this lift was proportional to the circulation of the flow around the surface of the body. Mathematically, the Kutta-Joukowski Theorem is given as:

$$L = \rho U \Gamma \qquad (26)$$

Where Γ is the strength of the circulation over the aerofoil. In potential flow, this theorem is used in conjunction with Kutta Condition. This condition requires the flow to depart the surface of the aerofoil smoothly at the tapered trailing edge, was realised. Simply put, Kutta's Condition implies that no flow separation occurs over the surface of the aerofoil. Thus, this requires the boundary layer over the aerofoil to be remain attached at all times and physically thin.

However, as previously mentioned, the use of potential flow theory in describing the aerodynamic lift generated by an aerofoil is one of the few instances where it is appropriate. Where the effects of vortices dominate a flow field, limitations of potential flow theory are observed. As such, alternative theories are required in an effort to explain the behaviour flow around structures other than aerofoils.

4.3.2 Bluff-Body

Potential flow is problematic as it has limited applicability to other cases other than aerofoil aerodynamics. This is particularly true in the context of fluid flow over a bridge section where bluff body aerodynamics dominates. A structure is deemed as being a bluff-body when the fluid flow is separated over a considerable portion of the body. This is an example when the Kutta Condition is not realised and the aerodynamic principles relevant to aerofoils become invalid. The bluff-body categorisation incorporates a variety of different shapes.

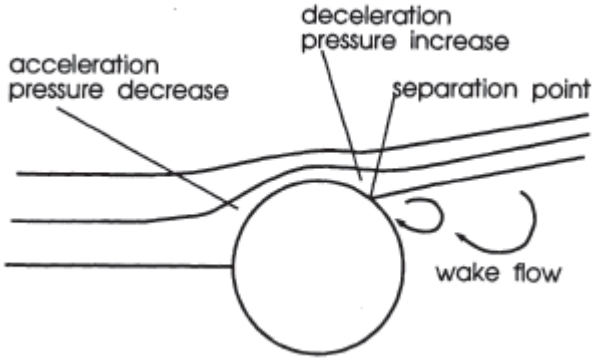

Figure 14: Flow interaction with a bluff-body [37]

Bluff-bodies are a major topic of consideration in civil engineering applications as opposed to aerospace engineering. This is due to the fact that they are representative of many common structures dealt with such as bridge decks. The flow over bluff bodies is characterised by boundary layer separation and the shedding of vortices resulting from geometrical features that are not conducive of streamlined flow. In this regard, it becomes obvious that the potential flow assumptions of inviscid and irrotational flow breakdown. Unlike the aforementioned potential flow theory, there is no readily available purely analytical formulation of the bluff-body

aerodynamic forces. Rather, complex numerical simulations or experimental data is often utilised to this end.

In bluff body aerodynamics, the Strouhal number is often used quantify the frequency of vortex shedding. This is a non-dimensional value defined as:

$$St = \frac{fB}{U} \qquad (27)$$

f is the frequency of vortex shedding and B is the reference length. The vortices that the Strouhal number pertains to are known as Karman vortices named after Theodore von Karman. A repetitive pattern of these vortices form a Karman vortex sheet and is caused by the separated and unsteady flow over a structure.

Figure 15: Karman vortices of a circular cylinder

4.4 Summary

Presented in this chapter are the concepts that have been deemed integral for an in depth analysis of both wing and bridge flutter. These concepts pertain to structural dynamics and aerodynamics and have been effective in laying the groundwork for further discussion. In addition, some of the aerodynamic concepts outlined here have provided a preliminary insight into the fundamental differences between wing and bridge flutter.

5 Flutter Specific Theory

A platform has been provided in the form of the key concepts outlined in the previous chapter to launch into an examination of the various forms of flutter that are of interest to this study. Initially, this chapter will endeavour to clarify the difference between flutter and mechanical resonance before the significance of the role played by various forms of coupling is discussed. From here, the different types of flutter will be differentiated and the more specific theories regarding each of these will be presented.

5.1 Flutter vs. Mechanical Resonance

As has been alluded to in previous chapters, there has been historically some conjecture concerning the similarities between flutter and mechanical resonance. Therefore, it is necessary at this point to highlight the fundamental differences between the two structural instabilities. It has been previously explained that flutter is a self-excited response of an elastic body immersed in a fluid flow. It is self-excited in that the energy derived from the fluid flow is used to create a positive feedback loop that the structural damping strives to eliminate. The source of energy, which is the free stream flow in most flutter cases, is deemed to be a steady source. Given the self-excitation, the body that is undergoing flutter determines the frequency at which it oscillates at.

In the instance of mechanical resonance, the frequency at which the corresponding oscillations occur is that of the natural frequency of the elastic body. The result of this is oscillations with significantly higher amplitudes than other frequencies which have a tendency to be destructive. The energy that produces the mechanical resonance stems from an oscillation force and is consequently termed a forced response problem.

Flutter and resonance do share a common theme in that they both potentially destructive behaviours that are primary design considerations. The underlying difference between the two is how they are initiated for an elastic body. Flutter of a structure is a natural response problem while resonance is a forced response problem. This is a distinguishing factor when considering the nature of the behaviour of an elastic body.

5.2 Coupling

A topic of great significance in the discussion of flutter is that of coupling and the role it has in initiating the aeroelastic phenomenon. There are two different types of coupling that are

pertinent to the analysis of flutter. Thus, it is necessary to examine these types of coupling in detail to further understand the mechanisms of flutter.

Inertial coupling is the first type and the one that is most commonly associated with flutter. Inertial coupling occurs when the vertical motion induces a twisting force by virtue of the inertia forces present [38]. As will be seen this is prevalent in the case of classical wing and bridge flutter. However, given that the torsional mode of vibration dominates the in the cases of an aerofoil experiencing stall flutter and the flutter case of the Tacoma Narrows bridge, inertial coupling becomes irrelevant.

The interaction between the fluttering motion of a structure and the aerodynamic forces acting upon it is referred to as aerodynamic coupling. A rotation of the structure in an airflow will result in a change in lift acting on the body which causes a change in translation. Essentially, aerodynamic coupling entails a variation of lift produced by wing rotation or translation. Therefore, aerodynamic coupling is more applicable to the description of torsional bridge flutter and stall flutter. Again, this will become apparent in future discussion of the different examples of flutter.

5.3 Classical Wing Flutter

Traditionally, classical flutter, also referred to as binary flutter, has been the most common form of flutter to be analysed. This is attributed to the fact that many aircraft structures are susceptible to this type of flutter. While the typical analysis considers classical flutter in the context of a wing, there have been other instances throughout history where other structures have been known to induce this type of flutter. The potential for catastrophic failure is high when flutter is encountered regardless of the particular structures that are effected.

If a disturbance of some form is encountered by a wing that is stable then, following an initial response to the disturbance, the wing will return to its previously stable condition. This is due to the structural and aerodynamic damping being adequate in ensuring that the wing returns to an equilibrium position. In regards to flutter, the previously described sequence of events will occur below a critical velocity known as the flutter boundary. At or above this critical velocity the wing becomes unstable and flutter is said to transpire. This is not unique to classical wing flutter, however it does provide a foundation for the following discussion.

There must be some means of disturbance to instigate the wing instability. For classical wing flutter, an initial increase in the lift force acting on the wing causes a resulting moment that alters the angle of attack of the wing. Above the flutter boundary, instead of being damped, the

response of the wing is seen to increase exponentially [35] and is said that that negative damping is being provided by the air.

Physically, classical flutter is characterised by the coupling of the bending and torsional modes of vibration. When this occurs the response of the structure is deemed to be self-excited whereby the response of one mode will cause a response in the other mode. In this sense, the wing during flutter forms a positive feedback loop where the energy from one mode of vibration is used to sustain the other. The coupling of modes is characterised by the coalescence of the respective frequencies of bending and torsional vibration. Thus, it is now apparent the role that inertial coupling plays in the context of classical wing flutter.

5.4 Torsional Bridge Flutter

Classical flutter in an aeronautical context has made up a large part of aeroelastic studies in the last century. The collapse of the bridge at Tacoma Narrows is generally accepted as being at the foremost example of large structure flutter. In the immediate years after the bridge collapse, the ensuing flutter analysis mirrored that of a classical wing flutter scenario. However, through further testing and with advancements in computing capabilities, this method has since been rendered inappropriate.

Prior to delving into the theory behind the type of flutter that was prevalent in the Tacoma Narrows incident some background will be provided regarding the design of this particular bridge. At the time, the relatively light weight and high aspect ratio design was considered to be revolutionary. The length of the bridge rendered it as one of the longest suspension cable bridges in the world [39]. However, it would eventually be realised that, from a structural dynamics perspective, these attributes would be contributing factors to the onset of flutter. The substantial length, in conjunction with the relatively narrow deck, diminished the torsional stiffness of the bridge.

While the aforementioned structural characteristics accentuated the possibility of flutter, the profile geometry of the bridge deck was conceded to be the root cause of the collapse. The H-section profile that was adopted for the bridge deck was deemed to be a true bluff-body shape. As such, the presence of Karman vortices were mandatory in the fluid-structure interaction in the case of the Tacoma Narrows bridge so much so that Theodore von Karman postulated that these were the cause of the destructive vibrations. However, this was disputed on the grounds that the frequency of the vortex shedding was different to that of the frequency of the oscillations of the bridge [4].

Through wind tunnel experiments, it was verified that the Tacoma Narrows bridge failure was due to torsional flutter [29]. While it is accepted that a naturally developed Karman vortex sheet was present, it was not pertinent to the failure of the bridge. Rather, the flow separation over the bridge resulted in the formation of vortices that were adequate in causing a change in the angle of attack. Consequently, the motion induced by this caused further vortices to be shed and the creation of a flutter wake eventuated [4]. Thus, this process, in which the oscillatory motion of the structure accentuates the shedding of vortices, is one that is self-excited and therefore fulfils the requirements of flutter.

The flutter of the Tacoma Narrows bridge exhibited vibrations in the torsional mode only which differentiates this particular type of flutter to that of classical wing flutter discussed in 5.3. The physical mechanism for the torsional flutter is the flow separation that occurs over the structure due to profile of the bridge deck. Thus, it can be inferred that the defining feature between classical flutter and the torsional flutter discussed here is the geometrical characteristics of the structural profile. While this is true, there is still the potential for classical flutter to arise in the case of a bridge deck despite the prevalence of bluff body aerodynamics in the context of bridge flutter.

5.5 Classical Bridge Flutter

For bridges that possess a deck profile that is relatively streamlined, the flutter that is likely to be encountered is that of the classical form as opposed to the single, torsional mode. While not indicative of the collapse of the bridge at Tacoma Narrows, coupled bending torsion flutter is considered to be a problem for suspension bridges. The notion of classical bridge flutter has provided the foundation for many theoretical and experimental flutter investigations. However, in actuality, there have not been any recorded incidences of classical bridge flutter.

To reiterate, classical flutter involves the coupling of bending and torsion modes of vibration. The H-section used in the design of the Tacoma Narrows bridge guaranteed that flow separation occurred almost immediately during fluid-structure interaction. Considering a more streamlined bridge deck however, one which possess vertices of sorts at the leading and trailing edges, flow tends to remain attached for longer over the structure. This facilitates the initiation of classical form of flutter in that the vertical and twisting motion of the bridge are coupled which causes the self-excited forces.

5.6 Stall Flutter

The final flutter variant that will be presented and discussed here is that of stall flutter. As alluded to by its name, this is a phenomenon associated with the stalling conditions for a wing. It is an example of non-linear aeroelasticity and as such varies significantly from the previously documented classical wing flutter. A succinct description of the stall flutter phenomenon is as follows:

> ‘Stall flutter is an aeroelastic phenomenon that emerges from an energy transfer between a fluid and an elastic system undergoing dynamic stall’ [40].

Stall flutter is instigated by the separation of flow over the surface of the wing that occurs during operation at high angles of attack. Given the non-linear nature of flow separation, this type of flutter is inherently non-linear. Stall flutter is characterised as a one degree-of-freedom instability as it exhibits prominent torsional oscillations. It is here that parallels can be observed with the flutter incident that was the collapse of the Tacoma Narrows Bridge. The torsional oscillations that have been associated with the most notable example of bridge flutter are the same as those exhibited by a wing undergoing stall flutter. The torsional oscillatory behaviour is not the only similarity shared between a stalling aerofoil and a H-section bridge deck. The mechanism that initiates the two types of flutter is attributed to the separation of flow over the structure. In the case of stall flutter, the flow separation is caused by large angles of attack while by virtue of the geometry of the H-section bridge deck, separation of flow occurs.

5.6.1 Separation of Flow

The following subsection will be devoted to the explanation of flow separation and the role it plays in the instigation of stall flutter. This will serve the purpose of gaining an understanding of the fundamental disparities between not only classical wing flutter and stall flutter but also the between torsional bridge flutter and stall flutter. The necessity for this section is a result of the relative complexity that is involved.

It has already been alluded to that the separation of flow over the top surface of the aerofoil is the instigating mechanism of stall flutter. Thus, it is necessary to delve into the factors that can cause flow separation. Effectively, flow separation is a result of viscous effects of the flow passing over the immersed aerofoil. At low angles of attack, the fluid interacts with the aerofoil in a desirable manner, which sees the streamlines travel smoothly around the structure. The surface pressure is such that it is greater along the bottom surface than the top so that lift is generated. Towards the trailing edge, where the surface pressure begins to gradually increase,

having earlier reached a minimum, a region of adverse pressure gradient is said to originate [41]. For low angles of incidence, this adverse pressure gradient is moderate and therefore not a hindrance to lift generation. However, at larger angles of attack, it becomes particularly severe and the flow becomes separated.

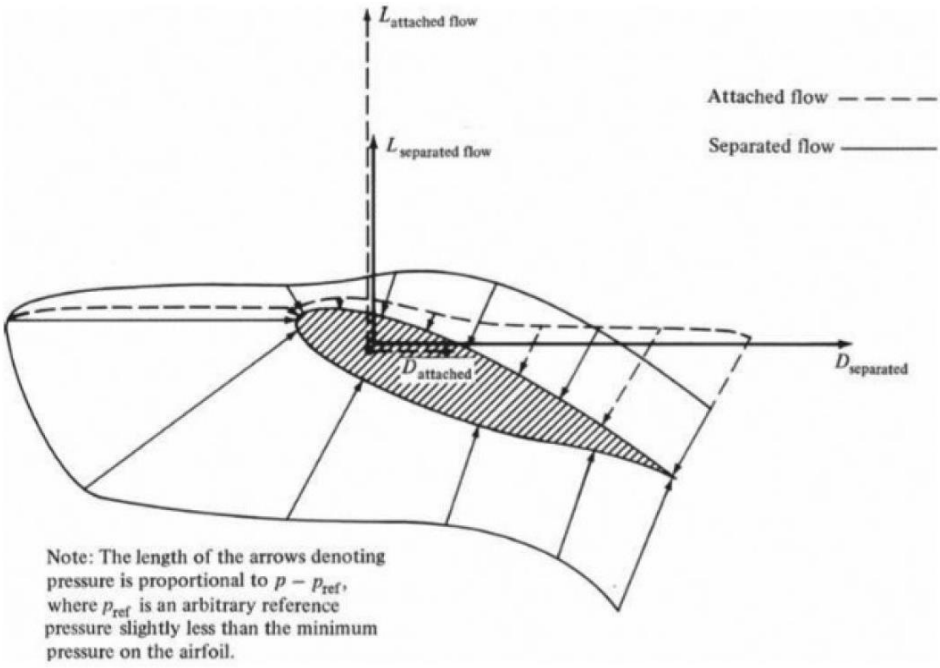

Figure 16: Attached and separated flow over an aerofoil [41]

The implication of flow separation on the generation of lift is illustrated in Figure 16. Using the vertical component of the net surface pressure distribution, the lift generated by the aerofoil can be derived. Hence, observing Figure 16, the net surface pressure distribution for the separated flow instance will be lesser than when it is attached and consequently, the lift is smaller. This loss of lift is the cause of stall. However, the phenomenon that is stall flutter entails a dynamic stalling effect which is differs to that to commonly regarded static stall.

5.6.2 Static Stall vs. Dynamic Stall

When discussing stall flutter, it is important to note the difference between static and dynamic stall. In the event of the flow stalling over a wing at a fixed angle of attack, static stall is said to occur. Conversely, dynamic stall is associated with the flow separation over a dynamic body, typically one undergoing pitching motion. The determination of static stall, and the corresponding lift and drag coefficients, is dependent upon a singular angle of attack. However, in the case of dynamic stall, these coefficients will be constantly changing given the variance in angle of attack. The coefficients predicted during dynamic stall can be dramatically different to those predicted by static stall.

The occurrence of dynamic stall is characterised by a particular process which will be described briefly here. With the onset of dynamic stall, a vortex is generated at the leading edge when the shear layer in the vicinity rolls up which allows for the provision of additional suction on the upper surface of the aerofoil [23]. Following an initial gain in lift and delay in stall, the leading edge vortex detaches from the aerofoil surface having become unstable. The result of this is a substantial loss of lift in conjunction with severe pitching.

Stall flutter is an embodiment of the cross-disciplined nature of flutter. While being prevalent in both an aerospace and civil engineering context, this type of flutter pervades many other areas of engineering. Advancements in the field of wind energy have been plagued by turbine blades experiencing the implications of aeroelasticity. The high angles of attach at which these blades operate at make them particularly susceptible to stall flutter. Furthermore, stall flutter has been known to effect helicopter rotor blades.

5.7 Aerodynamic Theories

A pertinent component in the discussion of flutter is the aerodynamic theories that are available for use. Over the years that the study of aeroelasticity has been of interest, a number of theories have been developed that attempt to model the effects of aerodynamics. These are mainly concerned with classical aerofoil flutter, however, as will be seen shortly, theories have been developed for bridge flutter. In this section the methods in which the aerodynamics associated with the flutter will be presented.

5.7.1 Quasi-Steady Aerodynamics

The assumption of quasi-steady aerodynamics allows for an easy introduction into the modelling of the airflow contributions when considering flutter problem. The quasi-steady approximation is an example of the aerodynamic theory developed on the foundation of a steady flow assumption. This approximation ignores the time history of the fluid flow and evaluates the aerodynamic forces given the instantaneous motion of the structure [17]. The effect of this is that the influence that the wake has on imparting forces onto the structure is disregarded. The quasi-steady lift force and the resulting moment are described by the following equations [11]:

$$L_{qs} = 2\pi\rho b U^2 \left[\frac{\dot{h}}{b} + b\left(\frac{1}{2} - a\right)\frac{\dot{\alpha}}{U} + \alpha\right] \quad (28)$$

$$M_{qs} = b\left(\frac{1}{2} + a\right)L_{qs} - \frac{\pi\rho U b^3}{2}\dot{\alpha} \quad (29)$$

In the context of wing flutter, from (28) and (29), b is the half chord length, U is the free-stream velocity and a is the location of the elastic axis normalised by the half-chord length. If

a is negative then it lies forward of the mid-chord and alternatively when it is positive it lies aft. α is the angle of attack and is representative of the pitch of the structure while $\dot{h}$ and $\dot{\alpha}$ are the time derivatives of the heave and pitch respectively.

While considered to be drastically less complex than an unsteady flow approach, the use of quasi-steady aerodynamics has proven to produce less accurate solutions to the flutter problem. This is due to the significance that the aforementioned wake effects have on the quantification of the aerodynamics forces in the flutter problem. Furthermore, these wake effects arise due to the oscillating motion of the structure during flutter and, thus, are considered fundamental to the flutter analysis. Therefore, the use of quasi-steady aerodynamics is often superseded by an unsteady aerodynamic model is thorough flutter investigations.

5.7.2 Unsteady Aerodynamics

It has become widely accepted that the use of unsteady aerodynamics will ultimately provide a more realistic solution to the flutter problem. The development of unsteady aerodynamic theory in the 1930's was vital to the progression of flutter analysis. Contrary to the quasi-steady approximation, the influence that the wake has is considered in this instance. Due to the motion of an oscillating object, the aerodynamic forces are inherently unsteady and as such necessitate a worthy model. Two methods have proven popular in the modelling of unsteady aerodynamics for the analysis of flutter. The first of these is embodied by the Wagner Function which provides an approach via the time domain while the second, Theodorsen's Function, is in the frequency domain.

5.7.2.1 Time Domain Aerodynamics

A solution to the flutter problem provided by the implementation of the Wagner function to account for unsteady aerodynamics has found use in aerofoil problems. As previously mentioned, this approach is one that allows for the representation of the lifting force and pitching moment in the time domain. Numerically, this lifting force according to Wagner's theory is expressed as:

$$L = 2\pi\rho U b w \phi(s) \qquad (30)$$

In (30), w is given by $Usin(\alpha)$ and describes the normal component of the velocity component. Similarly, $\phi(s)$ is the aforementioned Wagner Function as a expressed in terms of a dimensionless time s which itself is evaluated as:

$$s = \frac{Ut}{b} \qquad (31)$$

It is convenient to use an expression formulated by Jones [9] to approximate Wagner's Function again in terms of the dimensionless time.

$$\phi(s) = 1 - 0.165e^{-0.0455s} - 0.0335e^{-0.30s} \quad (32)$$

The value of Wagner's Function, in terms of the dimensionless time, is given by the following graph.

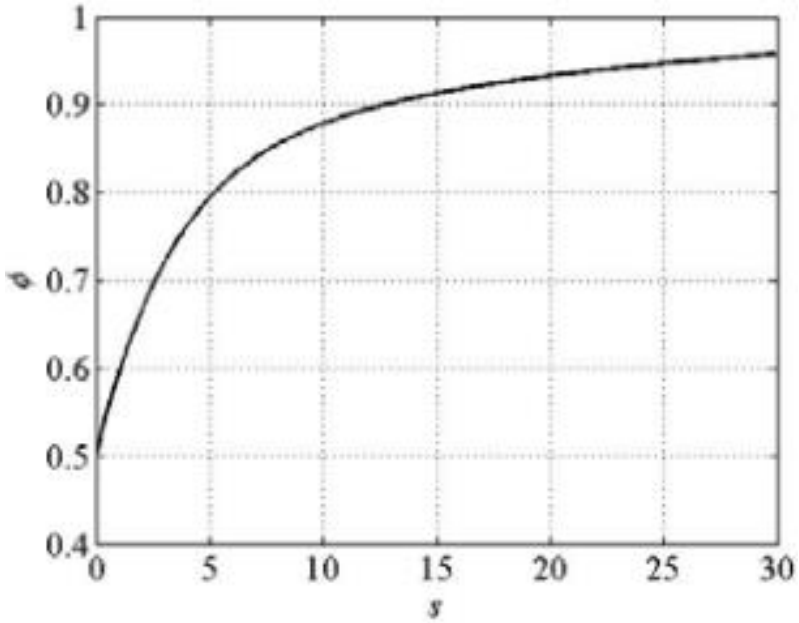

Figure 17: Wagner's Function for various non-dimensional times [43]

Wagner's theory regarding an unsteady aerodynamic model is important to consider when discussing flutter. While the approach outlined here is useful, it has been used sparingly in flutter analysis from literature. Alternatively, the frequency domain has proved to be more beneficial for the formulation of an unsteady aerodynamic model.

5.7.2.2 Frequency Domain Aerodynamics

For an aerofoil undergoing small oscillations, Theodorsen derived an exact theory that implemented an unsteady aerodynamic approach capable of producing a solution to the flutter problem. This theory gained traction in the analysis of flutter and has for many decades been successfully employed in the study of flutter. The work conducted by Theodorsen, and the subsequent theory, has been used in both aerofoil and bridge flutter modelling. It will be the objective of this subsection to provide an explanation of Theodorsen's Function and illustrate how it has been utilised initially for aerofoil flutter and modified for bridge flutter. The work of Theodorsen is based on a number of simplifying assumptions which include [44]:

1. Flow remains attached at all times
2. The wing can be considered as a flat plate

3. The wake is flat

Based on these assumptions, the dependence on potential flow theory can very much be inferred. Therefore, it is necessary to note the importance of potential flow to the derivation formulation of this model. Theodorsen's Function is given as [21]:

$$C(k) = \frac{H_1^{(2)}(k)}{H_1^{(2)}(k)+iH_0^{(2)}(k)} = F(k) - iG(k) \quad (33)$$

Where $H_0^{(2)}$,$H_1^{(2)}$ and $H_1^{(2)}$ are Hankel Functions of the second kind but are not particularly significant in this instance. In the form above, the real components of Theodorsen's Function are denoted as $F(k)$ while the imaginary components are denoted by $G(k)$. As was the case for Wagner's Function in the time domain, an expression has been formulated to offer an approximation of Theodorsen's Function in the frequency domain [22]:

$$C(k) = 1 - \frac{0.165}{1 - \frac{0.0455}{k}i} - \frac{0.335}{1 - \frac{0.3}{k}i} \quad (34)$$

Theodorsen's Function, and the Hankel Functions of which it features, are all functions of k, which is the reduced frequency and is expressed as:

$$k = \frac{\omega b}{U} \quad (35)$$

The reduced frequency is a dimensionless parameter that provides a measurement of sorts of the unsteadiness of the flow. Furthermore, it is analogous to the Strouhal Number, which was introduced in the previous chapter. Both dimensionless parameters are similar in that they find use in the modelling of unsteady flow. From literature, the Strouhal Number is prevalent in civil engineering applications while the reduced frequency is utilised in an aerofoil context. The notable distinction between these two parameters is the use of the half-chord length as the reference dimension for the reduced frequency whereas the Strouhal Number utilises the full structural width.

Returning to Theodorsen's Function, the real and imaginary parts of which it is comprised can be seen in Figure 18 below for a range of reduced frequencies.

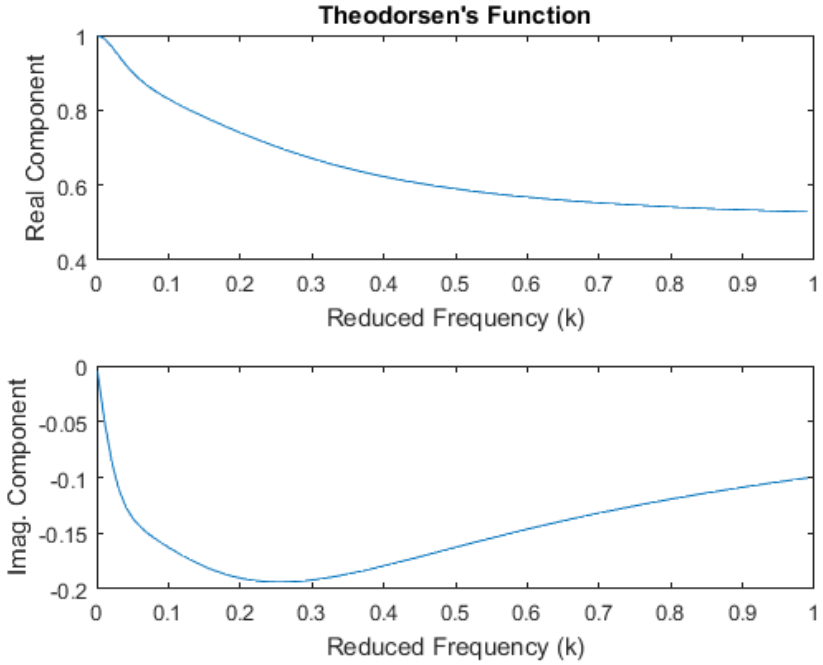

Figure 18: Real and imaginary components of Theodorsen's Function

The use of Theodorsen's Function ensures that the effects associated with unsteady aerodynamics are accounted for. Specifically, these are the circulatory and non-circulatory effects generated by an oscillating structure immersed in fluid flow. The non-circulatory effects are often referred to as mass apparent effects as they are associated with forces induced by the accelerating particles surrounding a structure in motion [18]. Essentially, these are the consequences of the structure displacing the fluid of which it is immersed in. Conversely, the circulatory effects are associated with the lift and moment generated by the circulation around the aerofoil. Included in this are also the implications of the vortices that are shed into the wake as a result of the motion of the aerofoil.

Thus, the lifting and pitching moment can be formulated with the aid of Theodorsen's Function in terms of varying reduced frequency. The lift and moment about the elastic axis of an aerofoil due to unsteady aerodynamics can be represented as

$$L = \rho\pi b^2[\ddot{h} + U\dot{\alpha} - ab\ddot{\alpha}] + 2\pi\rho UbC(k)\left[\dot{h} + U\alpha + b\left(\frac{1}{2} - a\right)\dot{\alpha}\right] \quad (36)$$

$$M = \rho\pi b^2\left[ab\ddot{h} + Ub\left(\frac{1}{2} - a\right)\dot{\alpha} - b^2\left(\frac{1}{8} + a\right)\ddot{\alpha}\right] + 2\pi\rho b^2 U\left(a + \frac{1}{2}\right)C(k)\left(\dot{h} + U\alpha + b\left(\frac{1}{2} - a\right)\dot{\alpha}\right) \quad (37)$$

These will provide the aerodynamic force and moment terms in the development of the aerofoil flutter model in the following chapter.

5.7.2.3 Bridge Aerodynamics

In the early years of bridge flutter investigation, it generally accepted that the work of Theodorsen was applicable to the analysis of bridge flutter. However, armed with the knowledge of bluff body aerodynamics, it is apparent that the assumptions upon which Theodorsen's is based upon becomes inapplicable. Particularly, the assumption that the flow remains attached is inappropriate as a defining feature of bluff bodies is the flow separation that occurs. Therefore, while attempts have been made to apply this approach, Theodorsen's theory does not provide an accurate representation of the unsteady aerodynamic forces in the study of bridge flutter.

The flow separation involved with bridge flutter renders it a problem that is inherently non-linear. As such. The formulation of expressions such as those of Theodorsen's and Wagner's in order to model the aerodynamic forces prevalent in the instance of bridge flutter has so far been unachievable. However, through scaled wing tunnel experimentation, flutter derivatives have been able to be extracted that allow for the conception of aerodynamic models pertaining to bridge flutter. As alluded to earlier in 5.4 and 5.5, the particular geometry plays an integral role in the corresponding aerodynamic characteristics. Consequently, the initial wind tunnel investigation produced flutter derivatives for a wide range of bridge decks [29]. These derivatives are beneficial as they allow for the linearisation of the previously non-linear aerodynamic models. Using the preliminary three derivative formulation in conjunction with the empirical flutter derivatives, the lift and moment equations for the case of bridge flutter are as follows [26]:

$$L = \frac{1}{2}\rho U^2 B\left[kH_1^*\frac{\dot{h}}{U} + kH_2^*\frac{B\dot{\alpha}}{U} + k^2H_3^*\alpha\right] \quad (38)$$

$$M = \frac{1}{2}\rho U^2 B^2\left[kA_1^*\frac{\dot{h}}{U} + kA_2^*\frac{B\dot{\alpha}}{U} + k^2A_3^*\alpha\right] \quad (39)$$

Where H_i^* and A_1^* are the flutter derivatives and B is the full bridge width. Just as Theodorsen's Function in the case of aerofoil flutter is expressed in terms of the reduced frequency, the flutter derivatives featured here are dependent on the inverse of the Strouhal Number. Further alterations arise between the two applications in the way that the aerofoil flutter derivatives are complex as opposed to the bridge flutter derivatives which are real [26]. Table 1 offers a concise explanation of the roles that the various flutter derivatives play.

Table 1: The role of the flutter derivatives

Derivative	Role
H_1^*	Indicative of the vertical motion when the torsional motion is initially inhibited
H_2^* and H_3^*	Indicative of the implications of the torsional oscillations on the response of the vertical motion
A_1^*	Indicative of the impact that vertical motion has on the torsional motion
A_2^*	Indicative of the torsional motion when the vertical motion is initially prohibited
A_3^*	Indicative of the aerodynamic damping on the torsional flutter frequency

The flutter derivatives are able to be translated to an aerofoil context in order to illustrate the relationship that exists with Theodorsen's Function [29].

$$
\begin{aligned}
H_1^* &= -\frac{2\pi F(k)}{k} \\
H_2^* &= -\frac{\pi}{k}\left(1 + F(k) + \frac{2G(k)}{k}\right) \\
H_3^* &= -\frac{2\pi}{k^2}\left[F(k) - \frac{G(k)}{2}k\right] \\
A_1^* &= \frac{\pi F(k)}{k} \\
A_2^* &= -\frac{\pi}{2k}\left(1 - F\,(k) - \frac{2G(k)}{k}\right) \\
A_3^* &= \frac{\pi}{k^2}\left[F(k) - \frac{G(k)}{2}k\right]
\end{aligned}
\qquad (40)\ (41)
$$

Recalling from Equation (33) that the $F(k)$ and $G(k)$ represent the real and imaginary components of Theodorsen's Function respectively. It is worth noting that the relationships developed above have been done for an aerofoil whose elastic axis is at the same location as the centre of mass.

5.8 Theory Summary

A vast amount of information regarding the various types of flutter and pertinent theory has been presented in this chapter. Therefore, it is meaningful to perform a subsequent critical

analysis of this information in order to offer some concluding remarks regarding the cross-disciplined nature of flutter. This will be beneficial in that it directly links the work completed here back to the purpose of the current study. The following table provides a concise summary of the significant attributes of the various flutter examples examined.

Table 2: Summary of the flutter examples

Flutter Type	**Vibration Modes**	**Flutter Mechanisms**
Classic Aerofoil Flutter	Bending and Torsion	Vibration Coupling
Torsional Bridge Flutter	Torsion	Flow Separation
Classic Bridge Flutter	Bending and Torsion	Vibration Coupling
Stall Flutter	Torsion	Flow Separation

Due to its significance in the flutter problem, the aerodynamic theory for both wing and bridge flutter has also been discussed here. The various aerodynamic models have been alluded to with particular attention given to the work of Theodorsen whose frequency domain approach has formed the foundation for many flutter investigations. In the discussion, Theodorsen's Function, which is used in accounting for the effects of the unsteady aerodynamics in the formulation of the lift and moment equations, is introduced. However, the assumptions upon which this function is based and the dependence on potential flow theory poses limitations when used in the application of bridge flutter. The aerodynamic equations for the case of the bridge flutter are known to be semi-empirical in nature. This is a consequence of the flutter derivatives used extracted from wind tunnel experiments to model the unsteady aerodynamics.

6 Model Development

With the knowledge of the relevant theory concerning wing and bridge flutter, a quantitative analysis of the two can be performed. In this chapter, the numerical models for aerofoil and bridge flutter will be developed. The physical models used to represent the aerofoil and bridge structures of interest will be presented and the corresponding equations of motion derived. Aerodynamic models are then re-introduced from the theory chapter and consolidated with the equations of motion to deliver the flutter model.

6.1 Methodology

To provide a clear outline of the model development, the methodology for this part of the project and has been included here.

1. Derive the aeroelastic equations of motion using Lagrangian mechanics
2. Consolidate equations of motion with the aerodynamic model to yield a flutter model
3. Generate numerical method for flutter boundary prediction
4. Validate numerical method with baseline results from literature
5. Implement solution process for a variety of aerofoil and bridge sections

This methodology will be followed in order to produce models for classical aerofoil and bridge flutter as well as torsional bridge flutter.

6.2 Assumptions

The assumptions that will be made during the model development and flutter simulations will be specified here.

- The flow is incompressible and subsonic
- The air is deemed to be an ideal gas
- The flow is such that it is a continuum mass
- The free-stream flow is of uniform velocity in all flutter cases examined with negligible change in direction and magnitude
- The motion of the structures at the point of flutter is sinusoidal in nature
- The wing is simple in nature. That is, it is rectangular and does not possess any external stores
- The bridges of interest are also simple in nature. They are considered to be symmetrical about the horizontal and vertical axes.

6.3 Physical Models

Being continuous structures, a wing and bridge possess an infinite degree of freedoms. As such, in the three dimensional form, an analytical investigation of flutter is difficult. To rectify this, the continuous structures are reduced to discrete, two dimensional section profiles. The models for the aerofoil and bridge shapes have been included below with the geometrical features of interest insinuated. All of the models are comprised of two degrees-of-freedom, plunge and pitch, which are denoted respectively by h and α.

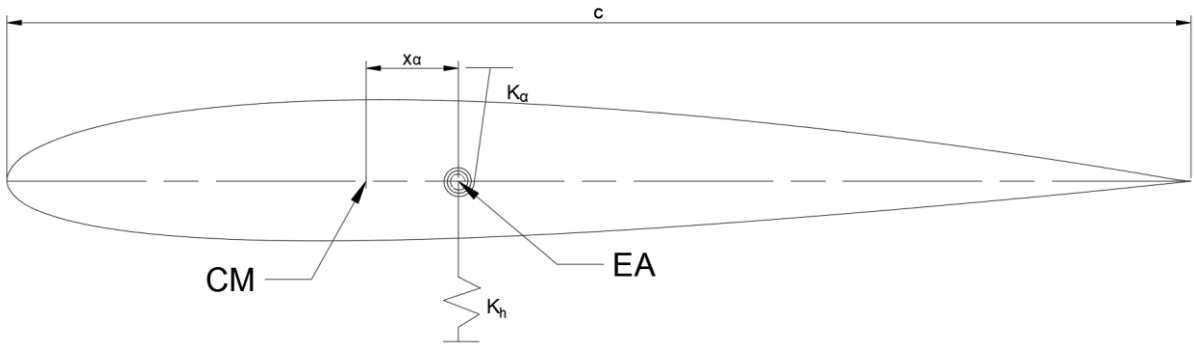

Figure 19: 2-DOF aerofoil model

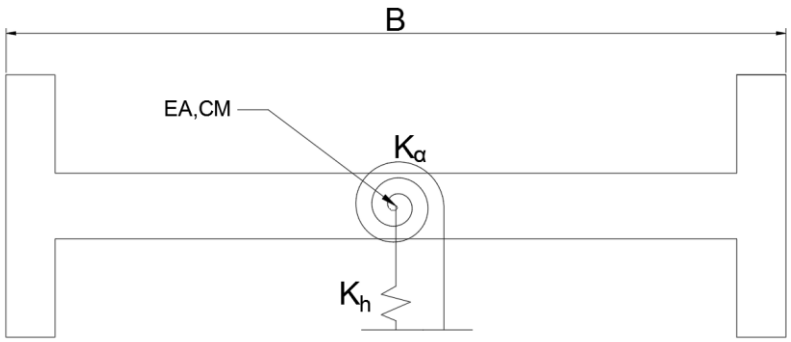

Figure 20: H-Section model for torsional flutter

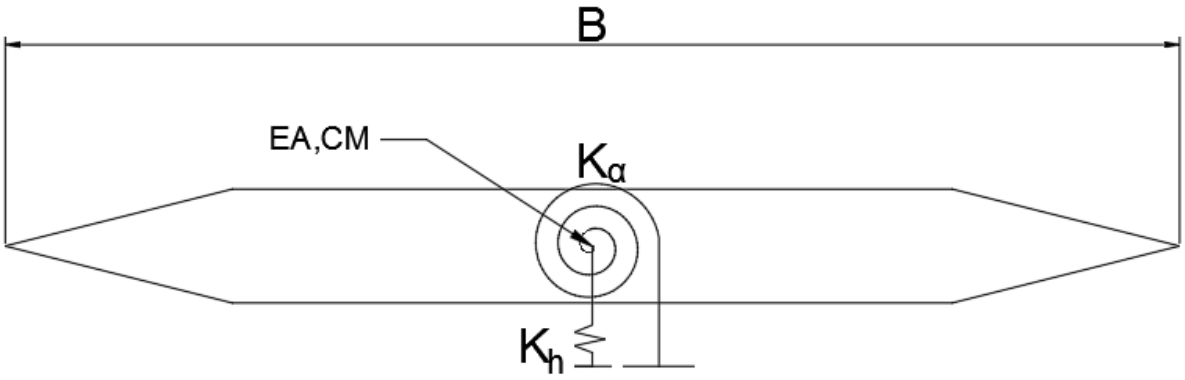

Figure 21: Streamlined deck model for classic bridge flutter

Figure 19 is an illustration of the profile for which the aerofoil flutter model will be developed. x_α denotes the distance between elastic axis and centre of mass. Figure 20 is a simple representation of the H-section used for the original Tacoma Narrows Bridge and will be used as the example for torsional bridge flutter. The streamlined deck seen in Figure 21 will be used to model classical bridge flutter.

The featured profiles have associated stiffnesses that resist bending and torsion represented by the springs K_h and K_α respectively. Similarly, while not depicted in the figures above, the models also possess intrinsic structural damping components that are denoted C_h and C_α. Other important geometrical parameters include the aerodynamic centre, elastic axis and the centre of mass. These are seen in Figure 22.

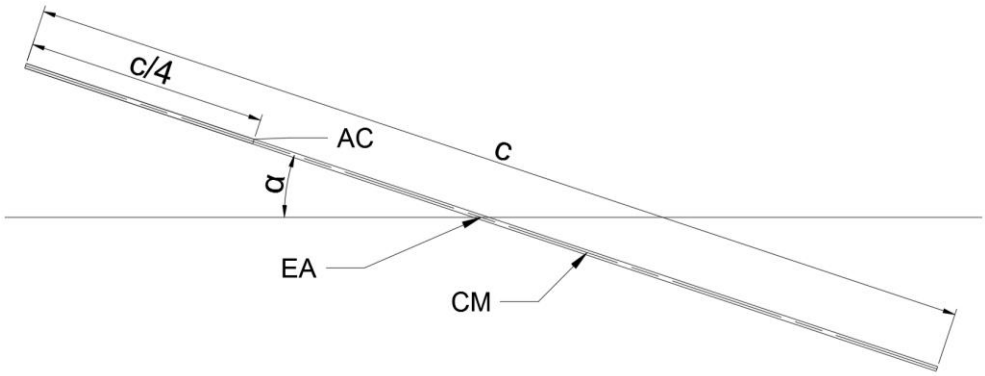

Figure 22: The geometric points of interest on an arbitrary flat plate

The elastic axis (EA) is defined in aeroelastic literature as the 'locus of shear centres of the cross sections of a beam' [4]. It is beneficial as it provides a natural reference line that assists in describing the manner in which a beam deforms elastically. In the case of a bridge section, the shear centre is a term that is synonymous with elastic axis. It is at this point where the plunge and pitch is measured rendering it essentially as the main reference point.

The centre of mass (CM), which is a common attribute of any structure or object, is the point through which the mass of a body acts. In the case of symmetrical structures, for example the two bridge sections analysed in this thesis, the centre of mass lies at the midpoint. The consequence of this is lack of a static mass unbalance that would otherwise be found in unsymmetrical structures such as an aerofoil. However, the offset between the elastic axis and the centre of mass is a structural characteristic that is pertinent in aerofoil flutter.

For the case of a two-dimensional aerofoil, the aerodynamic centre (AC) is located a quarter of the chord behind the leading edge. This location is useful as it is the point where the pitching moment does not vary with lift in the subsonic regime thus providing a means of simplification

to the analysis process. The aerodynamic centre is more important in the context of aerofoil flutter than that of bridge flutter due to the differences in aerodynamic models. With knowledge of these, the structural equations of motion can be generated.

6.4 Aerofoil Equations of Motion

The critical first step in the analysis of a dynamical structure is to describe the nature of its motion. This is achieved through the derivation of the equations of motion which can be accomplished most effectively by implementing the energy approach associated with Lagrange's Equation. Due to the approach necessitated by this method, both the potential and kinetic energy of the structure is required. The generalised coordinates that of interest are vertical plunge and rotational pitch, denoted h and α respectively. The simpler potential energy can be described as:

$$V = \frac{1}{2}K_h h^2 + \frac{1}{2}K_\alpha \alpha^2 \tag{42}$$

Formulating an expression for the kinetic energy becomes a more complex task because the displacement and rotation at the body's centre of mass is required. However, the desire is such for the flutter analysis that these are measured at the elastic axis. Therefore, it is necessary to determine how the action at the elastic axis corresponds to the behaviour of the structure at the centre of mass. Thus, the equation for the kinetic energy of the aerofoil is as follows [22] [35]:

$$T = \frac{1}{2}m\dot{h}^2 + bS_\alpha \dot{h}\dot{\alpha} + \frac{1}{2}I_\alpha \dot{\alpha}^2 \tag{43}$$

With expressions for the potential and kinetic energy, Lagrange's Equation can be employed. Recall that this equation for a particular generalised coordinate is given by:

$$\frac{d}{dt}\left(\frac{\partial T}{\partial \dot{q}_i}\right) - \frac{\partial T}{\partial q_i} + \frac{\partial V}{\partial q_i} = Q_i \tag{44}$$

Considering first the plunge generalised coordinate, this equation becomes

$$\frac{d}{dt}\left(\frac{\partial T}{\partial \dot{h}}\right) - \frac{\partial T}{\partial h} + \frac{\partial V}{\partial h} = Q_h \tag{45}$$

$$\frac{d}{dt}\left(\frac{\partial\left[\frac{1}{2}m\dot{h}^2 + bS_\alpha \dot{h}\dot{\alpha} + \frac{1}{2}I_\alpha \dot{\alpha}^2\right]}{\partial \dot{h}}\right) - \frac{\partial\left[\frac{1}{2}m\dot{h}^2 + bS_\alpha \dot{h}\dot{\alpha} + \frac{1}{2}I_\alpha \dot{\alpha}^2\right]}{\partial h} + \frac{\left[\partial \frac{1}{2}K_h h^2 + \frac{1}{2}K_\alpha \alpha^2\right]}{\partial h} = Q_h \tag{46}$$

$$m\ddot{h} + S_\alpha \ddot{\alpha} + K_h h = Q_h \tag{47}$$

Turning to the pitch generalised coordinate, a similar process can be followed to yield the corresponding equation of motion.

$$\frac{d}{dt}\left(\frac{\partial T}{\partial \dot{\alpha}}\right) - \frac{\partial T}{\partial \alpha} + \frac{\partial V}{\partial \alpha} = Q_\alpha \tag{48}$$

$$\frac{d}{dt}\left(\frac{\partial\left[\frac{1}{2}m\dot{h}^2 + bS_\alpha \dot{h}\dot{\alpha} + \frac{1}{2}I_\alpha \dot{\alpha}^2\right]}{\partial \dot{\alpha}}\right) - \frac{\partial\left[\frac{1}{2}m\dot{h}^2 + bS_\alpha \dot{h}\dot{\alpha} + \frac{1}{2}I_\alpha \dot{\alpha}^2\right]}{\partial \alpha} + \frac{\left[\partial \frac{1}{2}K_h h^2 + \frac{1}{2}K_\alpha \alpha^2\right]}{\partial \alpha} = Q_\alpha \tag{49}$$

$$S_\alpha \ddot{h} + I_{EA}\ddot{\alpha} + K_\alpha \alpha = Q_\alpha \tag{50}$$

If one assumes that there exists some structural damping, the generalised force terms in the equations of motion become:

$$Q_h = -C_h \dot{h} - L \tag{51}$$

$$Q_\alpha = -C_\alpha \dot{\alpha} + M \tag{52}$$

Therefore, substituting Equations (51) and (52) into (47) and (50) respectively, the behaviour of a two degree-of-freedom aerofoil can be described by:

$$m\ddot{h} + S_\alpha \ddot{\alpha} + C_h \dot{h} + K_h h = L \tag{53}$$

$$S_\alpha \ddot{h} + I_\alpha \ddot{\alpha} + C_\alpha \dot{\alpha} + K_\alpha \alpha = M \tag{54}$$

In (53) and (54), the term S_α is the static mass unbalance and is described as:

$$S_\alpha = mbx_\alpha \tag{55}$$

6.5 Aerofoil Aerodynamic Model

The lifting force and resulting pitching moment from Theodorsen's work were previously introduced in the theory section. Again, these are given as:

$$L = \rho\pi b^2[\ddot{h} + U\dot{\alpha} - ab\ddot{\alpha}] + 2\pi\rho UbC(k)\left[\dot{h} + U\alpha + b\left(\frac{1}{2} - a\right)\dot{\alpha}\right] \tag{56}$$

$$M = \rho\pi b^2\left[ab\ddot{h} + Ub\left(\frac{1}{2} - a\right)\dot{\alpha} - b^2\left(\frac{1}{8} + a\right)\ddot{\alpha}\right] + 2\pi\rho b^2 U\left(a + \frac{1}{2}\right)C(k)\left(\dot{h} + U\alpha + b\left(\frac{1}{2} - a\right)\dot{\alpha}\right) \tag{57}$$

Consolidating the Equations (56) and (57)with the structural equations of motion in Equations (53) and (54) yields the following numerical models for aerofoil flutter:

$$\ddot{h} + S_\alpha \ddot{\alpha} + C_h \dot{h} + m\omega_h^2 h = \rho\pi b^2[\ddot{h} + U\dot{\alpha} - ab\ddot{\alpha}] + 2\pi\rho UbC(k)\left[\dot{h} + U\alpha + b\left(\frac{1}{2} - a\right)\dot{\alpha}\right] \quad (58)$$

$$S_\alpha \ddot{h} + I_\alpha \ddot{\alpha} + C_\alpha \dot{\alpha} + I_\alpha \omega_\alpha^2 \alpha = \rho\pi b^2\left[ab\ddot{h} + Ub\left(\frac{1}{2} - a\right)\dot{\alpha} - b^2\left(\frac{1}{8} + a\right)\ddot{\alpha}\right] + 2\pi\rho b^2 U\left(a + \frac{1}{2}\right)C(k)\left(\dot{h} + U\alpha + b\left(\frac{1}{2} - a\right)\dot{\alpha}\right) \quad (59)$$

6.6 Bridge Equations of Motion

A similar process involving the use of Lagrange's Equation can be implemented in order to derive the equations of motion for a fluttering bridge deck. The equations of motion yielded from this are as follows:

$$m\ddot{h} + S_\alpha \ddot{\alpha} + C_h \dot{h} + K_h h = L \quad (60)$$

$$S_\alpha \ddot{h} + I_\alpha \ddot{\alpha} + C_\alpha \dot{\alpha} + K_\alpha \alpha = M \quad (61)$$

Based on the assumption that the bridge decks are symmetrical about the horizontal and vertical axes, there is no mass unbalance and, consequently, no need for the static imbalance term, S_α, in Equations (60) and (61) above. Subsequently, these become:

$$m\ddot{h} + C_h \dot{h} + K_h h = L \quad (62)$$

$$I_\alpha \ddot{\alpha} + C_\alpha \dot{\alpha} + K_\alpha \alpha = M \quad (63)$$

6.7 Bridge Aerodynamic Model

As was carried out for the aerofoil, the aerodynamic model for bridge flutter outlined previously can be reintroduced here:

$$L = \frac{1}{2}\rho U^2 B\left[kH_1^*\frac{\dot{h}}{U} + kH_2^*\frac{B\dot{\alpha}}{U} + k^2 H_3^*\alpha\right] \quad (64)$$

$$M = \frac{1}{2}\rho U^2 B^2\left[kA_1^*\frac{\dot{h}}{U} + kA_2^*\frac{B\dot{\alpha}}{U} + k^2 A_3^*\alpha\right] \quad (65)$$

Consolidating the structural model in (62) and (63) with the aerodynamic model in (64) and (65) yields:

$$m\ddot{h} + C_h \dot{h} + K_h h = \frac{1}{2}\rho U^2 B\left[kH_1^*\frac{\dot{h}}{U} + kH_2^*\frac{B\dot{\alpha}}{U} + k^2 H_3^*\alpha\right] \quad (66)$$

$$I_\alpha \ddot{\alpha} + C_\alpha \dot{\alpha} + K_\alpha \alpha = \frac{1}{2}\rho U^2 B^2\left[kA_1^*\frac{\dot{h}}{U} + kA_2^*\frac{B\dot{\alpha}}{U} + k^2 A_3^*\alpha\right] \quad (67)$$

Taking the mass terms as a common factor on the LHS of (66) and (67) allows for the simplification of the model in the following way:

$$\ddot{h} + 2\xi_h\omega_h\dot{h} + \omega_h^2 h = \frac{\rho U^2 B}{2m}\left[kH_1^*\frac{\dot{h}}{U} + kH_2^*\frac{B\dot{\alpha}}{U} + k^2H_3^*\alpha\right] \quad (68)$$

$$\ddot{\alpha} + 2\xi_\alpha\omega_\alpha\dot{\alpha} + \omega_\alpha^2\alpha = \frac{\rho U^2 B^2}{2I_\alpha}\left[kA_1^*\frac{\dot{h}}{U} + kA_2^*\frac{B\dot{\alpha}}{U} + k^2A_3^*\alpha\right] \quad (69)$$

The processes adopted to formulate the respective flutter models for the aerofoil and bridge are an illustration of some of the similarities and differences that exist between the two contexts. It should be noted that bridge numerical model established in Equations (68) and (69) is applicable to both forms of bridge flutter discussed in this thesis. That is, the torsional bridge flutter exhibited by the Tacoma Narrows bridge, despite the nature of oscillations being one degree of freedom, can be represented by the model. This is a result of the empirical flutter derivatives which enable the physical motion of the particular case of flutter to be captured. It is also worth noting that the lack of a mass unbalance means that inertial coupling cannot occur. Instead, aerodynamic coupling is to blame for the onset of flutter when this is the case.

6.7.1 Aerodynamic Database

The numerical model developed for the flutter of a bridge is not unique to the geometries of interest to this thesis. Rather, it can be employed in the context of any bridge section. The distinguishing feature of the specific bridge decks are the flutter derivatives that are used to linearise the inherently non-linear phenomenon of bridge flutter.

As previously stated, it was the experimental work of Scanlan and Tomko in the 1970's that yielded these flutter derivatives for a vast array of bridge sections. The summarised findings of these experiments are presented in a number of plots that provided a graphical representation of the flutter derivatives. The plots corresponding to the decks focused on in this study have been included in Appendix A. These plots express the flutter derivatives in terms of the reduced velocity, which is the inverse of reduced frequency.

The bridge flutter analysis that will be conducted necessitated the extraction of the relevant derivatives. Subsequently, an aerodynamic database of sorts has been generated in an effort to achieve this. In this form, the flutter derivatives are capable of being utilised in the identification of the flutter boundary. This aerodynamic database is in tabular form and can be viewed in Appendix B.

6.8 Dynamic Stall Model

The non-linear nature of stall flutter differentiates itself from the classical aerofoil flutter model developed in 0. Due to the complexity involved with the non-linear behaviour there has been several models proposed. Similarly, the various applications in which stall flutter has pervaded has seen the development of models suited to these. In this section, two of stall flutter models will be presented and discussed.

While the structural elements of the equations of motion remain the same for stall and classical flutter, it is the aerodynamic model that requires modification so that the flow separation is somewhat accounted for. Classical flutter theories are not equipped to predict the onset of stall flutter due to the lack of a non-linear force prediction capability. Consequently, it is common for computational fluid dynamic models to be employed in order to simulate stall flutter. Alternatively, semi-empirical dynamic stall models have been introduced to the traditional flutter models as a means of representing the aerodynamics associated with stall flutter.

6.8.1 Beddoes-Leishman Model

The Beddoes-Leishman Model is an example of the aforementioned semi-empirical models for dynamic stall. Arguably the most established and most utilised dynamic stall model, the Beddoes-Leishman Model was originally used to evaluate the loads on helicopter blades [24]. The model that was proposed is comprised four modules which form an open-loop system whereby the input for a module stems from the output of the one previous [24]. These subsystems are as follows:

- A model of the attached flow accounting for the linear, unsteady aerodynamic forces
- A model of the separated flow accounting for the non-linear aerodynamic forces
- A model indicative of the onset of dynamic stall
- A model of dynamic stall accounting for the vortex induced aerodynamic forces

The model describing the attached flow is generated using compressible indicial response functions that consist of the circulatory and non-circulatory elements. In order to compute the total attached flow lift force, the circulatory and non-circulatory terms are summed similar to that in the classical flutter model based on Theodorsen's work. The aerodynamic implications of the flow separating are accounted for by calculating a dynamic equivalent point of separation using the theory of Kirchhoff and Helmholtz in conjunction with previous angle of attacks.

There are several drawbacks that are associated with the Beddoes-Leishmann dynamic stall model. The most notable of these is the requirement for a substantial amount of empirical data

and implementation of this method can be a tedious process. Furthermore, the Beddoes-Leishmann method incorporates the effects of compressibility which is unnecessary in regards to this present study and many applications of stall flutter. The Beddoes-Leishmann model has provided the basis for the conception of many other dynamic stall models in the ensuing years.

6.8.2 ONERA Method

The second dynamic stall model that will be discussed is referred to as the ONERA model. Its foundation lies on the implementation of a set of ordinary differential equations (ODEs) to describe the unsteady aerofoil behaviour associated with dynamic stall. Like so many of the dynamic stall models, the ONERA method was originally developed for the application to helicopters [24]. However, in recent times it has been utilised to model the behaviour of many different structures experiencing dynamic stall.

The aforementioned set of ordinary differential equations consists of two equations of which one is used to describe the linear aerodynamics of the unsteady free stream and the other addresses the non-linear effects of flow separation [45]. The aerodynamic loads are yielded from this method through the summation of the linear and non-linear ODEs as follows:

$$c_{l,dynamic} = c_{l,1} + c_{l,2} \tag{70}$$

The linear differential equation is described as:

$$\dot{c}_{l,1} + \lambda_L c_{l,1} = \lambda_L c_{l,pot} + (\lambda_L s_L + \sigma_L)\dot{\alpha} + s_L \ddot{\alpha} \tag{71}$$

The non-linear differential is described as:

$$\ddot{c}_{l,2} + a_L \dot{c}_{l,2} + r_L c_{l,2} = -(r_L \Delta c_l + e_L \dot{\Delta} c_l) \tag{72}$$

The differentiation of those respective terms has been done so with respect to a non-dimensional time. Of particular interest in Equations (71) and (72) is the loss of lift term denoted by Δc_l. The parameters and their definitions have been tabulated as a means of easy explanation.

$c_{l,1}$	Linear lift coefficient	$c_{l,2}$	Non-linear lift coefficient
$c_{l,pot}$	Extrapolation of the static lift curve	a_L	Aerofoil dependent coefficient
λ_L	From unsteady experimental data	r_L	Aerofoil dependent coefficient
s_L	From unsteady experimental data	Δc_l	Loss of lift
σ_L	From unsteady experimental data	e_L	Aerofoil dependent coefficient
$\dot{\alpha}$	First time derivative of angle of attack	$\ddot{\alpha}$	Second time derivative for angle of attack

The geometrical dependency of several of the parameters outlined above is obvious. A main advantage of the ONERA model is its compatibility with typical structural equations of motion owing to its ordinary differential equation format. However, an inhibiting factor of the ONERA model in many applications is the underlying assumptions upon which it is formulated and the substantial coefficients that are required [24].

6.9 Model Comparison

Having developed numerical models for classical aerofoil, bridge and torsional bridge flutter, as well as engaging in a qualitative discussion of two pertinent dynamic stall models, it is an appropriate time to draw comparisons. Firstly, the structural equations of motion for the classical aerofoil model and the two bridge models are seen to be largely the same. The absence of a static unbalance term in the bridge model is attributed to the section being treated as symmetrical around the midline. Thus, there does not exist an offset between the elastic axis and the centre of mass. The implication of this is that there does not exist a term that indicates inertial coupling in the bridge models. As this is the case, it would appear at first that classical flutter is unable to manifest in the bridge context. This is untrue as aerodynamic coupling can contribute to a bridge deck incurring classical flutter.

Secondly, it can be observed that the structural damping is accounted for in the bridge model but not in the aerofoil one. This is in accordance with common practices outlined in literature whereby the structural damping of the wing is not typically considered in the flutter analysis. An explanation for this is the structural damping of a typical wing is negligible unlike that of a bridge.

Another difference in the development of the models is aerodynamic models used. It was previously noted from the theory chapters that the primary point of divergence between the flutter of wings and bridges stemmed from the aerodynamic behaviour. This was reiterated in the model development process. The case of the classical aerofoil flutter and the use of Theodorsen's theory renders it as the only type where a wholly analytical model is achievable. The models employed for bridge flutter rely upon empirical data as do the stall flutter models presented here.

7 Simulations

The purpose of the simulation component presented here is to identify the cross-discipline similarities of flutter in a numerical fashion. A logical and effective way in which to achieve this is to consider the structural and fluid dynamics aspects of flutter. In doing so, comparisons can be made to observe for notable similarities and differences between the different types

This chapter is concerned with the methodology involved with the numerical and CFD simulations of the various systems that are of interest to this study. Initially, the mathematical formulation of the solution methods for the prediction of the flutter boundary will be outlined. This will lead into a brief overview of the MATLAB code that has been constructed to execute the solution processes. Validation of the MATLAB code will follow whereby flutter case studies from literature will be evaluated. Upon completion of this task, and with confidence in the solution process, simulation methodology for the structural parameter dependency study will be outlined. Finally, the methodology in regards to the CFD simulations will be discussed.

7.1 Aerofoil Flutter Solution Process

Since Theodorsen first proposed a reliable solution to the problem of an oscillating aerofoil, many other solution techniques have been developed and utilised. Furthermore, the advancement in computing capabilities in the last few decades has also provided alternative forms of analysis in the mould of CFD solvers and finite element packages. However, given the nature of this study, the original solution method outlined by Theodorsen for the analysis of classical flutter is the most suitable. This process is advantageous in that it is implementable for both the case of aerofoil and bridge flutter.

The general procedure for the classical flutter analysis is explained well in [22] and [35]. The presumption that harmonic motion is predominant at the flutter boundary provides a solution to the flutter problem.

$$h = h_0 e^{i\omega t} \qquad \alpha = \alpha_0 e^{i\omega t} \tag{73}$$

With the solution of this form, the time derivatives present in the flutter model can be expressed in the form of the initial displacement. This is the premise of harmonic motion as alluded to in

4.2.4 and allows for the grouping of like terms in the two equations. This process can be seen in Appendix C.

The ultimate product from Theodorsen's solution for the aerofoil is the flutter determinant which is comprised of the non-dimensional variants of the flutter model. These non-dimensional parameters include:

$$\mu = \frac{m}{\rho \pi b^2} \quad (74)$$

$$r^2 = \frac{I_\alpha}{mb^2} \quad (75)$$

$$\sigma = \frac{\omega_h}{\omega_\alpha} \quad (76)$$

$$x_\alpha = \frac{S}{mb} \quad (77)$$

With the harmonic solution introduced, like terms are grouped. The real and imaginary components of each group of terms is separated and denoted as individual coefficients [22]. For convenience, these have been provided in Appendix D.

These components can then be used to formulate the constituents flutter determinant to produce the following [22]:

$$A = A_R + iA_i + \mu\sigma^2 X_A \quad (78)$$

$$B = B_R + iB_I \quad (79)$$

$$D = D_R + iD_I \quad (80)$$

$$E = E_R + iE_i + \mu r^2 X_A \quad (81)$$

The unknown in these equations, X_A, is the frequency ratio at the flutter boundary and is defined as:

$$X_A = \frac{\omega_\alpha}{\omega} \quad (82)$$

The flutter determinant is then established using Equations (78) to (81) and inputting them as the elements of a 4 × 4 matrix:

$$\begin{vmatrix} A & D \\ B & E \end{vmatrix} = \begin{vmatrix} A_R + iA_i + \mu\sigma^2 X_A & D_R + iD_I \\ B_R + iB_I & E_R + iE_i + \mu r^2 X_A \end{vmatrix} \quad (83)$$

The non-trivial solution of the determinant is found by equating it to zero which yields a quadratic equation in terms of X_A. Since the unsteady aerodynamics model is formulated in the frequency domain, this quadratic will be complex in nature. Thus, it will possess both real and imaginary parts which can be used to group terms accordingly to form two equations. These are seen to be the following:

$$\mu^2 r^2 \sigma^2 X_A^2 + (A_R r^2 + E_R \sigma^2)\mu X_A + (A_R E_R - E_R E_I - D_R B_R + D_I B_I) = 0 \quad (84)$$

$$(A_I r^2 + E_I \sigma^2)\mu X_A + (A_R E_I - A_I E_R - D_R B_I - D_I B_R) = 0 \quad (85)$$

Solving the equations for X_A, a plot can be generated that depicts the square root X_A on the y-axis and the inverse of the reduced frequency on the x-axis. The point of interest is where one of the real curves intersects the imaginary curve. The coordinates of this point can be used to compute the critical flutter velocity and flutter frequency for the system. An enticing feature of this solution method, as opposed to those that are more recent and widely used, is the ability for it to be effectively implemented for bridge flutter also.

7.2 Bridge Flutter Solution Process

This solution process for bridge flutter does draw parallels with the aerofoil solution. However, a number of nuisances are pivotal in discerning two. As was the case before, this process depends upon the response at the flutter boundary being one of harmonic motion so that a solution can be implemented. The extensive numerical formulation for the bridge flutter solution has been included in Appendix E. From the solution process, the following is yielded:

$$\begin{bmatrix} \left[(-X_B^2 + 1) + \left(2\xi_h X_B - \frac{\rho B^2}{2m} X_B^2 H_1^*\right) i\right] & -\left[\frac{\rho B^2}{2m} X_B^2 H_3^* + \left(\frac{\rho B^2}{2m} X_B^2 H_2^*\right) i\right] \\ \left[-\left(\frac{\rho B^4}{2I} X_B^2 A_1^*\right) i\right] & \left[\left(-X^2 - \frac{\rho B^2}{2I} X_B^2 A_3^* + \frac{\omega_\alpha^2}{\omega_h^2}\right) + \left(2\xi_\alpha \frac{\omega_\alpha}{\omega_h} - \frac{\rho B^4}{2I} X_B A_2^*\right) i\right] \end{bmatrix} \quad (86)$$

In this instance, the variable in (86) is described as:

$$X_B = \frac{\omega}{\omega_h} \quad (87)$$

The matrix depicted in (86) can be seen, in essence, to be quite similar to the aerofoil flutter determinant in (83) without the use of simplifying coefficients. In calculating the determinant of the matrix, the real and imaginary components of each of the elements are grouped together [46]. Doing so yields two equations in which coefficients can be introduced for convenience [43]. Taking the real parts first, the corresponding equation produced is:

$$R_4 X_B^4 + R_3 X_B^3 + R_2 X_B^2 + R_1 X_B + R_0 = 0 \quad (88)$$

Where R_i are the coefficients used to represent the groups of terms corresponding to each order of the unknown value. In a similar fashion, the imaginary components, termed as I_i, can be grouped together to generate the second equation in the form of:

$$I_3 X_B^3 + I_2 X_B^2 + I_1 X_B + I_0 = 0 \quad (89)$$

The formulas for the coefficients featured in Equations (88) and (89) can be seen in Appendix F. From here, the unknown X_B in (88) and (89) is solved for a range of reduced velocities, which is recalled as being the inverse of the reduced frequency, and the plots generated on a single graph. It can be seen that the two equations are of the fourth and third order and therefore must yield four and three roots respectively. However, only the positive roots will be considered which ensures the real equation produce only two useful roots and the imaginary equation produce one. From here, similar to the aerofoil process, the point of interest is where one of the real equations intersects with an imaginary root.

7.3 Flutter Boundary Prediction Code

Three separate MATLAB codes have been generated, each of which pertain to a type of flutter being analysed. In the MATLAB code for the classical aerofoil flutter, a list of reduced frequency values was generated that ranged from 0.1 to 1. This list was used as the range for a *for-loop* in which the corresponding value for Theodorsen's Function was calculated and separated into the real and imaginary components. These were then utilised to generate the four elements of the flutter determinant from Equation (83) which was subsequently equated to zero and solved to produce a quadratic equation.

In this form, the in-built MATLAB solve function was executed to produce the two real roots and a one imaginary roots of which the square roots of both was calculated. This process was performed for each reduced frequency value and the resulting real and imaginary roots were stored in a list. Plots were generated which featured the inverse of each reduced frequency value, which is the reduced velocity, on the x-axis.

A similar code was generated for the bridge flutter cases with consideration given to the various differences that were alluded to in the solution formulation. A *for-loop* was initiated that executed the program for a range of reduced velocity values. The aerodynamic database in Appendix B was utilised to call upon the specific flutter derivatives that corresponded to each individual reduced velocity value. The real and imaginary coefficients outlined previously were assembled and the corresponding equations formed. Having all the necessary components, the

real and imaginary equations were solved and the results stored in list form. Once more, plots were generated for each of the real and imaginary solutions.

As a whole the different codes are alike in essence as a result of the similar solution process upon which they are based. Individual codes are necessitated by the minor alterations between the aerofoil and bridge models. The MATLAB codes for each individual flutter boundary prediction have been provided in Appendix G.

7.4 Aerofoil Validation

In order to show that the process implemented in the MATLAB code for the aerofoil flutter analysis produces reasonable and accurate results, a case from literature [35] was used for the purpose of validation. The non-dimensional parameters that this case was based upon have been compiled in Table 3.

Table 3: Parameters for aerofoil validation

Non-Dimensional Parameter	Value
x_α	$1/10$
a	$-1/5$
μ	20
r	$\sqrt{6/25}$
σ	$2/5$

In literature, the solution to this validation example is obtained using the p-k method which determines the critical flutter speed at the point where the damping changes signs. From this solution, the critical speed and flutter frequency were deemed to be:

$$U_F = 2.170 b\omega_\alpha \qquad \omega_F = 0.6443\omega_\alpha$$

The parameters outlined in Table 3 above were implemented in the MATLAB code devised here for the aerofoil flutter analysis. The subsequent plot that was generated is depicted in Figure 23 below.

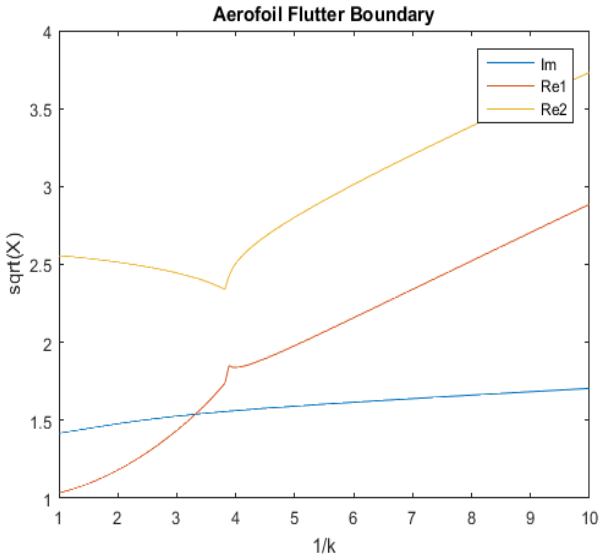

Figure 23: Validation plot for the aerofoil solution process

The intersection point of the imaginary curve and the first real curve can be seen to occur at $1/k = 3.314$ and $\sqrt{X} = 1.539$. These can be used to evaluate the flutter frequency and critical velocity via the following relations:

$$\omega_F = \frac{\omega_\alpha}{\sqrt{X_A}} \qquad U_F = \frac{\omega_\alpha b}{k\sqrt{X_A}} \qquad (90)$$

$$\omega_F = 0.650\omega_\alpha \qquad U_F = 2.15\omega_\alpha b$$

Tabulating these results allows for comparison with those results previously presented from literature.

Table 4: Comparison of results for validation purposes

	Theodorsen's Method	Validation Case	Difference (%)
Flutter Frequency	$0.650\omega_\alpha$	$0.6443\omega_\alpha$	0.88
Critical Speed	$2.15\omega_\alpha b$	$2.170b\omega_\alpha$	0.926

The differences recorded in Table 4 are quite small, both less than 1%. This suggests that the solution process implemented in the MATLAB code is capable of ascertaining the flutter boundary with a high degree of accuracy.

7.5 Bridge Deck Validation

Similarly, a validation case was sourced from literature in order to legitimise the results produced by the bridge flutter solution process. The bridge deck featured in this example is geometrically similar to that of the bridge deck used to illustrate classical flutter in this study. The physical parameters in this instance have been obtained from [27] and can be seen in the following table.

Table 5: Parameters for bridge validation

Parameter	Value	Units
Width	31	m
Mass	23687	kg/m
Mass Moment of Inertia	2.501×10^6	$kg\ m^2/m$
Bending Natural Frequency	0.622	rad/s
Torsional Natural Frequency	1.709	rad/s
Bending Damping Ratio	0.001	–
Torsion Damping Ratio	0.001	–

Using the MATLAB code developed for the streamlined deck, a plot was produced and can be seen below in Figure 24. Again, the point of interest is the location where the imaginary and one of the real curves intersect.

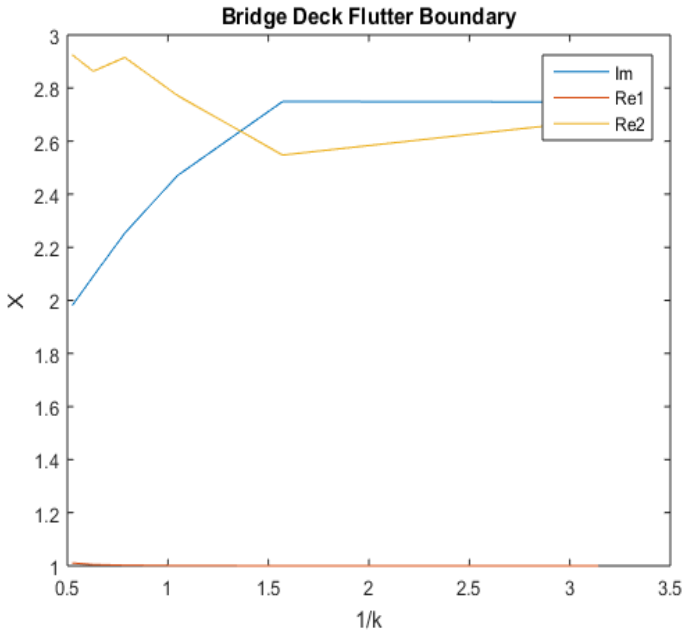

Figure 24: Validation plot for the bridge solution process

Figure 24 indicates that the intersection point occurs approximately at $1/k = 1.3610$ and $X = 2.6375$. With these coordinates, the critical velocity can be calculated in the following manner:

$$U_F = \frac{B\omega_h X_B}{k} \tag{91}$$

Performing this calculation yields a flutter velocity of $69.213\ m/s$. Comparing these results with those from literature offers an illustration of the reliability of the current solution process.

Table 6: Comparison of results from literature

Source	Flutter Velocity (m/s)
Present Work	69.213
CFD [27]	63-65
Wind Tunnel [27]	74

While there is some discrepancy in the results, the critical flutter speed that was produced in this study falls within the theoretical and experimental results of the validating case. The difference between the results can be attributed to the sensitivity of each method.

There are a number of noteworthy attributes that differ between the plots produced by the aerofoil and bridge solution methods. Due to the intricacies involved in the formulation of the respective solutions, the y-axis depicts different versions of X. In regards to the aerofoil solution, the y-axis is representative of $\sqrt{X_A}$ while in the instance of the bridge solution it is just X_B.

Another point of difference is evident when considering the aerodynamic components of each process. For the aerofoil, the reduced frequency is assumed *a priori* and thus, there can be an infinite number of reduced frequencies over which the process can be evaluated. Conversely, the flutter derivatives for the bridge analysis are experimentally obtained and, as such, there is only a limited range of integer-based reduced velocities that can be assessed.

7.6 Structural Parameters for Test Cases

The validation processes that have been performed here, concerning the flutter analysis for both the aerofoil and bridge deck, have established the capability of the respective solution methods. This enables the application of these methods to the test cases that have been formulated for this study. For the aerofoil, the parameters have been sourced from a case study that is commonly used for the purpose of flutter analysis [47] [48].

For the bridge cases, the streamlined deck is treated as having a width of 31 metres and the H-section a width of 11.9 metres. This is done so that they correspond to real world examples, those specifically being the Great Belt East Bridge and the Tacoma Narrows Bridge respectively. However, these are the only attributes that are translated from a real world context to this theoretical study. The other structural parameters have been tailored so that they produce identical non-dimensional parameters as each other and the aerofoil case. The reason for this is

to allow a normalised field for effective comparison of flutter results. Table 7 and Table 8 feature the structural parameters for the various cases.

Table 7: Dimensional structural parameters

Parameter	Units	Aerofoil	Streamlined	H-Section
Chord/Width	m	0.236	31	11.9
Mass	kg	0.739	51037.387	7520.712
Elastic Axis	m	0.04838	15.5	5.95
Moment of Inertia	$kg\ m^2$	0.0262	4414223.643	95850.725
Bending Natural Frequency	rad/s	34.6	0.622	0.622
Torsional Natural Frequency	rad/s	88	1.583	1.583
Bending Damping Ratio	-	0	0.001	0.001
Torsional Damping Ratio	-	0	0.001	0.001

Table 8: Non-dimensional structural parameters

Parameter	Aerofoil	Streamlined	H-Section
μ	13.8	13.8	13.8
x_α	0.15	0	0
a	-0.41	1	1
r	0.09	0.09	0.09
σ	0.393	0.393	0.393

7.7 Parametric Study

In order to ascertain the implications of various structural parameters on the flutter boundary, a number of simulations were run where selected properties were varied. These parameters include the pitch and plunge natural frequencies and the mass and mass moment of inertia. The geometrical features of the structures were not varied as the experimentally obtained flutter derivatives in the case of the bridge decks are based on a set width.

The first parameter varied was the torsional natural frequency of each structure. Following this, the same process was carried out for the bending natural frequency. For both of these

simulations, the normalised frequency ratio resulting from the varying frequencies was also calculated and employed as the dependent variable for the flutter boundary. This was necessary as it enabled comparisons of the results for the three flutter cases that possessed significantly different natural frequencies.

The flutter boundary was also simulated for varying mass properties of the system. It was noted that in changing the mass of the system, it is unrealistic to assume that the mass moment of inertia remains the same. Therefore, in altering the structural mass, the normalised parameter represented by the radius of gyration was held constant and the mass moment of inertia computed accordingly. However, a similar course of action was not applied for the natural frequencies or damping coefficients of the system. Rather, these were treated as being immune to any mass properties alteration and were subsequently held constant.

7.8 CFD Simulations

As has been discussed in the theory chapters, a fundamental point of difference between the flutter of a wing and that of a bridge is the manner in which fluid-structure interaction occurs. Given the significance of this, a range of CFD simulations were performed to illustrate the difference in fluid flow over the respective structures. It must be noted that the intention of these simulations was not to model flutter but rather demonstrate the implications of the profile geometry on the behaviour of the fluid flow.

These simulations were performed with the free-stream velocity set at 20 m/s. Initially, the structures were positioned so that the angle of attack was zero. For each simulation, a change in angle of attack of the structure was enforced by calculating the corresponding x- and y-components of the free-stream velocity. The respective meshes were generated in *OpenFoam* and the flow solution produced using the *simpleFoam* solver. The scripts used to generate each of the structures have been provided in Appendix H. Due to the flow separation that is associated with the different types of flutter, a turbulence model was necessitated. The Spalart-Allmaras model was employed due to its familiarity and economical computation of boundary layers in external flow [49].

8 Results and Discussions

The purpose of this chapter is to firstly present the results obtained from the numerical investigation that has been conducted. These results will allow for an ensuing interpretation and discussion of their meaning and significance. From this, it is desired that meaningful quantifiable comparisons of flutter in the various contexts can be made.

8.1 Flutter Boundary Estimation

Undoubtedly, the most effective means of comparison between the various types of flutter is the velocity at which the flutter boundary exists. With this in mind, the results produced by the first numerical analysis include the reduced velocity and frequency ratio at the flutter boundary.

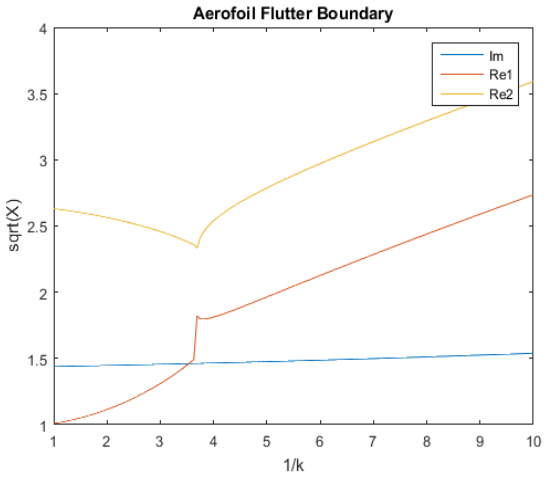

Figure 25: The aerofoil flutter boundary

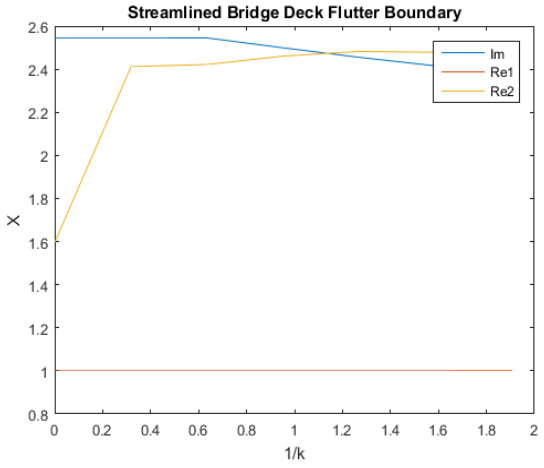

Figure 26: The streamlined deck flutter boundary

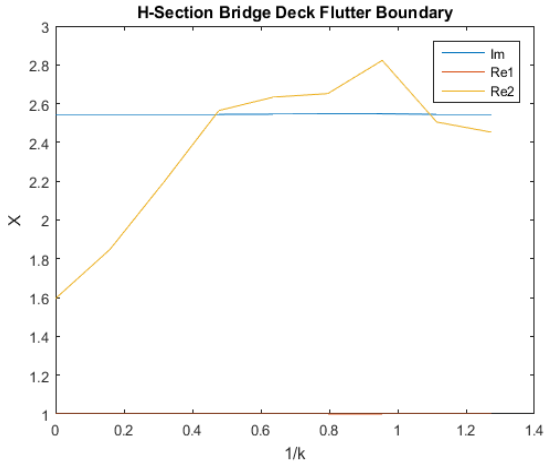

Figure 27: The H-section deck flutter boundary

Thus, the coordinates at the point of intersection have been extracted and tabulated as follows.

Table 9: Results from the flutter boundary analysis

Flutter Boundary Characteristic	Aerofoil	Streamlined	H-section
Reduced Velocity $(1/k)$	3.5353	0.9321	0.4132
Flutter Frequency Ratio (X)	2.1348	2.4753	2.5446

Using the reduced velocity values above, an initial comparison can be completed. It is advantageous to use this non-dimensional velocity as it allows for comparison between structures that possess vastly different properties. Recalling that the reduced velocity is the reciprocal of the reduced frequency, it can be quantitatively described, at the flutter boundary, for the aerofoil and bridge deck respectively as:

$$\left(\frac{1}{k}\right)_A = \frac{U_f}{b\omega_F} \qquad \left(\frac{1}{k}\right)_B = \frac{U_f}{B\omega_F} \qquad (92)$$

From the results in Table 9, an ordering of flutter boundaries for the different structures can be observed. It is worth noting that a higher flutter boundary corresponds to a higher critical velocity necessary to initiate flutter. The results indicate that the aerofoil has the highest flutter boundary. The streamlined bridge deck was deemed to have a flutter boundary at a reduced velocity of 1.0947 which rendered it as the second highest. The lowest flutter boundary was that of the H-section bridge deck.

Similarly, the frequency ratio results also offer an indication of how the flutter characteristics of the different structures compare. In this instance, the frequency ratio for the aerofoil is the smallest while that of the H-section is the largest. Hence, it appears that for a higher reduced velocity at the flutter boundary the flutter frequency ratio is smaller. From this preliminary numerical investigation, it has been established that the H-section bridge deck, renowned for the torsional flutter oscillations that it exhibits, has the lowest flutter boundary in terms of critical velocity. Meanwhile, results portray the aerofoil as the structure with the highest flutter boundary.

The two flutter boundary characteristics obtained in the preliminary analysis can be collaborated to give an indication of the flutter velocity. This is achieved in conjunction with Equations (90) and (91). The results have been compiled in Table 10.

Table 10: Comparison of the flutter velocities

	Aerofoil	Streamlined Deck	H-section Deck
Normalised Velocity	$2.4196(b\omega_\alpha)$	$2.3072(B\omega_h)$	$1.0514(B\omega_h)$
Velocity (m/s)	25.125	44.487	7.782

The results depicted above further indicate that the velocity at the flutter boundary for the H-section deck is significantly lower than the other two structures. Initial observations would suggest that the wind velocity required for the onset of flutter in the case of the H-section is unrealistically low. This is true, however several comments can be made to support the value that has been yielded. Firstly, the wind speed that initiated the torsional flutter that destroyed the Tacoma Narrows Bridge was recorded at 64 km/hr or 17.78 m/s. So initially it can be seen that the torsional flutter does not require substantially high velocities in order to occur. Secondly, the lower velocity here is a result of the tailored structural parameters that have been utilised in this study. Parameters such as the modal natural frequencies, damping ratios and mass properties were less than those of the Tacoma Narrows Bridge.

Thus, while velocity for the H-section deck is low it is valid. Furthermore, it illustrates the clear difference in the velocity necessary for the two types of flutter. It can be inferred from this initial flutter analysis that torsional flutter is likely to occur earlier than that of the classical form. The effect of various structural properties on this flutter boundary will be alluded to in the results of the parametric study featured in the proceeding chapter.

8.2 Parametric Study Results

The results featured in this section relate to the investigation that was conducted in an effort to understand the influence that various structural parameters have on the flutter boundary. The individual plots that were generated for each of the structures have been included in Appendix I. With these results, a comparison of the structural characteristics of the three types of flutter was engaged. The intention of this was to examine the role that the structural aspects play in the various types of flutter and, in doing so, identify the similarities and differences that exist. To put the implications of the different parameter variations into perspective, the flutter boundary characteristics were plotted against the pertinent normalised structural parameters. This was first done for the torsional natural frequency.

8.2.1 Torsional Natural Frequency

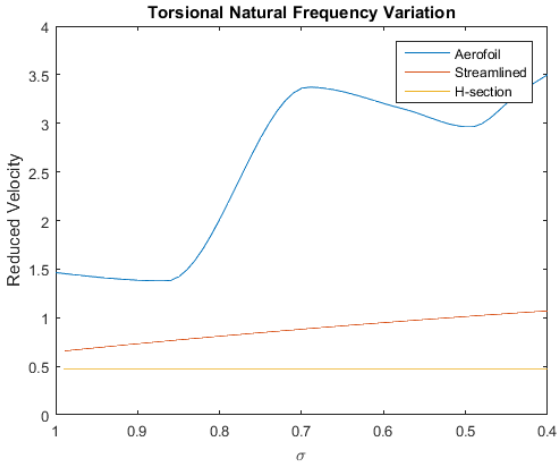

Figure 28: Comparison of the torsional natural frequency effect on reduced velocity

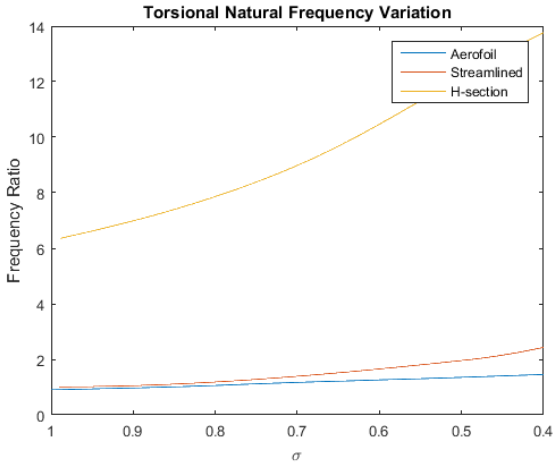

Figure 29: Comparison of the torsional natural frequency effect on frequency ratio

The plots in Figure 28 and Figure 29 show the impact that the non-dimensional frequency parameter, σ, has on the flutter boundary. Recalling that this parameter is defined as the ratio between the bending natural frequency and the torsional natural frequency offers a preliminary explanation as to why both the reduced velocity and flutter frequency ratio behaves the way they do. By definition, as the torsional natural frequency is made larger, the non-dimensional frequency ratio decreases accordingly which is reflected by the x-axis of both Figure 28 and Figure 29.

In general, all three of the cases responded in a positive manner to the increase in torsional frequency. Figure 28 shows that the reduced velocity at the flutter boundary increases noticeably for the aerofoil and streamlined deck. While the trend of the aerofoil curve is irregular, generally it follows an upward path. There appears to be little variation in the H-section reduced velocity however the increase that it shows in regards to the frequency ratio in Figure 29 is substantial. Similarly, for the aerofoil and streamlined deck, the frequency ratio becomes larger as the torsional natural frequency is increased.

8.2.2 Bending Natural Frequency

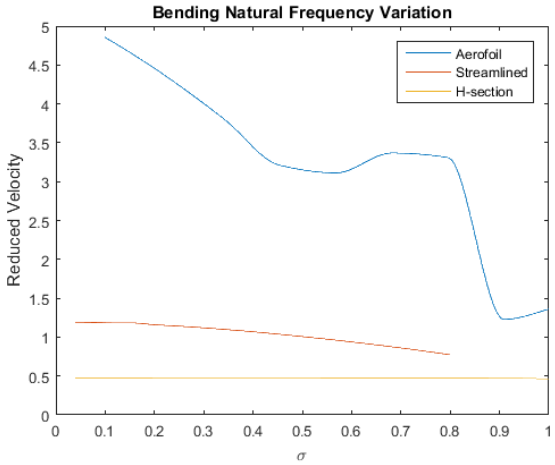

Figure 30: Comparison of the bending natural frequency effect on reduced velocity

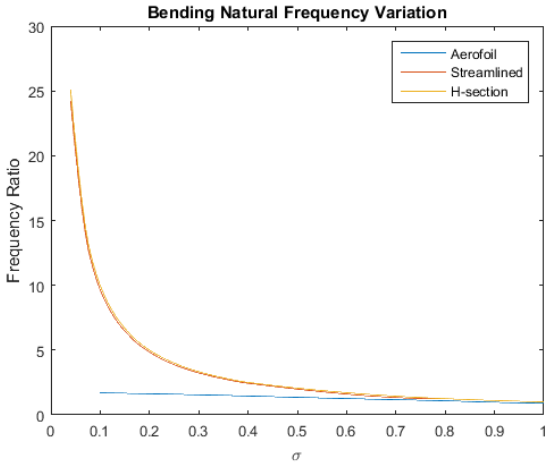

Figure 31: Comparison of the bending natural frequency effect on frequency ratio

The figures above are concerned with the effects of a changing bending natural frequency. Considering the non-dimensional frequency parameter once more, it is recognised that, for a rising bending natural frequency, this parameter will become larger. Thus, the x-axis scale in both Figure 30 and Figure 31 is that of a gradually increasing non-dimensional frequency.

Figure 30 shows that higher bending natural frequency induces flutter at a lower reduced velocity for the aerofoil and streamlined deck. As was the case for the torsional natural frequency variation, the reduced frequency of the H-section changed a negligible amount. The frequency ratio of the two bridge cases is influenced most significantly by the bending natural frequency. This is attributed to the fact that the frequency ratio at the flutter boundary in the context of the bridges is defined as being inversely proportional to the bending natural frequency. The frequency ratio at the aerofoil flutter boundary decreased minimally, if at all, with a rising bending natural frequency. Thus, in this regard, there is a noticeable difference between the influence of torsional natural frequency and bending natural frequency with the two having polar effects on the flutter boundaries.

8.2.3 Mass Properties

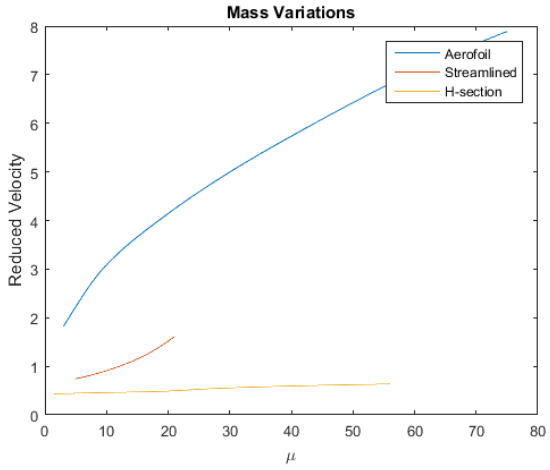

Figure 32: Comparison of mass effect on reduced velocity

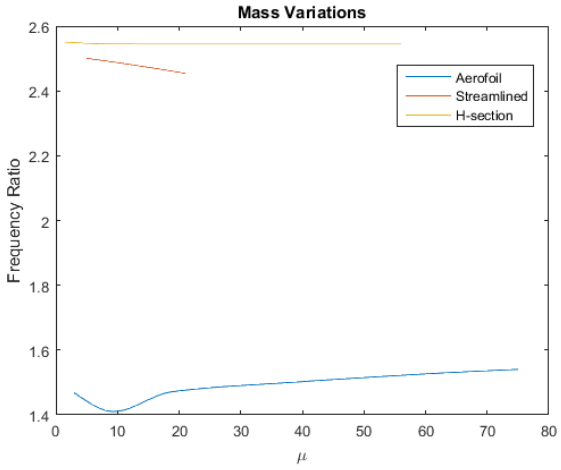

Figure 33: Comparison of mass effect on frequency ratio

The non-dimensional parameter used to normalise the mass variation results is that of the mass-to-air ratio. It can be seen in Figure 32, that an increasing mass-to-air ratio results in an increased reduced for all three flutter cases. Of particular interest from this figure is the plot of the streamlined deck which only extends for a small range. This was due to the lack of intersecting real and imaginary roots for masses above approximately 80000 kilograms. As such, there was a distinct lack of flutter boundary characteristics to record above this mass. Despite this however, the results plotted provide an adequate indication of the influence of the structural mass properties.

The response of the frequency ratio differs for all three examples as alluded to in Figure 33. Despite an initial drop, a heavier aerofoil tends to cause the frequency ratio to enlarge which is the opposite to what is seen to occur in the instance of the streamlined deck. Once more, the response of the H-section is one that is of little significance. Of the parameters that have been varied, this is the first indication of a significant deviation in the manner in which each structure behaves.

8.2.4 Critical Velocity Comparison

Thus far, the impact of varying structural parameters on the individual non-dimensional characteristics at the flutter boundary has been investigated. However, the extent of the insight that these are capable of providing is limited. Hence, an appropriate course of action now is to

utilise these particular characteristics to calculate the actual critical velocity for varying properties. In doing so, an explicit understanding of the influence of the various parameters will be attained. As before, this was first carried out for the torsional natural frequency with the results plotted below.

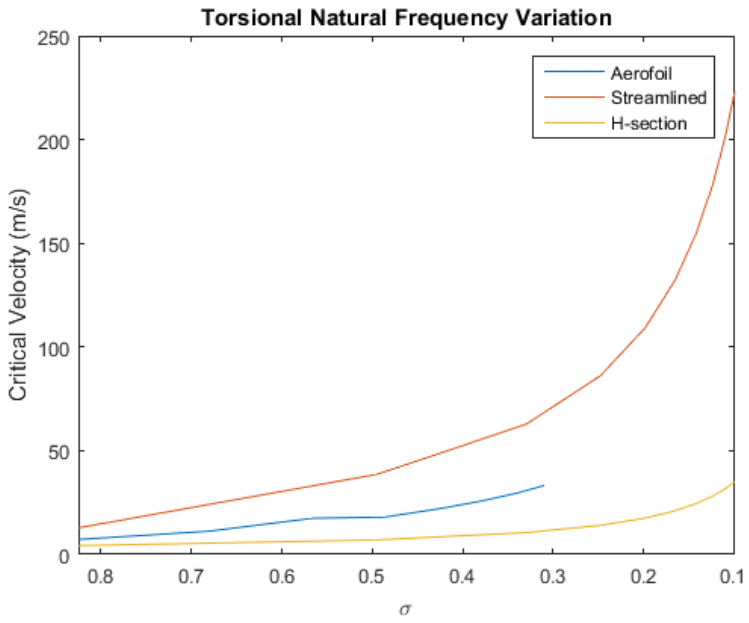

Figure 34: The critical velocity for decreasing non-dimensional frequency

Figure 34 clearly indicates that an increased torsional natural frequency or, alternatively, a reduced non-dimensional ratio, has a profound impact on the critical velocity in all three cases. Given that the definition of the non-dimensional frequency on the x-axis is a ratio of the bending natural frequency to torsional natural frequency, it can be inferred that a larger difference between the two will result in a smaller non-dimensional value.

For the two instances of classical flutter, where the two modes of vibration coalesce, enlarging the difference between the natural frequency of both of these renders it more difficult for modal coupling to occur. This offers an explanation for the prominent increase of the critical velocity for these two types of flutter. For the H-section deck, which is prone to torsional flutter, it is intuitive that a higher torsional natural frequency would have positive implications on the flutter boundary. In fact, it can be recalled that a detrimental feature of the Tacoma Narrows Bridge was its inadequate torsional stiffness which entailed a reduced natural frequency of the torsional mode of vibration.

It is demonstrated that the initiation of the three types of flutter investigated in this study can be impeded through an increase of the torsional natural frequency. There a number of means through which the torsional natural frequency can be made larger. Given that, by definition,

natural frequency is proportional to structural stiffness, it becomes obvious that these remedies revolve around increasing the torsional stiffness of the structure in question. An example of this is the use of physical stiffeners which has been applied in various forms to both wings and bridges. It can be recalled that this was a remedying action first proposed by Lancaster in the first flutter analysis in the early 20th century.

Alternatively, reducing the mass moment of inertia of the system would also increase the torsional natural frequency. The mass moment of inertia is defined as:

$$I_\alpha = \int_Q x_\alpha^2 dm \qquad (93)$$

Where, from the model development chapter, the distance between the elastic axis and the centre of mass is x_α. In (93), the integral is performed over the entire mass, Q, of the system. Therefore, two courses of action will yield a smaller mass moment of inertia, the first of which is a reduction in structural mass. Although, as will be seen later, enhanced mass properties can also be advantageous to the structures ability to reject the onset of flutter. The second is to reduce the offset distance between the elastic axis and centre of mass.

The key concluding point from Figure 34 is that, regardless of the type of flutter, the velocity at which it will be initially encountered becomes higher as the natural frequency for the torsional mode of vibration is increased. Thus, an illustration of the cross-discipline nature of flutter has been observed. The importance of torsional stiffness as a means of prevention is pertinent in all three flutter cases analysed.

In a similar manner to that of the torsional natural frequency, a comparison of the critical speed in response to a changing bending natural frequency for the three types of flutter has been conducted. The results of this are depicted in the following figure.

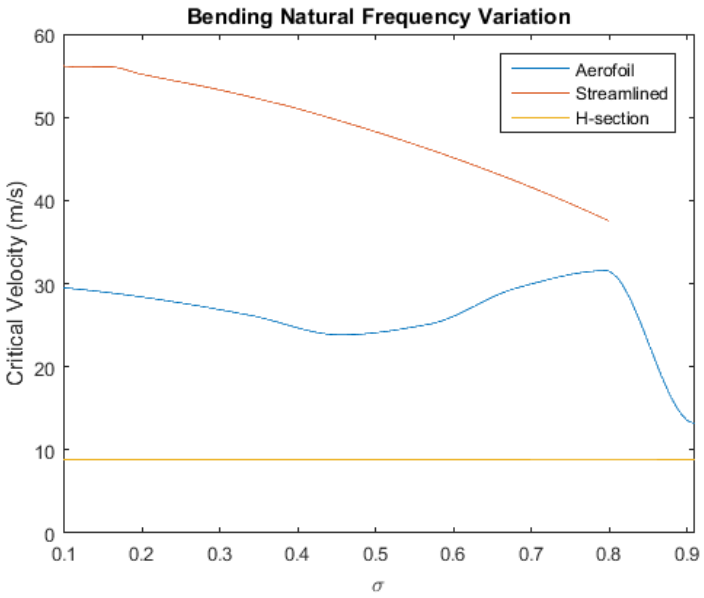

Figure 35: The critical velocity for varying increasing non-dimensional frequency

The plots in Figure 35 demonstrate that, generally, an increase in the bending natural frequency is likely to reduce the velocity at the flutter boundary for the classical types. This is due to the natural frequency of the two ratios gradually becoming more similar which in turn renders the structure more susceptible to flutter. Similar natural frequencies are a hindering factor as there is a less of a requirement for them to coalesce and lead to flutter. For this reason, the two examples of classical flutter can be seen to react more severely to an increased bending natural frequency. Essentially, this effect is the opposite to what was observed from the corresponding plot for the torsional natural frequency.

Whereas, the H-section flutter model is not influenced at all by the changing bending natural frequency. An immediate explanation of this is that this section exhibits torsional oscillations only. For this reason, a changing bending natural frequency will not contribute significantly in influencing this response. In this way, torsional bridge flutter distinguishes itself from the classical varieties.

The most common physical means of achieving a reduced bending natural frequency is to increase the structural mass. This is most effective when performed in conjunction with the lowering of the structural bending stiffness. However, it was deduced in the interpretation of the torsional natural frequency results that the critical velocity could be raised by reducing the mass of the system. This is where the implementation of mass balancing methods has been a popular method of flutter prevention. This technique has been utilised in the both wing and bridge applications. The comparison of the mass properties effect will offer an explicit

indication of how the flutter velocity is influence. The results of this are seen in Figure 36 below.

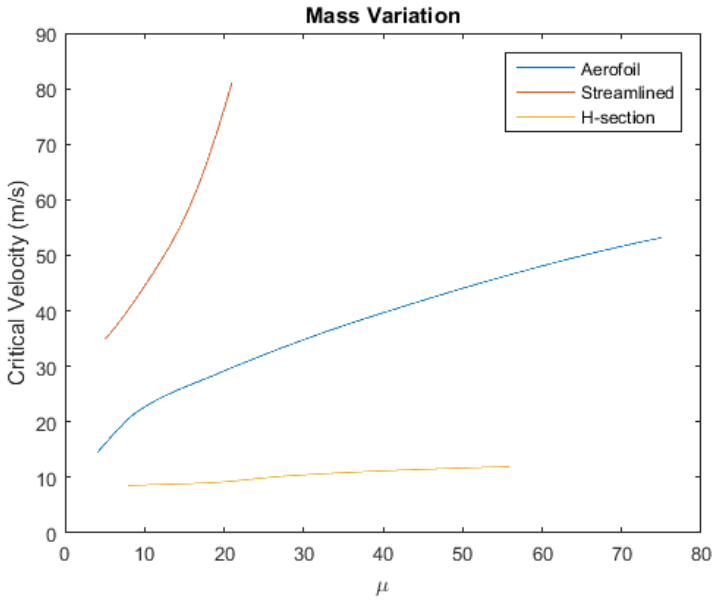

Figure 36: The critical velocity for varying mass properties

The general inference from Figure 36 is that increased structural mass properties have the effect of raising the velocity at the flutter boundary. All three forms of flutter are seen to be preventable through an increase in mass properties. The implications of this is a reduction in the flexibility of the structures which hinders the sustenance of oscillations due to flutter. As previously alluded to, the high flexibility of the Tacoma Narrows Bridge was a contributing factor to its destruction. From the results presented here, a heavier design would have assisted in delaying the onset of flutter.

In carrying out the mass properties dependency study, the consequences of varying mass and mass moment of inertia were not applied to the corresponding natural frequencies. Thus, this specific parametric dependency simulation solely demonstrated the pertinence that system mass has on the onset of flutter. The effect of mass variation on the different natural frequencies is referred to in previous discussion of Figure 34 and Figure 35.

The structural based simulations that have been performed, and the results that have been yielded, allow for a number of conclusions to be made. These will the topic of further discussion in a later section. Attention is now turned to the results obtained from the CFD simulations.

8.3 CFD Results

The parametric dependency study was intended to illustrate how the structural characteristics of wing and bridge flutter compare. The results of the CFD simulations that are presented here are intended to provide a visualisation of the fluid-structure interaction for the different flutter cases. In doing so, the flow behaviour that facilitates the different types of flutter will be divulged.

8.3.1 0 Degrees Angle of Attack

The first set of simulations involved a free-stream velocity of 20 m/s at an angle of attack (AoA) of 0 degrees. Figure 37, Figure 38 and Figure 39 below pertain to the flow solutions for the aerofoil, streamlined deck and H-section deck respectively.

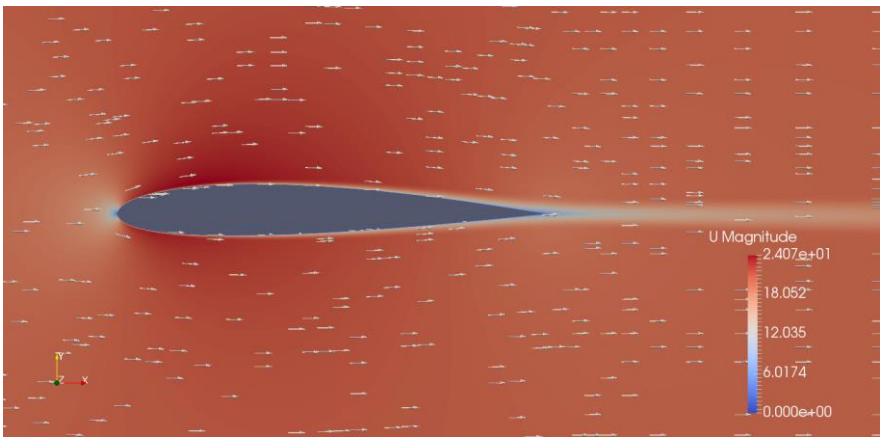

Figure 37: Velocity vectors for the aerofoil simulation at 0 degrees

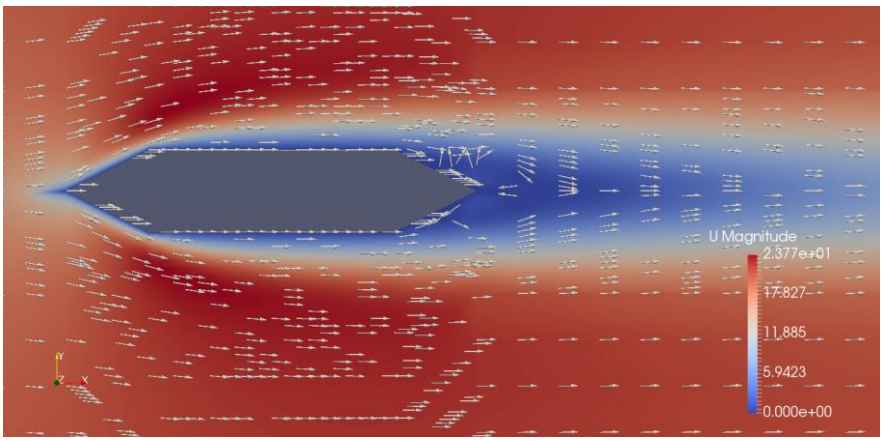

Figure 38: Velocity vectors for the streamlined deck simulation at 0 degrees

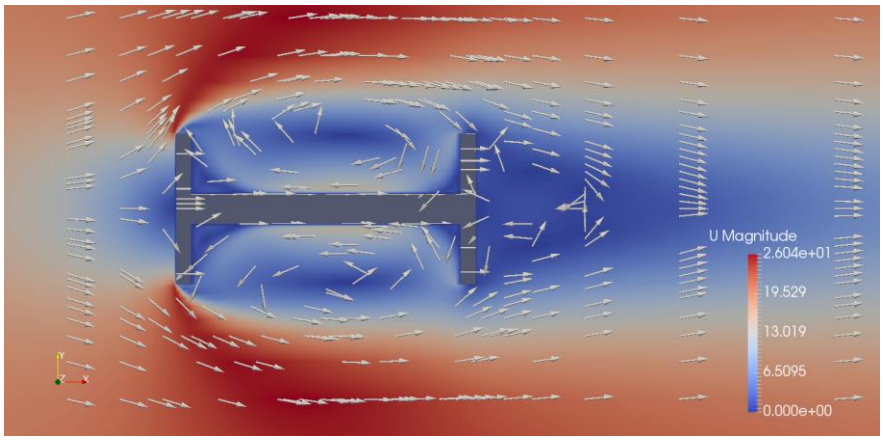

Figure 39: Velocity vectors for the H-section deck simulation at 0 degrees

The simulation results illustrate the difference in the flow fields for the various structures. Figure 37 shows that the flow remains attached over the entire structure for the aerofoil at an AoA of 0 degree. Here, an extremely thin boundary layer can be observed along the surface. Conversely, in the instance of the streamlined deck depicted in Figure 38, the boundary layer becomes separated as the flow travels over the diagonal sections of the upper and lower surfaces at the leading edge. While this is the case, the formation of vortices is delayed until the flow departs at the trailing edge of the structure. This is evidenced by the directional change of the velocity vectors in this region. For the H-section in Figure 39 however, flow separation is profound with the boundary layer being effectively tripped almost immediately. Vortices can be seen to form on both the upper and lower sections of the structure. In addition to this, there is evidence of vortices in the wake behind the structure.

8.3.2 5 Degrees Angle of Attack

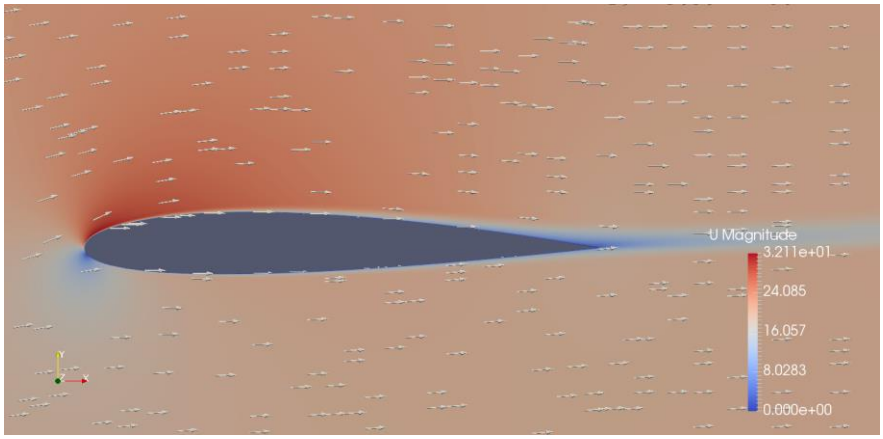

Figure 40: Velocity vectors for the aerofoil simulation at 5 degrees

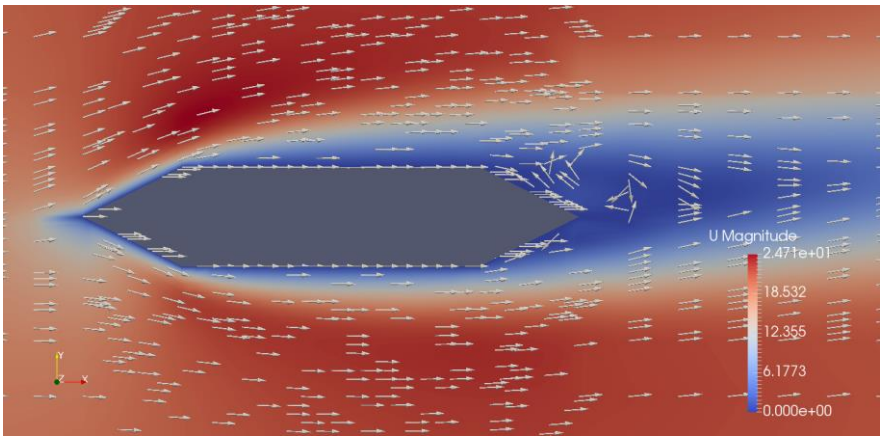

Figure 41: Velocity vectors for the streamlined deck simulation at 5 degrees

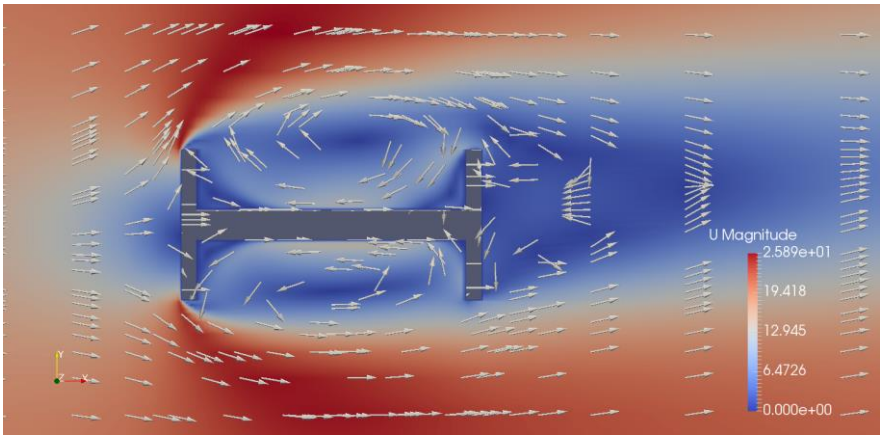

Figure 42: Velocity vectors for the H-section deck simulation at 5 degrees

The results presented above refer to the simulations at 20 m/s and AoA of 5 degrees. For the aerofoil, Figure 40 shows that, despite the change in angle of attack, the flow remains largely attached to the surface. A gradual increase in boundary layer can be seen at the trailing edge. The flow interaction with the streamlined deck in Figure 41 exhibits are more pronounced effect. It can be observed that the change in AoA has accentuated the flow separation with an increase in the vortex formed at the upper face of the trailing edge. The H-section responds in a similar fashion in Figure 42 with the vortex at the upper face becoming larger with the increased AoA.

8.3.3 10 Degrees Angle of Attack

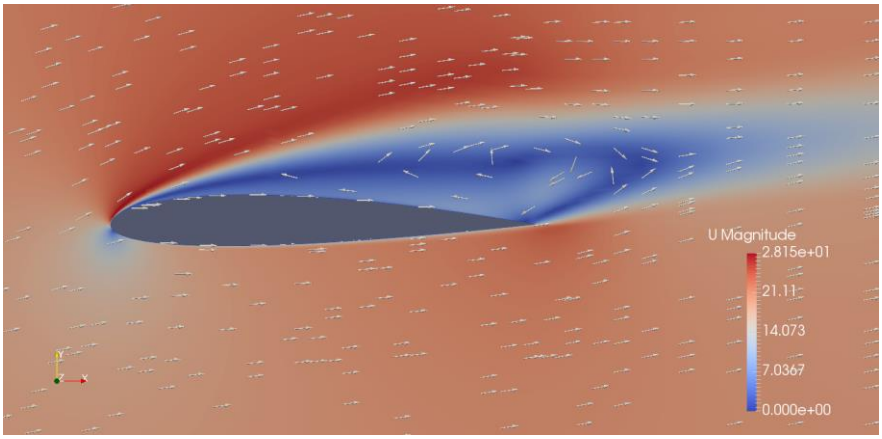

Figure 43: Velocity vectors for the aerofoil simulation at 10 degrees

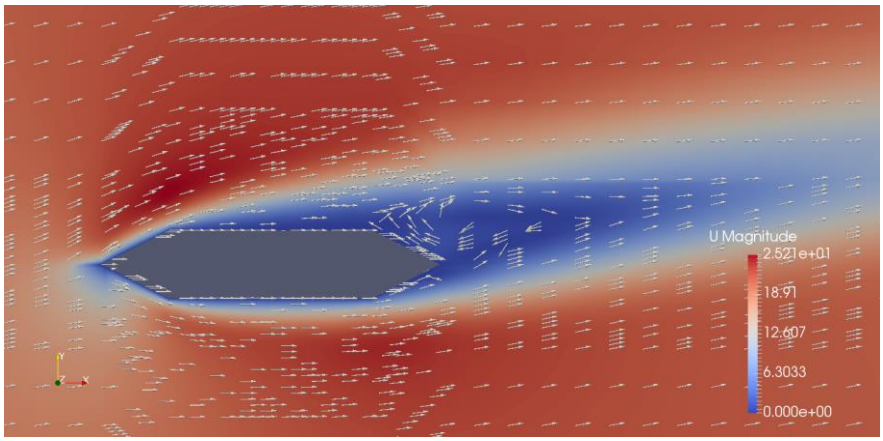

Figure 44: Velocity vectors for the streamlined deck simulation at 10 degrees

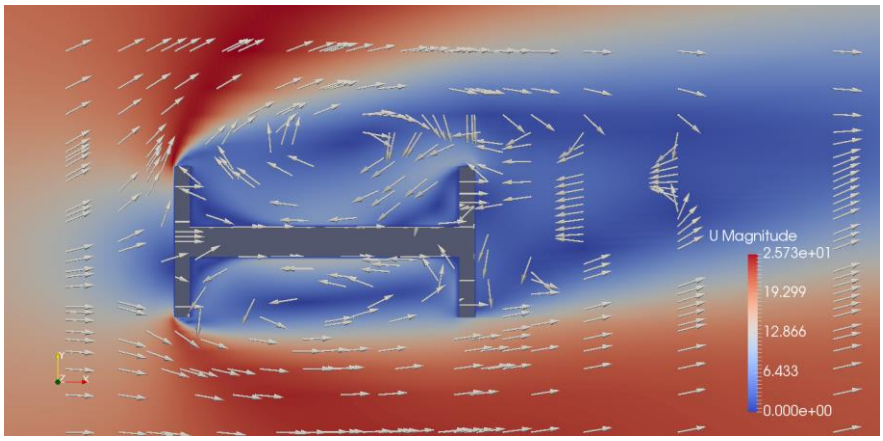

Figure 45: Velocity vectors for the H-section deck simulation at 10 degrees

At an AoA of 10 degrees flow separation can be seen to occur over the surface of the aerofoil in Figure 43. It is apparent that this flow separation occurs reasonably close to the leading edge. Furthermore, the formation of a vortex can be observed in the separated region. Figure 44

indicates an increase in the extent of the flow separation for the streamlined deck with the vortex at the leading edge again becoming more pronounced and larger than previously seen. The same is true in Figure 45 where the separation of flow over the H-section is prominent. Furthermore, the vortex that is formed increases in size and the vortices in the wake are intensified.

8.4 Discussion

As has been previously mentioned, the results presented in this chapter allow for an insight into the structural and fluid dynamic aspects of the different flutter types investigated. This section will offer concluding points that have been drawn from the simulation results. Additionally, potential sources of error in the numerical simulation process will be alluded to and remedies for this proposed.

It was concluded from the preliminary flutter analysis, that the H-section structure, which is known to facilitate self-excited torsional oscillations, was prone to flutter at lower velocities. Therefore, it can be gathered that the fluid-structure interaction that is associated with this type of flutter is more troublesome than that of the classical aerofoil or bridge flutter. This would suggest that, in a bid to prevent the initiation of flutter, utilising a profile that allows for the flow to remain attached over the majority of the surface is preferred.

In regards to the overall aim of this study, the structural simulations indicated that each type of flutter was influenced in a largely similar manner by most of the structural parameter variations. However, a notable exception to this was the fact that the H-section flutter velocity was unimpeded by a changing bending natural frequency. Thus is because the flutter associated with this structure is characterised by torsional oscillations. Conversely, for the classical flutter cases, extending the difference between the natural frequencies is seen to heighten the flutter boundary. This is achieved by either reducing the bending natural frequency or making bigger the torsional natural frequency. In an all three cases, the flutter boundary was positively impacted by an increase in the structural mass properties. While this was the case for the bending natural frequency, the flutter boundary in all three cases was improved through an increase in torsional natural frequency.

The results obtained from the CFD simulations consolidated the outcomes of the structural simulations. These were beneficial in understanding the flow behaviour induced by the different types of flutter. It is immediately apparent the impact that the profile geometry had on the flow. The torsional flutter is facilitated by flow separation and formation of vortices over a large part

of structure as is evidenced by the results for the H-section. Similarly, it can be seen that classical flutter occurs when flow separation is not prevalent and vortices formation does not occur over the surface of the structure. The flow separation that occurs over the aerofoil at an AoA of 10 degrees is a situation that is potentially conducive to stall flutter.

The CFD solutions also indicate that high angles of attack of the aerofoil are required to induce a similar flow behaviour as that of the H-section. This flow separation is replicating stall in the instance of the aerofoil which, in the context of flutter, can result in stall flutter. The angle of attack required to induce stall varies for different aerofoil geometries. To this end, like torsional bridge flutter, it can be asserted that stall flutter is also geometry dependent.

8.4.1 Error Analysis

The assumption that the physical models are simple in nature is not particularly representative of real-world environments. In actuality, there would be various aspects of the wing and bridge structures would result in the manifestation of structural non-linearities in the system. For example, the presence of external stores or hardware on a wing or that of vehicles in the case of a bridge would incur a non-linear response. The consideration of non-linear effects in regards to flutter has been topic of a multitude of previous studies.

There are a number of sources from which error could have been derived from in the theoretical flutter analysis. In the case of the wing flutter prediction, the solution process relied upon an approximation for Theodorsen's Function that was complex in nature to represent the unsteady behaviour of the aerodynamics. Being an approximation only, there is likely to be elements that divulge from real world scenarios. The fact that a number of slightly different approximations can be found in literature supports this claim.

Regarding the bridge flutter analysis, the extraction of the flutter derivatives from the original graphs is an example of a potential error source. The rudimentary nature of these graphs made it difficult obtaining precise and consistent values. In a similar sense, the discrete range of flutter derivatives meant that the solution process was not as extensive as that of the aerofoil analysis. Therefore, there is the possibility that the results produced in the bridge flutter analysis are erroneous.

9 Conclusions and Recommendations

9.1 Conclusions

A qualitative and quantitative analysis of flutter concerning both wings and bridges has been carried out. The aim of this study was to compare the flutter phenomenon in these two contexts in an effort to explicitly illustrate the similarities and differences that exist. This was achieved via a number of different approaches that were believed would best capture the pertinent aspects of flutter.

The first element of this thesis was concerned with a historical review of the major flutter events over the past century. Similarly, this was also able to highlight the key developments in the understanding of flutter. The conclusions drawn from this are as follows:

- Wing flutter has been more of a prominent issue than that of bridge flutter.
- For a significant amount of time, flutter was only perceived to be an issue for aircraft. This was due to the high frequency of flutter incidence involving aircraft and a distinct lack of bridge flutter cases. As such, much of the flutter theory that was developed is based around an aerofoil profile.
- In 1940, this perception was dismissed with the collapse of the Tacoma Narrows Bridge. While many explanations were proposed for the collapse of this bridge it was eventually deemed to be a result of flutter
- The Tacoma Narrows incident brought revealed a number of design issues that have allowed for necessary measures to ensure that bridge flutter has not occurred since.
- On the other hand, the progression of aircraft capability has been paralleled by the development of new type of flutter.
- While destructive flutter incidents are rare nowadays, both aircraft and bridge flutter continue to be a pertinent design concern today.

Having reviewed the history, a number of flutter variants were discussed. This was followed by the presentation of the major theories that have been developed over the years. From the theory component of the study, it was concluded that:

- Flutter is a dynamic instability that discerns itself from other instabilities in that it is self-excited and, as such, relies upon its prior motion as the forcing function.
- There are a numerous types of flutter that are distinguishable by differing mechanisms of instability.

- For classical forms of flutter, in the application to both a wing and bridge, the flow is required to remain attached over the structure and the formation of vortices is delayed until the flow departs at the trailing edge.
- For torsional bridge flutter and stall flutter, flow separation must occur early along the structure and the formation of vortices dominate the flow field.
- An exact form solution to classical wing flutter was first proposed by Theodorsen and is capable of determining the speed and frequency at the flutter boundary.
- In this solution, Theodorsen's Function is prevalent and is used to account for the effects of unsteady aerodynamics
- Regardless of the type, bridge flutter is an inherently non-linear instability as flow separation is prominent. As such, an exact solution like the one available for classical wing flutter is not available. Rather, empirical flutter derivatives that are geometry dependent are used to linearise the bridge flutter problem.
- The application of wing flutter theory to the bridge flutter problem is inappropriate due to dependency on potential flow theory.

With the theory integral to the understanding of flutter presented, model development and simulations followed. The models developed pertained to that of classical wing and bridge flutter as well as torsional bridge flutter. The simulations were effective in identifying the role that the structural and fluid dynamics aspects played in the onset of the different types of flutter. From these chapters it was found that:

- The aerodynamic model for the aerofoil came in a purely analytical form while the bridge model featured experimentally obtained flutter derivatives.
- The unbalance between the centre of mass and elastic axis in the case of the aerofoil facilitated inertial coupling. Whereas, in the instance of the bridge models, the elastic axis and centre of mass were assumed be at the same location, thus aerodynamic coupling was a defining factor.
- From the flutter analysis, it was deemed that the normalised flutter boundary was the lowest for the torsional bridge flutter. Thus, it was inferred that torsional bridge flutter is particularly dangerous as it does not necessarily require high wind speeds to occur.
- The simulations from the parametric study revealed that all three types of flutter were delayed through increasing the torsional stiffness and mass properties of the structure.
- The CFD simulations illustrated that the flow over the streamlined deck and aerofoil was similar in that the shedding of vortices were minimal at low angles of attack.

- The H-section deck, which is associated with torsional flutter, demonstrated severe flow separation and the formation of notable vortices at all angles of attack.
- As the angle of attack increased, flow separation became prevalent over the aerofoil and vortices were shed. Similarly, the higher angle of attack accentuated the flow separation of the bridge decks.

9.2 Recommendations

The recommendations stemming from this thesis come in the form of suggestions for future research and continuation of the current work. Given the theoretical nature of the investigation conducted in this thesis, several alternative routes can be taken.

An experimental investigation of the cross-disciplined nature of flutter can be performed to verify the work completed here. This would involve conducting wind tunnel testing to observe for the onset of flutter for a wing and a number of bridge structures. Particular attention should be given to the fluid-structure interaction in these wind tunnel tests. Additionally, experimental work could also be conducted in order to verify the results from the parametric dependency study.

A previous University of Queensland thesis investigated flutter via CFD simulations [14]. Thus, a similar approach could be taken to consider the similarities between wing and bridge flutter. This would see a continuation of the CFD simulations performed in this current work which were used only for flow visualisation.

Finally, further work could be completed in regards to the stall flutter phenomenon. Due to its complex nature and extent of work that stall flutter simulations necessitate, a quantitative analysis was not included here. However, future work could build on the preliminary theory and models presented regarding stall flutter in an effort to make a more comprehensive comparison to bridge flutter.

References

[1] Kehoe, M. (1995). *A Historical Overview of Flight Flutter Testing*. Washington, DC: NASA.

[2] Garrick, I. & Reed III, W. (1981). *Historical Development of Aircraft Flutter*. *Journal Of Aircraft*, *18*(11), 897-912. http://dx.doi.org/10.2514/3.57579

[3] Ranter, H. (2016). *ASN Aircraft accident Caproni Ca.48 registration unknown Verona*. *Aviation-safety.net*. Retrieved 23 October 2016, from https://aviation-safety.net/database/record.php?id=19190802-0

[4] Billah, K. (1991). *Resonance, Tacoma Narrows bridge failure, and undergraduate physics textbooks*. *American Journal Of Physics*, *59*(2), 118. http://dx.doi.org/10.1119/1.16590

[5] Hartman, E. (1968). Flight Research. In E. Hartman, *SP-4302 Adventures in Research: A History of Ames Research Center 1940-1965* (1st ed.). NACA. Retrieved from http://history.nasa.gov/SP-4302/ch1.10.htm

[6] Abzug, M. & Larrabee, E. (2002). *Airplane stability and control*. Cambridge, UK: Cambridge University Press.

[7] Chen, P., Liu, D., & Scarcello, J. (2008). *Studies of F-16 Limit-Cycle-Oscillation Mechanism Using Medium fidelity Aeroelastic Simulation Tool*. U.S. Air Force research Laboratories.

[8] Tewari, A. (1999). *Flutter*. *Iitk.ac.in*. Retrieved 13 June 2016, from http://www.iitk.ac.in/infocell/Archive/dirjan1/flutter.html

[9] Curry, R. (2015). *UAV to Climb to 90000 ft Without an Engine*. *UAS Vision*.

[10] Lim, A. (2007). *Modelling and Nonlinear Analysis of Aircraft Wing Flutter* (Undergraduate). University of Queensland.

[11] Saverin, J. (2009). *Modelling and Nonlinear Analysis of Aircraft Wing Flutter using a Compressible Flow Approximation* (Undergraduate). University of Queensland.

[12] Varghese, J. (2009). *Development of Melnikov Criteria for Chaos in a Fluttering Airfoil with Structural Nonlinearities* (Undergraduate). University of Queensland.

[13] Schmidt, C. (2010). *Aeroelastic Analysis of Flutter in Helicopter Rotor Blades with a Comparison to the Effect in Fixed Wing Aircraft* (Undergraduate). University of Queensland.

[14] Turner, P. (2013). *Flutter Analysis of a 2D Wing using OpenFOAM* (Undergraduate). University of Queensland.

[15] Collar, A. (1978). *The First Fifty Years of Aeroelasticity*. Aerospace, *5*, 12-20.

[16] Atkins, T. & Escudier, M. (2013). Kutta Condition. *A Dictionary of Mechanical Engineering*. Oxford University Press.

[17] E. H. Dowell (2004). *A Modern Course in Aeroelasticity*, Springer.

[18] Haddadpour, H. and R. D. Firouz-Abadi (2006). *Evaluation of Quasi-steady Aerodynamic Modelling for Flutter Prediction of Aircraft Wings in Incompressible Flow*. Thin-Walled Structures 44(9): 931-936.

[19] Birnbaum, W. (1924). *The Plane Problem of the Oscillating Wing*. Journal of Applied Mathematics and Mechanics 4: 277-292

[20] Wagner, H. (1925). *Dynamic Lift of Wings*. Journal of Applied Mathematics and Mechanics 5:17-35

[21] Theodorsen, T. (1935). *General Theory of Aerodynamic Instability and the Mechanism of Flutter*. National Advisory Committee for Aeronautics – Report 496.

[22] Fung, Y. C. (2002). *An Introduction to the Theory of Aeroelasticity*, Dover Publications.

[23] Lof, B. (2015). *Flutter of a Wind Turbine Airfoil* (Master of Science). Delft University of Technology.

[24] Leishman, J. & Beddoes, T. (1989). *A Semi-Empirical Model for Dynamic Stall*. *Journal Of The American Helicopter Society*, *34*(3), 3-17. http://dx.doi.org/10.4050/jahs.34.3

[25] Holierhoek, J., de Vaal, J., van Zuijlen, A., & Bijl, H. (2012). *Comparing different dynamic stall models*. *Wind Energy*, *16*(1), 139-158. http://dx.doi.org/10.1002/we.548

[26] Simiu, E. & Scanlan, R. (1978). *Wind Effects on Structures*. New York: Wiley.

[27] Zhan, H. & Fang, T. (2012). *Flutter Stability Studies of Great Belt East Bridge and Tacoma Narrows Bridge by CFD Numerical Simulation* (Ph.D). The Seventh International Colloquium on Bluff Body Aerodynamics and Applications.

[28] von Karman, T. and Dunn, L., (1942). *Preliminary Report on the Aerodynamic Investigations for the Design of the Tacoma Narrows Bridge*. Board of Consulting Engineers.

[29] Scanlan, R. & Tomko, J. (1971). *Airfoil and Bridge Deck Flutter Derivaitves*. *Journal Of The Engineering Mechanics Division*, (December,1971).

[30] Selvam, R. P. and Govindaswamy, S. (2001). *A report on aeroelastic analysis of bridge girder section using computer modelling*. Fayetteville, Ark.; [Springfield, VA], University of Arkansas, Mack-Blackwell National Rural Transportation Study Center

[31] Bisplinghoff, R. (1955). *Aeroelasticity*. Cambridge, Mass.: Addison-Wesley Pub. Co.

[32] Fitzpatrick, R. (2011). *Generalized Coordinates*. *Farside.ph.utexas.edu*. Retrieved 17 July 2016, from http://farside.ph.utexas.edu/teaching/336k/Newtonhtml/node75.html

[33] Daniel, B. and Meehan, P. (2015). *MECH3200: Advanced Dynamics and Vibrations* (Lecture Notes), University of Queensland

[34] Rao, S. (2004). *Mechanical vibrations*. Upper Saddle River, N.J.: Pearson Prentice Hall.

[35] Hodges, D. & Pierce, G. (2002). *Introduction to Structural Dynamics and Aeroelasticity*. Cambridge [England]: Cambridge University Press.

[36] Jahn, I. (2016). *MECH4480: Computational Fluid Dynamics – Potential Flow Theory* (Lecture Notes), University of Queensland

[37] Buresti, G. (2000). *Bluff-Body Aerodynamics*. Lecture, Genoa, Italy.

[38] Megson, T. (2007). *Aircraft structures for engineering students*. Oxford: Butterworth-Heinemann.

[39] Petroski, H. (2009). *Tacoma Narrows Bridges*. *American Scientist*, *97*(2), 103. http://dx.doi.org/10.1511/2009.77.103

[40] Li, J. (2007). *Experimental investigation of the low speed stall flutter of an airfoil*. Manchester: University of Manchester.

[41] Anderson, J. (1978). *Introduction to flight*. New York: McGraw-Hill.

[42] Jones, R. (2016). *The Unsteady Lift of a Wing of Finite Aspect Ratio*. Langley Field: NACA.

[43] Stathopoulos, T. & Baniotopoulos, C. (2007). *Wind effects on buildings and design of wind-sensitive structures.*. Wien: Springer.

[44] Dimitriadis, G. (2015). *Unsteady Aerodynamics - Theodorsen*. Lecture, Universite de Liege.

[45] Tang, D. & Dowell, E. (1996). *Comments On The Onera Stall Aerodynamic Model And Its Impact On Aeroelastic Stability*. *Journal Of Fluids And Structures*, *10*(4), 353-366. http://dx.doi.org/10.1006/jfls.1996.0023

[46] Scanlan, R. (1981). *State-of-the-art methods for calculating flutter, vortex-induced, and buffeting response of bridge structures*. Washington, D.C.: The Division.

[47] Shao, S. et al. "Flutter Of A Two-Dimensional Wing With Asymmetry At Low Mach Numbers". *Proceedings of the Institution of Mechanical Engineers, Part G: Journal of Aerospace Engineering* 228.1 (2012): 86-96. Web.

[48] Shahrad, P. and Mahzoon M. *Limit Cycle Flutter Of Airfoils In Steady And Unsteady Flows*. *Journal of Sound and Vibration* 256.2 (2002): 213-225. Web.

[49] Jahn, I. (2016). *MECH4480: Computational Fluid Dynamics – Finite Volume Formulation* (Lecture Notes), University of Queensland

[50] Balevi, T. (2012). *Flutter Analysis and Simulated Flutter Test of Wings* (Thesis), Middle Eastern Technical University

Appendix A: Flutter Derivatives

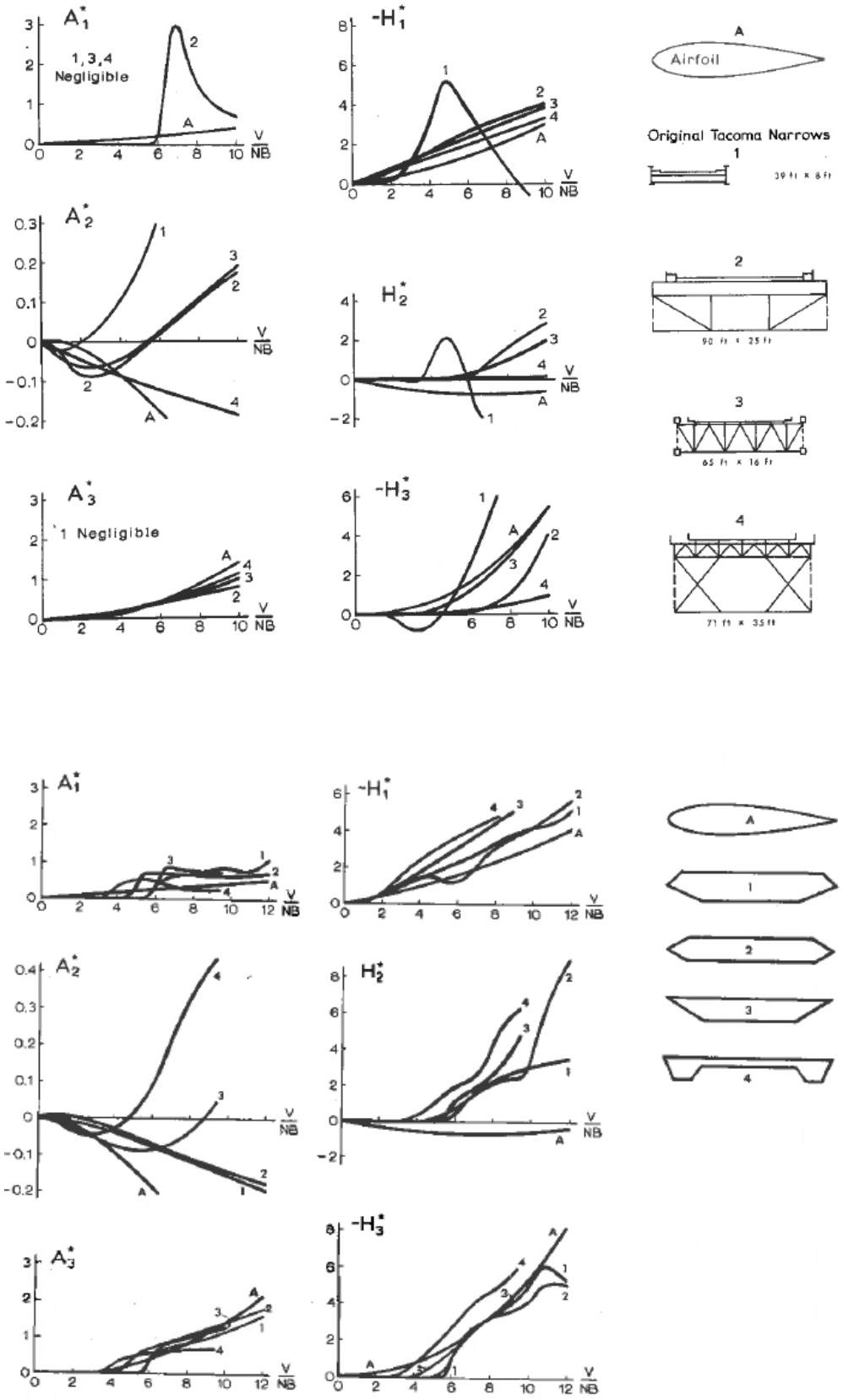

Appendix B: Aerodynamic Databases

Streamlined Deck

$1/k$	A_1^*	A_2^*	A_3^*	H_1^*	H_2^*	H_3^*
0	0	0	0	0	0	0
2	0	0	0	-0.67	0	0
4	0	-0.3	0	-1.5	0	-0.05
6	0.75	-0.5	0.5	-2.05	0.7	-1.25
8	0.7	-0.1	1	-3.25	2.25	-3.35
10	0.68	-0.14	1.46	-4.25	4.25	-4
12	0.7	-0.16	1.69	-5.5	8.9	-5

H-section Deck

$1/k$	A_1^*	A_2^*	A_3^*	H_1^*	H_2^*	H_3^*
0	0	0	0	0	0	0
1	0	-0.02	0	-0.1	0	0
2	0	-0.007	0	-0.25	0	0.1
3	0	-0.035	0	-1.4	-0.1	0.35
4	0	0.11	0	-3.2	1	0.22
5	0	0.19	0	-5	1.99	0.9
6	0	0.3	0	-3.8	-0.8	2.8
7	0	0	0	-2.3	0	5.4
8	0	0	0	-0.95	0	0

Appendix C: Aerofoil Solution Process

Substituting the solution forms of harmonic motion, the lift and moment equations prescribed by Theodorsen can be taken as [50]:

$$L = \Big[\rho\pi b^2[-\omega^2 h_0 + Ui\omega\alpha_0 + ab\omega^2\alpha_0] + 2\pi\rho Ub(F+iG)\left[i\omega h_0 + U\alpha_0 + b\left(\frac{1}{2}-a\right)i\omega\alpha_0\right]\Big]e^{i\omega t} \quad (94)$$

$$M = \left[\rho\pi b^2\left[-ab\omega^2 h_0 - Ub\left(\frac{1}{2}-a\right)i\omega\alpha_0 + b^2\left(\frac{1}{8}+a\right)\omega^2\alpha_0\right] + 2\pi\rho b^2 U\left(a+\frac{1}{2}\right)(F+iG)\left[i\omega h_0 + U\alpha_0 + b\left(\frac{1}{2}-a\right)i\omega\alpha_0\right]\right]e^{i\omega t} \quad (95)$$

Taking the necessary steps, (94) and (95) are then represented as:

$$L = -\rho\pi b^3\omega^2\left[\left(1 - \frac{2i(F+iG)}{k}\frac{h_0}{b}\right) + \left[-a - \frac{i\big(1+(1-2a)(F+iG)\big)}{k} - \frac{2(F+iG)}{k^2}\right]\alpha_0\right]e^{i\omega t} \quad (96)$$

$$M = \rho\pi b^4\omega^2\left[\left[-a + \frac{i(2a+1)C(k)}{k}\frac{h_0}{b}\right] + \left[\frac{1}{8} + a^2 - \frac{i\left(\frac{1}{2}-a\right)\big(1-(2a+1)(F+iG)\big)}{k} + \frac{(2a+1)(F+iG)}{k^2}\right]\right]\alpha_0 e^{i\omega t} \quad (97)$$

These can be appended with the flutter determinant to produce the flutter coefficients in Appendix D.

Appendix D: Aerofoil Coefficients

$$A_R = -(\mu + 1) - \frac{2G}{k} \quad (98)$$

$$B_R = -(\mu x_\alpha - a) + \frac{2F}{k^2} - \left(\frac{1}{2} - a\right)\frac{2G}{k} \quad (99)$$

$$D_R = (-\mu x_\alpha - a) + \left(\frac{1}{2} + a\right)\frac{2G}{k} \quad (100)$$

$$E_R = -\left(\mu r^2 + a^2 + \frac{1}{8}\right) + \left(\frac{1}{4} - a^2\right)\frac{2G}{k} - \left(\frac{1}{2} + a\right)2F \quad (101)$$

$$A_I = \frac{2F}{k} \quad (102)$$

$$B_I = \frac{1}{k}\left[1 + \frac{2G}{k} + \left(\frac{1}{2} - a\right)2F\right] \quad (103)$$

$$D_I = -\left(\frac{1}{2} + a\right)2F \quad (104)$$

$$E_I = \frac{1}{k}\left[\left(\frac{1}{2} - a\right) - \left(\frac{1}{2} + a\right)\frac{2G}{k} - \left(\frac{1}{4} - a^2\right)2F\right. \quad (105)$$

Appendix E: Bridge Flutter Solution Process

$$\ddot{h} + 2\xi_h\omega_h\dot{h} + \omega_h^2 h = \frac{\rho U^2 B}{2m}\left[KH_1^*\frac{\dot{h}}{U} + KH_2^*\frac{B\dot{\alpha}}{U} + K^2H_3^*\alpha\right] \quad (106)$$

$$\ddot{\alpha} + 2\xi_\alpha\omega_\alpha\dot{\alpha} + \omega_\alpha^2\alpha = \frac{\rho U^2 B^2}{2I}\left[KA_1^*\frac{\dot{h}}{U} + KA_2^*\frac{B\dot{\alpha}}{U} + K^2A_3^*\alpha\right] \quad (107)$$

The solution process is initiated by introducing a non-dimensional time parameter defined as:

$$\tau = \frac{Ut}{B} \quad (108)$$

Therefore, it follows that the derivatives of the respective vertical and twist components in the equations of motion are also transformed. These are now taken as:

$$(\dot{\ }) = (\ )'\frac{U}{B} \quad (109)$$

$$(\ddot{\ }) = (\ )''\frac{U^2}{B^2} \quad (110)$$

These relationships shown in (109) and (110) can be substituted into the equations of motion where necessary. After multiplying through by B/U^2 and B^2/U^2, Equations (106) and (107) are reduced to:

$$\frac{h''}{B} + 2\xi_h\omega_h\frac{h'}{U} + \omega_h^2 h\frac{B}{U^2} = \frac{\rho B^2}{2m}\left[KH_1^*\frac{h'}{B} + KH_2^*\alpha' + K^2H_3^*\alpha\right] \quad (111)$$

$$\alpha'' + 2\xi_\alpha\omega_\alpha\alpha'\frac{B}{U} + \omega_\alpha^2\,\alpha\frac{B^2}{U^2} = \frac{\rho B^4}{2I}\left[KA_1^*\frac{h'}{B} + KA_2^*\alpha' + K^2A_3^*\alpha\right] \quad (112)$$

Parameters that take a similar form to that of the reduced frequency, seen below in Equation (113), are substituted into (111) and (112).

$$\bar{K}_h = \frac{B}{U}\omega_h \qquad \bar{K}_\alpha = \frac{B}{U}\omega_\alpha \quad (113)$$

$$\frac{h''}{B} + 2\xi_h\bar{K}_h\frac{h'}{B} + \bar{K}_h^2\frac{h}{B} = \frac{\rho B^2}{2m}\left[KH_1^*\frac{h'}{B} + KH_2^*\alpha' + K^2H_3^*\alpha\right] \quad (114)$$

$$\alpha'' + 2\xi_\alpha \overline{K}_\alpha \alpha' + \overline{K}_\alpha^2 \, \alpha = \frac{\rho B^4}{2I}\left[KA_1^* \frac{h'}{B} + KA_2^* \alpha' + K^2 A_3^* \alpha\right] \quad (115)$$

At this point in the process, the presumption is made that the response of the system at the flutter boundary is harmonic [26]. Consequently, solutions of the form below can be employed:

$$\frac{h}{B} = \frac{h_0}{B} e^{i\omega t} = \frac{h_0}{B} e^{iKs} \quad (116)$$

$$\alpha = \alpha e^{i\omega t} = \alpha e^{iKs} \quad (117)$$

Making the necessary substitutions of (116) and (117) reduces Equations (114) and (115) to the form of:

$$\left[\frac{-K^2}{B} + 2i\xi_h \overline{K}_h \frac{K}{B} + \overline{K}_h^2 - \frac{\rho B^2}{2m}\frac{K^2 i}{B} H_1^*\right] h_0 + \left[-\frac{\rho B^2}{2m} iK^2 H_2^* - \frac{\rho B^2}{2m} K^2 H_3^*\right] \alpha_0 = 0 \quad (118)$$

$$\left[\frac{\rho B^4}{2I}\frac{K^2 i}{B} A_1^*\right] h_0 + \left[-K^2 + 2i\xi_\alpha K \overline{K}_\alpha + \overline{K}_\alpha^2 - \frac{\rho B^4}{2I} iK^2 - \frac{\rho B^4}{2I} K^2 A_3^*\right] \alpha_0 = 0 \quad (119)$$

From Equations (118) and (119) it can be seen that matrix form can be used:

$$\begin{bmatrix} \frac{-K^2}{B} + \frac{2i\xi_h \overline{K}_h K}{B} + \overline{K}_h^2 - \frac{\rho B^2}{2m}\frac{K^2 i}{B} H_1^* & -\frac{\rho B^2 iK^2}{2m} H_2^* - \frac{\rho B^2}{2m} K^2 H_3^* \\ \frac{\rho B^4}{2I}\frac{K^2 i}{B} A_1^* & -K^2 + 2i\xi_\alpha K \overline{K}_\alpha + \overline{K}_\alpha^2 - \frac{\rho B^4 iK^2}{2I} A_2^* - \frac{\rho B^4 K^2}{2I} A_3^* \end{bmatrix} \begin{Bmatrix} h_0 \\ \alpha_0 \end{Bmatrix} = \begin{bmatrix} 0 \\ 0 \end{bmatrix}$$

Each element of the 4×4 matrix above can be arranged in a way that the real and imaginary components are grouped. Furthermore, an unknown frequency ratio, analogous to that of the flutter frequency ratio in (82), can be introduced into the equation. This is given by:

$$X_B = \frac{K}{\overline{K}_h} = \frac{B\omega/U}{B\omega_h/U} = \frac{\omega}{\omega_h} \quad (120)$$

Appendix F: Bridge Coefficients

$$R_4 = 1 + \frac{\rho B^4}{2I} A_3^* - \frac{\rho B^2}{2m}\frac{\rho B^4}{2I} A_2^* H_1^* + \frac{\rho B^4}{2I}\frac{\rho B^2}{2m} H_2^* A_1^* \quad (121)$$

$$R_3 = 2\xi_\alpha \frac{\omega_\alpha}{\omega_h}\frac{\rho B^2}{2m} H_1^* + 2\xi_h \frac{\rho B^4}{2I} A_2^* \quad (122)$$

$$R_2 = -\frac{\omega_\alpha^2}{\omega_h^2} - 4\xi_h\xi_\alpha \frac{\omega_\alpha}{\omega_h} - 1 - \frac{\rho B^2}{2I} A_3^* \quad (123)$$

$$R_1 = 0 \quad (124)$$

$$R_0 = \frac{\omega_\alpha^2}{\omega_h^2} \quad (125)$$

$$I_3 = \frac{\rho B^4}{2I} A_2^* + \frac{\rho B^2}{2m} H_1^* + \frac{\rho B^4}{2I}\frac{\rho B^2}{2m} H_1^* A_3^* - \frac{\rho B^2}{2m}\frac{\rho B^4}{2I} A_1^* H_3^* \quad (126)$$

$$I_2 = -2\xi_\alpha \frac{\omega_\alpha}{\omega_h} - 2\xi_h \frac{\rho B^4}{2I} A_3^* - 2\xi_h \quad (127)$$

$$I_1 = \frac{\rho B^2}{2m} H_1^* \frac{\omega_\alpha^2}{\omega_h^2} - \frac{\rho B^4}{2I} A_2^* \quad (128)$$

$$I_0 = 2\xi_\alpha \frac{\omega_\alpha}{\omega_h}\frac{\rho B^2}{2m} H_1^* + 2\xi_h \frac{\rho B^4}{2I} A_2^* \quad (129)$$

Appendix G: MATLAB Scripts

---- Aerofoil Flutter Analysis

```
clc
close
```

---- Input Parameters

```
a = -0.41;              %distance to EA
mu = 13.8;              %Mass Ratio
r = 0.3^0.5;            %Radius of Gyration
w_pitch = 88;           %Pitch natural frequency
w_plunge = 34.6;        %Plunge natural frequency
sig = w_plunge/w_pitch; %Natural Frequency Ratio
x = 0.15;               %Offset distance
X = sym ('X');
```

----Specify iterative parameters

```
k_inv_list1 = [];       %Empty list for reduced velocity
k_list = linspace(0.1,1,201);
```

----Set up empty lists for later storage

```
Re_C_list = [];         %Empty list for real Theodorsen Function
Im_C_list = [];         %Empty list for imag. Theodorsen Function
Real_list1 = [];        %Empty list for real roots
Imag_list1 = [];        %Empty list for imag roots
Real_list2 = [];        %Empty list for 2nd real roots
```

---- Inititate for-loop

```
for k = k_list
    disp(k)
    %Theodorsen's Function
    C = 1-(0.165/(1-(0.041i/k)))-(0.335/(1-(0.32i/k)));
    F = real(C);
    G = imag(C);
    Re_C_list = [Re_C_list,G];
    Im_C_list = [Im_C_list,F];
    %Generate indiviual components for matrix entries
    A_R = -(mu+1)-(2*G/k);
    A_I = 2*F/k;
    B_R = -(mu*x - a)+(2*F/k^2)-(0.5-a)*(2*G/k);
    B_I = (1/k)*(1+(2*G/k)+(0.5-a)*2*F);
    D_R = -(mu*x - a)+(0.5+a)*(2*G/k);
    D_I = -(0.5+a)*(2*F/k);
    E_R = -(mu*r^2+a^2+(1/8))+(0.25-a^2)*(2*G/k)-(0.5+a)*(2*F/k^2);
    E_I = (1/k)*((0.5-a)-(0.5+a)*(2*G/k)-(0.25-a^2)*2*F);
    %Matrix entries
    A = A_R+i*A_I + mu*(sig)^2*X;
    B = B_R + i*B_I;
    D = D_R + i*D_I;
    E = E_R + i*E_I + mu*r^2*X;
```

```
    %Set up matrix,f
    f = [A B; D E];
    %Calculate determinant of f
    Flut_Det = det(f);
    %Separate determinant into real and imag. parts
    delta_R = real(Flut_Det);
    delta_I = imag(Flut_Det);
    %Equate to 0 for non-trivial solutions
    eqn_R = delta_R == 0;
    eqn_I = delta_I == 0;
    %Solve for X
    ROOTS_R = solve(eqn_R,X);
    ROOTS_I = solve(eqn_I,X);
    %Take the square root of X
    Real = sqrt(ROOTS_R);
    Imag = sqrt(ROOTS_I);
    %Store results in list
    Real_list1 = [Real_list1,Real(1)];  %Update first real list
    Real_list2 = [Real_list2,Real(2)];  %Update second real list
    Imag_list1 = [Imag_list1,Imag(1)];  %Update imaginary list
    k_inv_list1 = [k_inv_list1,1/k];
end
%Plots
 subplot(1,1,1);
 plot(k_inv_list1,Imag_list1);
 hold on
 plot(k_inv_list1,Real_list1);
 hold on
 plot(k_inv_list1,Real_list2);
 legend('Im','Re1','Re2')
 title ('Aerofoil Flutter Boundary')
 xlabel ('1/k')
 ylabel ('sqrt(X)')
```

---- Streamlined Deck Flutter Analysis

```
clc
close
```

---- Input Parameters

```
w_alp = 0.2519*2*pi;        %Pitch natural frequency
w_h = 0.099*2*pi;           %Plunge natural frequency
z_alp = 0.005;              %Pitch Damping
z_h = 0.005;                %Plunge Damping
sig = w_h/w_alp;            %Natural Frequency Ratio
rho = 1.225;                %Density
B = 31;                     %Deck width
m = 51037.387;              %Mass
I = 4414223.643;            %Moment of inertia
mu1 = (rho*B^2)/m
mu2 = (rho*B^4)/I
mu3 = ((rho^2)*(B^6))/(m*I)
X = sym ('X');
```

---- Flutter Derivatives List

```
A_1 = [0 0        0       0.75    0.7     0.68    0.7];
A_2 = [0 0        -0.03   -0.05   -0.1    -0.14   -0.16];
A_3 = [0 0        0       0.5     1       1.46    1.69];
A_4 = [0 0 0 0 0 0 0 0];
H_1 = [0 -0.67    -1.5    -2.05   -3.25   -4.25   -5.5];
H_2 = [0 0        0       0.7     2.25    4.25    8.9];
H_3 = [0 0        -0.05   -1.25   -3.35   -4      -5];
H_4 = [0 0 0 0 0 0 0 0];
```

---- Empty Lists for Storage

```
X1 = [];
X2 = [];
X3 = [];
%------ Reduced Velocity List ------%
v_list = [0 2 4 6 8 10 12];
for n = 1:length(v_list)
    ROOTS1_list = [];
    ROOTS2_list = [];
    disp(n)
    A1 = A_1(n);
    A2 = A_2(n);
    A3 = A_3(n);
    A4 = A_4(n);
    H1 = H_1(n);
    H2 = H_2(n);
    H3 = H_3(n);
    H4 = H_4(n);
    %Generate indiviual components for matrix entries
    R4 = 1+(mu2)*A3-(mu1)*H4+(mu3)*A2*H1+(mu3)*A3*H4+(mu3)*H2*A1-(mu3)*A1*H3;
```

```
    R3 = 2*z_h*(mu2)*A2+2*z_alp*(mu1)*(1/sig)*H1;
    R2 = -(1/sig)^2-4*z_h*z_alp*(1/sig)-1-(mu2)*A3-(mu1)*(1/sig)^2*H4;
    R1 = 0;
    R0 = (1/sig)^2;
    I3 = mu2*A2+(mu1)*H1+mu3*H1*A2-(mu3)*A1*H3;
    I2 = -2*z_alp*(1/sig)-2*z_h-2*z_h*mu2*A3;
    I1 = -(mu1)*H1*(1/sig)^2-mu2*A2;
    I0 = 2*z_h*(1/sig)^2+2*z_alp*(1/sig);
    %Matrix entries
    eqn1 = R4*X^4 + R3*X^3 + R2*X^2 + R1*X + R0;
    eqn2 = I3*X^3 + I2*X^2 + I1*X + I0;
    CC1 = [R4,R3,R2,R1,R0];
    CC2 = [I3,I2,I1,I0];
    %Find roots
    ROOTS1 = roots(CC1)
    ROOTS2 = roots(CC2)
    %Solve for X
    ROOTS1_list = [ROOTS1_list,ROOTS1(ROOTS1>=0)];
    ROOTS2_list = [ROOTS2_list,ROOTS2(ROOTS2>=0)];
    %Store results in list
    X1 = [X1,ROOTS1_list(1)];
    X2 = [X2,ROOTS1_list(2)];
    X3 = [X3,ROOTS2_list(1)];
end
% ------ Plots ------%
 subplot(1,1,1);
 plot(v_list/(2*pi),X1);
 hold on
 plot(v_list/(2*pi),X2);
 hold on
 plot(v_list/(2*pi),X3);
 legend('Im','Re1','Re2')
 title ('Streamlined Bridge Deck Flutter Boundary')
 xlabel ('1/k')
 ylabel ('X')
```

```
---- H-section Flutter Analysis
clc
close
```

------- Input Parameters

```
w_alp = 0.2519*2*pi;     %Pitch natural frequency
w_h = 0.099*2*pi;        %Plunge natural frequency
z_alp = 0.005;           %Pitch Damping
z_h = 0.005;             %Plunge Damping
sig = w_h/w_alp;         %Natural Frequency Ratio
rho = 1.225;             %Density
B = 11.9;                %Deck width
m = 7520.712;            %Mass
I = 95850.725;           %Moment of inertia
mu1 = (rho*B^2)/m
mu2 = (rho*B^4)/I
mu3 = ((rho^2)*(B^6))/(m*I)
X = sym ('X');
```

---- Flutter Derivatives List

```
A_1 = [0 0        0        0        0        0        0        0        0];
A_2 = [-0.02      -
0.007    0.035    0.11     0.19     0.3      0        0        0        0];
A_3 = [0 0        0        0        0        0        0        0        0];
A_4 = [0 0        0        0        0        0        0        0        0];
H_1 = [-0.1       -0.25    -1.4     -3.2     -5       -3.8     -2.3     -
0.95     0        0];
H_2 = [0 0        -0.1     1        1.99     -0.8     0        0        0];
H_3 = [0 0.1      0.35     0.22     0.9      2.8      5.4      0        0];
H_4 = [0 0        0        0        0        0        0        0        0];
```

---- Empty Lists for Storage

```
X1 = [];
X2 = [];
X3 = [];
```

---- Reduced Velocity List

```
v_list = [1 2 3 4 5 6 7 8 9 10];
for n = 1:length(v_list)
    ROOTS1_list = [];
    ROOTS2_list = [];
    disp(n)
    A1 = A_1(n);
    A2 = A_2(n);
    A3 = A_3(n);
    A4 = A_4(n);
    H1 = H_1(n);
    H2 = H_2(n);
    H3 = H_3(n);
```

```
    H4 = H_4(n);
    %Generate indiviual components for matrix entries
    R4 = 1+(mu2)*A3-(mu1)*H4+(mu3)*A2*H1+(mu3)*A3*H4+(mu3)*H2*A1-(mu3)*A1*H3;
    R3 = 2*z_h*(mu2)*A2+2*z_alp*(mu1)*(1/sig)*H1;
    R2 = -(1/sig)^2-4*z_h*z_alp*(1/sig)-1-(mu2)*A3-(mu1)*(1/sig)^2*H4;
    R1 = 0;
    R0 = (1/sig)^2;
    I3 = mu2*A2+(mu1)*H1+mu3*H1*A2-(mu3)*A1*H3;
    I2 = -2*z_alp*(1/sig)-2*z_h-2*z_h*mu2*A3;
    I1 = -(mu1)*H1*(1/sig)^2-mu2*A2;
    I0 = 2*z_h*(1/sig)^2+2*z_alp*(1/sig);
    %Matrix entries
    eqn1 = R4*X^4 + R3*X^3 + R2*X^2 + R1*X + R0;
    eqn2 = I3*X^3 + I2*X^2 + I1*X + I0;
    CC1 = [R4,R3,R2,R1,R0];
    CC2 = [I3,I2,I1,I0];
    %Find roots
    ROOTS1 = roots(CC1)
    ROOTS2 = roots(CC2)
    %Solve for X
    ROOTS1_list = [ROOTS1_list,ROOTS1(ROOTS1>=0)];
    ROOTS2_list = [ROOTS2_list,ROOTS2(ROOTS2>=0)];
    %Store results in list
    X1 = [X1,ROOTS1_list(1)];
    X2 = [X2,ROOTS1_list(2)];
    X3 = [X3,ROOTS2_list(1)];
end
% ------ Plots ------%
 subplot(1,1,1);
 plot(v_list/(2*pi),X1);
 hold on
 plot(v_list/(2*pi),X2);
 hold on
 plot(v_list/(2*pi),X3);
 legend('Im','Re1','Re2')
 title ('H-Section Bridge Deck Flutter Boundary')
 xlabel ('1/k')
 ylabel ('X')
```

Appendix H: OpenFoam Scripts

Aerofoil Mesh

```
# Aerofoil.py
from numpy import pi, sin, cos
from math import atan
# define points along NACA profile
C = 0.236       # set chord length
t = C           # set thickness as a percentage of chord length. E.g.
12 = 12% thickness
BL  = 0.05 * C  #inner mesh offset
BL2 = 4.0 * C   #outer mesh offset
BL3 = 4.0 * C   #rear offset
#wing Shape
tf=0.12
m=0.01
p=0.4
job_title = "Aerofoil example"
print job_title
def wingshape(x,c=C,tf=tf,m=m,p=p):
    t=c*tf
    if 0.<=x<=p*c:
        yt=5.0*t*(0.2969*(x/c)**(0.5)-0.1260*(x/c)-
0.3516*(x/c)**(2.0)+0.2843*(x/c)**(3.0)-
0.1015*(x/c)**4.0)+m*x/(p**2.0)*(2.0*p-x/c)
        yb=-5.0*t*(0.2969*(x/c)**(0.5)-0.1260*(x/c)-
0.3516*(x/c)**(2.0)+0.2843*(x/c)**(3.0)-
0.1015*(x/c)**4.0)+m*x/(p**2.0)*(2.0*p-x/c)
    if p*c<=x<c:
        yt=5.0*t*(0.2969*(x/c)**(0.5)-0.1260*(x/c)-
0.3516*(x/c)**(2.0)+0.2843*(x/c)**(3.0)-0.1015*(x/c)**4.0)+m*(c-x)/((1-
p)**2.0)*(1-2.0*p+x/c)
        yb=-5.0*t*(0.2969*(x/c)**(0.5)-0.1260*(x/c)-
0.3516*(x/c)**(2.0)+0.2843*(x/c)**(3.0)-0.1015*(x/c)**4.0)+m*(c-x)/((1-
p)**2.0)*(1-2.0*p+x/c)
    if x==c:
        yt=0.0
        yb=0.0
    if x>c: print "Error"
    return[yt,yb]
def grad(pt1,pt2,m1,m2):
    c1 = pt1.y - m1*pt1.x
    c2 = pt2.y - m2*pt2.x
    x = (c2 - c1)/(m1 - m2)
    y = m2 * x + c2
    return [x,y]
def wingdx(x,c=C,tf=tf,m=m,p=p):
    t = c * tf
    if x==0:
        dyt=10e20
        dyb=-10e20
    if 0.<x<=p*c:
        dyt=5.0*t*(0.14845*(1/(x*c))**(0.5)-0.1260*(1/c)-
0.7032*x*(1/c)**(2.0)+0.8529*x**2*(1/c)**(3.0)-
0.406*x**3*(1/c)**4.0)+(2*c*m*p-2*m*x)/(c*p**2.0)
```

```
        dyb=-5.0*t*(0.14845*(1/(x*c))**(0.5)-0.1260*(1/c)-
0.7032*x*(1/c)**(2.0)+0.8529*x**2*(1/c)**(3.0)-
0.406*x**3*(1/c)**4.0)+(2*c*m*p-2*m*x)/(c*p**2.0)
    if p*c<=x<=c:
        dyt=5.0*t*(0.14845*(1/(x*c))**(0.5)-0.1260*(1/c)-
0.7032*x*(1/c)**(2.0)+0.8529*x**2*(1/c)**(3.0)-
0.406*x**3*(1/c)**4.0)+(2.0*m*(c*p-x))/(c*(-1+p)**2)
        dyb=-5.0*t*(0.14845*(1/(x*c))**(0.5)-0.1260*(1/c)-
0.7032*x*(1/c)**(2.0)+0.8529*x**2*(1/c)**(3.0)-
0.406*x**3*(1/c)**4.0)+(2.0*m*(c*p-x))/(c*(-1+p)**2)
    if x>c: print "Error"
    return[dyt,dyb]
def wing(pt1, pt2, C, side) :
    if side == "top":
        K = 0
    else:
        K = 1
    m1 = wingdx(pt1.x, C)[K]
    m2 = wingdx(pt2.x, C)[K]
    c1 = pt1.y - m1*pt1.x
    c2 = pt2.y - m2*pt2.x
    x = (c2 - c1)/(m1 - m2)
    y = m2 * x + c2
    return[x,y]
#individual attributes of the global data object.
gdata.dimensions = 2
gdata.title = job_title
gdata.axisymmetric_flag = 0
# top edge coordinates
A3  = Node(0.0 * C, wingshape(0.0 * C)[0], label="A3")
A2  = Node(0.1 * C, wingshape(0.1 * C)[0], label = "A2")
A1 = Node(0.4 * C, wingshape(0.4 * C)[0], label="A1")
A0 = Node(1.00 * C,wingshape(1.0 * C)[0], label="A0")
A7 = Node(A0.x +BL3, A0.y)
# bottom edge coordinates
A4  = Node(0.05 * C, wingshape(0.05 * C)[1], label = "A4")
A5 = Node(0.4 * C, wingshape(0.4 * C)[1], label="A5")
A6 = Node(1.00 * C, wingshape(1.00 * C)[1], label="A6")
A8 = Node(A6.x +BL3, A6.y)
#fine mesh external
bz10 = Node(wing(A1,A0,C,"top")[0], wing(A1,A0,C,"top")[1])
bz21 = Node(wing(A2,A1,C,"top")[0], wing(A2,A1,C,"top")[1])
bz32 = Node(wing(A3,A2,C,"top")[0], wing(A3,A2,C,"top")[1])
bz43 = Node(wing(A4,A3,C,"bot")[0], wing(A4,A3,C,"bot")[1])
bz54 = Node(wing(A5,A4,C,"bot")[0], wing(A5,A4,C,"bot")[1])
bz65 = Node(wing(A6,A5,C,"bot")[0], wing(A6,A5,C,"bot")[1])
alpha1=-atan(1/wingdx(A1.x,C)[0])
alpha2=atan(1/wingdx(A2.x,C)[0])
alpha4=-atan(1/wingdx(A4.x,C)[1])
alpha5=atan(1/wingdx(A5.x,C)[1])
B0 = Node(A0.x, A0.y + BL, label="B0")
B1 = Node(A1.x+BL*cos(alpha1), A1.y+BL*sin(alpha1))
B2 = Node(A2.x-BL*cos(alpha2), A2.y+BL*sin(alpha2), label="B2")
B3 = Node(A3.x-BL, A3.y)
B4 = Node(A4.x-BL*cos(alpha4), A4.y-BL*sin(alpha4), label="B4")
B5 = Node(A5.x+BL*cos(alpha5), A5.y-BL*sin(alpha5))
B6 = Node(A6.x, A6.y - BL)
B7 = Node(A7.x, B0.y)
B8 = Node(A8.x, B6.y)
```

```
b10z =
Node(grad(B0,B1,wingdx(A0.x,C)[0],wingdx(A1.x,C)[0])[0],grad(B0,B1,wing
dx(A0.x,C)[0],wingdx(A1.x,C)[0])[1], label = "b10")
b21z =
Node(grad(B2,B1,wingdx(A2.x,C)[0],wingdx(A1.x,C)[0])[0],grad(B2,B1,wing
dx(A2.x,C)[0],wingdx(A1.x,C)[0])[1], label='b21')
b32z =
Node(grad(B2,B3,wingdx(A2.x,C)[0],wingdx(A3.x,C)[0])[0],grad(B2,B3,wing
dx(A2.x,C)[0],10000)[1], label='b32')
b43z =
Node(grad(B4,B3,wingdx(A4.x,C)[1],wingdx(A3.x,C)[1])[0],grad(B4,B3,wing
dx(A4.x,C)[1],10000)[1], label = 'b43')
b54z =
Node(grad(B4,B5,wingdx(A4.x,C)[1],wingdx(A5.x,C)[1])[0],grad(B4,B5,wing
dx(A4.x,C)[1],wingdx(A5.x,C)[1])[1], label='b54')
b65z =
Node(grad(B6,B5,wingdx(A6.x,C)[1],wingdx(A5.x,C)[1])[0],grad(B6,B5,wing
dx(A6.x,C)[1],wingdx(A5.x,C)[1])[1], label='b54')
#course mesh external nodes
C1 = Node(B1.x, A1.y+BL2*sin(alpha1))
C0 = Node(A0.x, C1.y, label="C0")
C2 = Node(A2.x-BL2*cos(alpha2), A2.y+BL2*sin(alpha2), label="C2")
C3 = Node(A3.x-BL2, A3.y)
C4 = Node(A4.x-BL2*cos(alpha4), A4.y-BL2*sin(alpha4), label="C4")
C5 = Node(B5.x, A5.y-BL2*sin(alpha5))
C6 = Node(A6.x, C5.y)
C7 = Node(A7.x, C1.y)
C8 = Node(A8.x, C5.y)
c21z =
Node(grad(C2,C1,wingdx(A2.x,C)[0],wingdx(A1.x,C)[0])[0],grad(C2,C1,wing
dx(A2.x,C)[0],wingdx(A1.x,C)[0])[1], label='c21')
c32z =
Node(grad(C2,C3,wingdx(A2.x,C)[0],wingdx(A3.x,C)[0])[0],grad(C2,C3,wing
dx(A2.x,C)[0],10000)[1], label='c32')
c54z =
Node(grad(C4,C5,wingdx(A4.x,C)[1],wingdx(A5.x,C)[1])[0],grad(C4,C5,wing
dx(A4.x,C)[1],wingdx(A5.x,C)[1])[1], label='c54')
c43z =
Node(grad(C4,C3,wingdx(A4.x,C)[1],wingdx(A3.x,C)[1])[0],grad(C4,C3,wing
dx(A4.x,C)[1],10000)[1], label = 'c43')
# Create lines that form aerofoil profile
a1a0 = Bezier([A1,bz10,A0])
a2a1 = Bezier([A2,bz21,A1])
a3a2 = Bezier([A3,bz32,A2])
a4a3 = Bezier([A4,bz43,A3])
a5a4 = Bezier([A5,bz54,A4])
a6a5 = Bezier([A6,bz65,A5])
a0a7 = Line(A0,A7)
a8a6 = Line(A8,A6)
# Wing to BL lines
a0b0 = Line(A0, B0)
a1b1 = Line(A1, B1)
a2b2 = Line(A2, B2)
a3b3 = Line(A3, B3)
a4b4 = Line(A4, B4)
a5b5 = Line(A5, B5)
a6b6 = Line(A6, B6)
a7b7 = Line(A7, B7)
a8b8 = Line(A8, B8)
# BL1 to BL2 lines
```

```
b0c0 = Line(B0, C0)
b1c1 = Line(B1, C1)
b2c2 = Line(B2, C2)
b3c3 = Line(B3, C3)
b4c4 = Line(B4, C4)
b5c5 = Line(B5, C5)
b6c6 = Line(B6, C6)
b7c7 = Line(B7, C7)
b8c8 = Line(B8, C8)
# BL lines
b1b0 = Bezier([B1, b10z, B0])
b2b1 = Bezier([B2, b21z, B1])
b3b2 = Bezier([B3, b32z, B2])
b4b3 = Bezier([B4, b43z, B3])
b5b4 = Bezier([B5, b54z, B4])
b6b5 = Bezier([B6, b65z, B5])
b0b7 = Line(B0,B7)
b8b6 = Line(B8,B6)
c1c0 = Line(C1,C0)
c2c1 = Bezier([C2,c21z,C1])
c3c2 = Bezier([C3,c32z,C2])
c4c3 = Bezier([C4,c43z,C3])
c5c4 = Line(C5,C4)
c6c5 = Line(C6,C5)
c0c7 = Line(C0,C7)
c8c6 = Line(C8,C6)
#cluster objects
cf0 = HypertanClusterFunction(0.1666,2.0)
cf1 = HypertanClusterFunction(1,1)
cf2 = HypertanClusterFunction(0.11,1.0)
cf3 = HypertanClusterFunction(2.0,0.1)
cf4 = HypertanClusterFunction(0.2,2.0)
cf5 = HypertanClusterFunction(0.015,2.0)
cf6 = HypertanClusterFunction(2.0,0.015)
#Blocks
blk_0 = Block2D(make_patch(b1b0, a0b0, a1a0, a1b1), nni = 20, nnj = 10,
label = 'block0', cf_list=[cf3, cf0,cf3,cf0])
blk_1 = Block2D(make_patch(b2b1, a1b1, a2a1, a2b2), nni = 10, nnj = 10,
label = 'block1', cf_list=[None, cf0,None,cf0])
blk_2 = Block2D(make_patch(b3b2, a2b2, a3a2, a3b3), nni = 20, nnj = 10,
label = 'block2', cf_list=[None, cf0,None,cf0])
blk_3 = Block2D(make_patch(b4b3, a3b3, a4a3, a4b4), nni = 20, nnj = 10,
label = 'block3',cf_list=[None, cf0, None,cf0])
blk_4 = Block2D(make_patch(b5b4,a4b4, a5a4, a5b5), nni = 7, nnj = 10,
label ='block4', cf_list=[cf1, cf0, cf1, cf0])
blk_5 = Block2D(make_patch(b6b5, a5b5, a6a5, a6b6), nni = 20, nnj = 10,
label = 'block5',cf_list=[cf4, cf0, cf4,cf0])
blk_6 = Block2D(make_patch(b8b6, a6b6, a8a6, a8b8), nni = 25, nnj = 10,
label = 'block6',cf_list=[cf6, cf0, cf6,cf0])
blk_7 = Block2D(make_patch(b0b7, a7b7, a0a7, a0b0), nni = 25, nnj = 10,
label = 'block7',cf_list=[cf5, cf0, cf5,cf0])
blk_8 = Block2D(make_patch(c1c0, b0c0, b1b0, b1c1), nni = 20, nnj = 56,
label = 'block8', cf_list=[cf3, cf2,cf3,cf2])
blk_9 = Block2D(make_patch(c2c1, b1c1, b2b1, b2c2), nni = 10, nnj = 56,
label = 'block9', cf_list=[None, cf2,None,cf2])
blk_10 = Block2D(make_patch(c3c2, b2c2, b3b2, b3c3), nni = 20, nnj =
56,
label = 'block10', cf_list=[None, cf2,None,cf2])
blk_11 = Block2D(make_patch(c4c3, b3c3, b4b3, b4c4), nni = 20, nnj =
56,
```

```
label = 'block11',cf_list=[None, cf2, None,cf2])
blk_12 = Block2D(make_patch(c5c4,b4c4, b5b4, b5c5), nni = 7, nnj = 56,
label ='block12', cf_list=[cf1, cf2, cf1, cf2])
blk_13 = Block2D(make_patch(c6c5, b5c5, b6b5, b6c6), nni = 20, nnj =
56,
label = 'block13',cf_list=[cf4, cf2, cf4,cf2])
blk_14 = Block2D(make_patch(c8c6, b6c6, b8b6, b8c8), nni = 25, nnj =
56,
label = 'block14',cf_list=[cf6, cf2, cf6,cf2])
blk_15 = Block2D(make_patch(c0c7, b7c7, b0b7, b0c0), nni = 25, nnj =
56,
label = 'block15',cf_list=[cf5, cf2, cf5,cf2])
# Command to identify internal face connections
identify_block_connections()
# Set boundary conditions.
blk_8.bc_list[NORTH] = ExtrapolateOutBC(label="OF_inlet_00")
blk_9.bc_list[NORTH] = ExtrapolateOutBC(label="OF_inlet_00")
blk_10.bc_list[NORTH] = ExtrapolateOutBC(label="OF_inlet_00")
blk_11.bc_list[NORTH] = ExtrapolateOutBC(label="OF_inlet_00")
blk_12.bc_list[NORTH] = ExtrapolateOutBC(label="OF_inlet_00")
blk_13.bc_list[NORTH] = ExtrapolateOutBC(label="OF_inlet_00")
blk_14.bc_list[NORTH] = ExtrapolateOutBC(label="OF_inlet_00")
blk_15.bc_list[NORTH] = ExtrapolateOutBC(label="OF_inlet_00")
blk_0.bc_list[SOUTH] = ExtrapolateOutBC(label="OF_wall_00")
blk_1.bc_list[SOUTH] = ExtrapolateOutBC(label="OF_wall_00")
blk_2.bc_list[SOUTH] = ExtrapolateOutBC(label="OF_wall_00")
blk_3.bc_list[SOUTH] = ExtrapolateOutBC(label="OF_wall_00")
blk_4.bc_list[SOUTH] = ExtrapolateOutBC(label="OF_wall_00")
blk_5.bc_list[SOUTH] = ExtrapolateOutBC(label="OF_wall_00")
blk_6.bc_list[WEST] = ExtrapolateOutBC(label="OF_outlet_00")
blk_7.bc_list[EAST] = ExtrapolateOutBC(label="OF_outlet_00")
blk_14.bc_list[WEST] = ExtrapolateOutBC(label="OF_outlet_00")
blk_15.bc_list[EAST] = ExtrapolateOutBC(label="OF_outlet_00")
# command to write BC labels
sketch.prefer_bc_labels_on_faces()
# plot .svg
sketch.xaxis(0.0, 1.1 * C, 0.2 * C, -0.5 * C)
sketch.yaxis(-0.55 * C, 0.55 * C, 0.02 * C, -0.25 * C)
sketch.window(0.0, -0.6 * C, 1.2 * C, 0.6 * C, 0.05, 0.05, 0.17, 0.17)
```

Streamlined Mesh

```
# STREAMLINED.py
job_title = "STREAMLINED BRIDGE SECTION"
print job_title
# We can set individual attributes of the global data object.
gdata.dimensions = 2
gdata.title = job_title
gdata.axisymmetric_flag = 0
# Set up 3 rectangles in the (x,y)-plane by first defining
# the corner nodes, then the lines between those corners.
a = Node(0.0, 0.0, label="A")
b = Node(0.4, 0.0, label="B")
c = Node(0.0, 0.5, label="C")
d = Node(0.4, 0.5, label="D")
e = Node(0.0,1.0, label="E")
f = Node(0.4,1.0, label="F")
g = Node(0.44, 1.0, label="G")
h = Node(0.44, 0.52, label="H")
i = Node(0.56,1.0, label="I")
j = Node(0.56,0.52, label = "J")
k = Node(0.6,1.0, label = "K")
l = Node(0.6,0.5, label = "L")
m = Node(1.0,1.0, label = "M")
n = Node(1.0,0.5, label = "N")
o = Node(1.0,0.0, label = "O")
p = Node(0.6,0.0, label = "p")
q = Node(0.56,0.0, label = "Q")
r = Node(0.56,0.48, label = "R")
s = Node(0.44,0.48, label = "S")
t = Node(0.44,0.0, label = "T")
u = Node(0.4,0.45, label = "U")
v = Node(0.4,0.55, label = "V")
w = Node(0.44,0.59, label = "W")
x = Node(0.56,0.59, label = "X")
y = Node(0.6,0.55, label = "Y")
z = Node(0.6,0.45, label = "Z")
aa = Node(0.56,0.41, label = "AA")
bb = Node(0.44,0.41, label = "BB")
cc = Node(0.0,0.45, label = "CC")
dd = Node(0.0,0.55, label = "DD")
ee = Node(1.0,0.55, label = "EE")
ff = Node(1.0,0.45, label = "FF")
# Define Lines connecting blocks
#Horizontal Lines + angled lines
ab = Line(a, b); bt = Line(b, t); tq = Line(t, q); qp = Line(q, p); po
= Line(p,o)
cd = Line(c, d); ds = Line(d, s); sr = Line(s, r); rl = Line(r,l); ln =
Line(l,n)
dh = Line(d, h); hj = Line(h, j); jl = Line(j,l); ln = Line(l,n);
ef = Line(e,f); fg = Line(f,g); gi = Line(g,i); ik = Line(i,k); km =
Line(k,m)
#Vertical Lines
acc = Line(a, cc); dde = Line(dd, e);
bu = Line(b, u); vf = Line(v, f);
tbb = Line(t, bb); wg = Line(w, g);
qaa = Line(q, aa); xi = Line(x, i);
pz = Line(p,z); yk = Line(y,k);
off = Line(o,ff); eem = Line(ee,m);
```

```
ccu = Line(cc,u); ubb = Line(u,bb); bbaa = Line(bb,aa); aaz =
Line(aa,z); zff = Line(z,ff)
ddv = Line(dd,v); vw = Line(v,w); wx = Line(w,x); xy = Line(x,y); yee =
Line(y,ee)
ccc = Line(cc,c); cdd = Line(c,dd)
ud = Line(u, d); dv = Line(d, v)
bbs = Line(bb,s); hw = Line(h,w)
aar = Line(aa,r); jx = Line(j,x)
zl = Line(z,l); ly = Line(l,y)
ffn = Line(ff,n); nee = Line(n,ee)
# Define the blocks, with particular discretisation.
nx0 = 20; nx1 = 20; ny0 = 20; ny1 = 20
blk_0 = Block2D(make_patch(ccu, bu, ab, acc), nni=nx0, nnj=ny0,
                label="BLOCK-0")
blk_1 = Block2D(make_patch(cd, ud, ccu, ccc), nni=nx1, nnj=ny1,
                label="BLOCK-1")
blk_2 = Block2D(make_patch(ddv, dv, cd, cdd), nni=nx1, nnj=ny1,
                label="BLOCK-2")
blk_3 = Block2D(make_patch(ef, vf, ddv, dde), nni=nx0, nnj=ny0,
                label="BLOCK-3")
blk_4 = Block2D(make_patch(vw, hw, dh, dv), nni=nx0, nnj=ny1,
                label="BLOCK-4")
blk_5 = Block2D(make_patch(fg, wg, vw, vf), nni=nx1, nnj=ny1,
                label="BLOCK-5")
blk_6 = Block2D(make_patch(gi, xi, wx, wg), nni=nx0, nnj=ny0,
                label="BLOCK-6")
blk_7 = Block2D(make_patch(wx, jx, hj, hw), nni=nx0, nnj=ny1,
                label="BLOCK-7")
blk_8 = Block2D(make_patch(ik, yk, xy, xi), nni=nx1, nnj=ny1,
                label="BLOCK-8")
blk_9 = Block2D(make_patch(xy, ly, jl, jx), nni=nx0, nnj=ny0,
                label="BLOCK-9")
blk_10 = Block2D(make_patch(km, eem, yee, yk), nni=nx0, nnj=ny0,
                label="BLOCK-10")
blk_11 = Block2D(make_patch(yee, nee, ln, ly), nni=nx1, nnj=ny1,
                label="BLOCK-11")
blk_12 = Block2D(make_patch(ln, ffn, zff, zl), nni=nx1, nnj=ny1,
                label="BLOCK-12")
blk_13 = Block2D(make_patch(zff, off, po, pz), nni=nx0, nnj=ny0,
                label="BLOCK-13")
blk_14 = Block2D(make_patch(aaz, pz, qp, qaa), nni=nx0, nnj=ny1,
                label="BLOCK-14")
blk_15 = Block2D(make_patch(rl, zl, aaz, aar), nni=nx1, nnj=ny1,
                label="BLOCK-15")
blk_16 = Block2D(make_patch(bbaa, qaa, tq, tbb), nni=nx0, nnj=ny0,
                label="BLOCK-16")
blk_17 = Block2D(make_patch(sr, aar, bbaa, bbs), nni=nx0, nnj=ny1,
                label="BLOCK-17")
blk_18 = Block2D(make_patch(ubb, tbb, bt, bu), nni=nx1, nnj=ny1,
                label="BLOCK-18")
blk_19 = Block2D(make_patch(ds, bbs, ubb, ud), nni=nx0, nnj=ny0,
                label="BLOCK-19")
# Cammand to identify internal face connections
identify_block_connections()
# Set boundary conditions.
blk_0.bc_list[WEST] = ExtrapolateOutBC(label="OF_inlet_00")# labelling
inlet B/C
blk_1.bc_list[WEST] = ExtrapolateOutBC(label="OF_inlet_00")
blk_2.bc_list[WEST] = ExtrapolateOutBC(label="OF_inlet_00")
blk_3.bc_list[NORTH] = ExtrapolateOutBC(label="OF_inlet_00")
```

```
blk_3.bc_list[WEST] = ExtrapolateOutBC(label="OF_inlet_00")
blk_5.bc_list[NORTH] = ExtrapolateOutBC(label="OF_inlet_00")
blk_6.bc_list[NORTH] = ExtrapolateOutBC(label="OF_inlet_00")
blk_8.bc_list[NORTH] = ExtrapolateOutBC(label="OF_inlet_00")# labelling
inlet B/C
blk_10.bc_list[NORTH] = ExtrapolateOutBC(label="OF_inlet_00")
blk_13.bc_list[SOUTH] = ExtrapolateOutBC(label="OF_inlet_00")
blk_14.bc_list[SOUTH] = ExtrapolateOutBC(label="OF_inlet_00")#
labelling inlet B/C
blk_16.bc_list[SOUTH] = ExtrapolateOutBC(label="OF_inlet_00")
blk_18.bc_list[SOUTH] = ExtrapolateOutBC(label="OF_inlet_00")
blk_0.bc_list[SOUTH] = ExtrapolateOutBC(label="OF_inlet_00")
blk_4.bc_list[SOUTH] = ExtrapolateOutBC(label="OF_wall_00") # labelling
wall B/C
blk_7.bc_list[SOUTH] = ExtrapolateOutBC(label="OF_wall_01")
blk_9.bc_list[SOUTH] = ExtrapolateOutBC(label="OF_wall_02")
blk_15.bc_list[NORTH] = ExtrapolateOutBC(label="OF_wall_03")
blk_17.bc_list[NORTH] = ExtrapolateOutBC(label="OF_wall_04")
blk_19.bc_list[NORTH] = ExtrapolateOutBC(label="OF_wall_05")
blk_10.bc_list[EAST] = ExtrapolateOutBC(label="OF_outlet_00")#
labelling outlet B/C
blk_11.bc_list[EAST] = ExtrapolateOutBC(label="OF_outlet_00")
blk_12.bc_list[EAST] = ExtrapolateOutBC(label="OF_outlet_00")#
labelling outlet B/C
blk_13.bc_list[EAST] = ExtrapolateOutBC(label="OF_outlet_00")
# command to write BC labels
sketch.prefer_bc_labels_on_faces()
# plot .svg
sketch.xaxis(-0.05, 1.05, 0.2, -0.05)
sketch.yaxis(-0.05, 1.05, 0.2, -0.05)
sketch.window(-0.05, -0.05, 1.05, 1.05, 0.05, 0.05, 0.17, 0.17)
```

H-section Mesh

```
# H-Section.py
# Code for H-Section bridge deck
gdata.dimensions = 2
gdata.title = job_title
gdata.axisymmetric_flag = 0
#Nodes
a = Node(0.0, 0.0, label="A")
b = Node(0.45, 0.0, label="B")
c = Node(0.0, 0.475, label="C")
d = Node(0.45, 0.475, label="D")
e = Node(0.455,0.0, label="E")
f = Node(0.455,0.475, label="F")
g = Node(0.0, 0.525, label="G")
h = Node(0.45, 0.525, label="H")
i = Node(0.0,1.0, label="I")
j = Node(0.45,1.0, label = "J")
k = Node(0.545,0.0, label = "K")
l = Node(0.545,0.475, label = "L")
m = Node(0.455,0.495, label = "M")
n = Node(0.545,0.495, label = "N")
o = Node(0.455,0.505, label = "O")
p = Node(0.455,0.525, label = "p")
q = Node(0.545,0.525, label = "Q")
r = Node(0.545,0.505, label = "R")
s = Node(0.455,1.0, label = "S")
t = Node(0.545,1.0, label = "T")
u = Node(0.55,1.0, label = "U")
v = Node(0.55,0.525, label = "V")
w = Node(1.0,0.525, label = "W")
x = Node(1.0,1.0, label = "X")
y = Node(1.0,0.475, label = "Y")
z = Node(0.55,0.475, label = "Z")
aa = Node(1.0,0.0, label = "AA")
bb = Node(0.55,0.0, label = "BB")
#Nodes for a additional blocks
cc = Node(0.5,0.0, label = "CC")
dd = Node(0.5,0.475, label = "DD")
ee = Node(0.5,0.525, label = "EE")
ff = Node(0.5,1.0, label = "FF")
# Define Lines connecting blocks
#Horizontal Lines
ab = Line(a, b); be = Line(b, e); ek = Line(e, k); kbb = Line(k, bb);
bbaa = Line(bb,aa)
cd = Line(c, d); df = Line(d, f); fl = Line(f, l); lz = Line(l,z); zy =
Line(z,y)
mn = Line(m,n)
orr = Line(o,r)
gh = Line(g, h); hp = Line(h, p); pq = Line(p,q); qv = Line(q,v); vw =
Line(v,w)
ij = Line(i,j); js = Line(j,s); st = Line(s,t); tu = Line(t,u); ux =
Line(u,x)
#Vertical Lines
ac = Line(a, c); cg = Line(c, g); gi = Line(g,i)
bd = Line(b, d); dh = Line(d, h); hj = Line(h,j)
ef = Line(e, f); fm = Line(f, m); op = Line(o,p); ps = Line(p,s)
kl = Line(k, l); ln = Line(l, n); rq = Line(r,q); qt = Line(q,t)
bbz = Line(bb,z); zv = Line(z,v); vu = Line(v,u);
```

```
aay = Line(aa,y); yn = Line(y,n); wx = Line(w,x);yw = Line(y,w)
#Lines for additional blocks
ecc = Line(e, cc)
cck = Line(cc, k)
fdd = Line(f, dd)
ddl = Line(dd, l)
pee = Line(p, ee)
eeq = Line(ee, q)
sff = Line(s, ff)
fft = Line(ff, t)
ccdd = Line(cc, dd)
eeff = Line(ee, ff)
#Clustering
cf0 = HypertanClusterFunction(2,0.01)
cf1 = HypertanClusterFunction(0.01,2)
cf2 = HypertanClusterFunction(2,0.01)
cf3 = HypertanClusterFunction(0.01,2)
cf2 = HypertanClusterFunction(2,0.01)
# Define the blocks, with particular discretisation.
nx0 = 12; nx1 = 12; ny0 = 12; ny1 = 12 ;  nx3 = 6
blk_0 = Block2D(make_patch(cd, bd, ab, ac), nni=nx0, nnj=20,
                label="BLOCK-0",cf_list=[cf0, cf2,cf0,cf2])
blk_1 = Block2D(make_patch(gh, dh, cd, cg), nni=nx1, nnj=30,
                label="BLOCK-1",cf_list=[cf0, None,cf0,None])
blk_2 = Block2D(make_patch(ij, hj, gh, gi), nni=nx1, nnj=20,
                label="BLOCK-2",cf_list=[cf0, cf3,cf0,cf3])
blk_3 = Block2D(make_patch(js, ps, hp, hj), nni=nx3, nnj=20,
                label="BLOCK-3",cf_list=[None, cf3,None,cf3])
blk_4 = Block2D(make_patch(st, qt, pq, ps), nni=50, nnj=20,
                label="BLOCK-4",cf_list=[None, cf3,None,cf3])
blk_5 = Block2D(make_patch(pq, rq, orr, op), nni=50, nnj=20,
                label="BLOCK-5")
blk_6 = Block2D(make_patch(tu, vu, qv, qt), nni=nx3, nnj=20,
                label="BLOCK-6",cf_list=[None, cf3,None,cf3])
blk_7 = Block2D(make_patch(ux, wx, vw, vu), nni=nx0, nnj=20,
                label="BLOCK-7",cf_list=[cf1, cf3,cf1,cf3])
blk_8 = Block2D(make_patch(vw, yw, zy, zv), nni=nx1, nnj=20,
                label="BLOCK-8",cf_list=[cf1, None,cf1,None])
blk_9 = Block2D(make_patch(zy, aay, bbaa, bbz), nni=nx0, nnj=20,
                label="BLOCK-9",cf_list=[cf1, cf2,cf1,cf2])
blk_10 = Block2D(make_patch(lz, bbz, kbb, kl), nni=nx3, nnj=20,
                label="BLOCK-10",cf_list=[None, cf2,None,cf2])
blk_11 = Block2D(make_patch(fl, kl, ek, ef), nni=50, nnj=20,
                label="BLOCK-11",cf_list=[None, cf2,None,cf2])
blk_12 = Block2D(make_patch(mn, ln, fl, fm), nni=50, nnj=20,
                label="BLOCK-12")
blk_13 = Block2D(make_patch(df, ef, be, bd), nni=nx3, nnj=20,
                label="BLOCK-13",cf_list=[None, cf2,None,cf2])
# Cammand to identify internal face connections
identify_block_connections()
# Set boundary conditions.
blk_0.bc_list[WEST] = ExtrapolateOutBC(label="OF_inlet_00")# labelling
inlet B/C
blk_1.bc_list[WEST] = ExtrapolateOutBC(label="OF_inlet_00")
blk_2.bc_list[WEST] = ExtrapolateOutBC(label="OF_inlet_00")
blk_0.bc_list[SOUTH] = ExtrapolateOutBC(label="OF_inlet_00")# labelling
inlet B/C
blk_13.bc_list[SOUTH] = ExtrapolateOutBC(label="OF_inlet_00")
blk_11.bc_list[SOUTH] = ExtrapolateOutBC(label="OF_inlet_00")
```

```
blk_10.bc_list[SOUTH] = ExtrapolateOutBC(label="OF_inlet_00")#
labelling inlet B/C
blk_9.bc_list[SOUTH] = ExtrapolateOutBC(label="OF_inlet_00")
blk_2.bc_list[NORTH] = ExtrapolateOutBC(label="OF_inlet_00")
blk_3.bc_list[NORTH] = ExtrapolateOutBC(label="OF_inlet_00")# labelling
inlet B/C
blk_4.bc_list[NORTH] = ExtrapolateOutBC(label="OF_inlet_00")
blk_6.bc_list[NORTH] = ExtrapolateOutBC(label="OF_inlet_00")
blk_7.bc_list[NORTH] = ExtrapolateOutBC(label="OF_inlet_00")
blk_1.bc_list[EAST] = ExtrapolateOutBC(label="OF_wall_01") # labelling
wall B/C
blk_3.bc_list[SOUTH] = ExtrapolateOutBC(label="OF_wall_02")
blk_5.bc_list[WEST] = ExtrapolateOutBC(label="OF_wall_03")
blk_5.bc_list[SOUTH] = ExtrapolateOutBC(label="OF_wall_04")
blk_5.bc_list[EAST] = ExtrapolateOutBC(label="OF_wall_05")
blk_6.bc_list[SOUTH] = ExtrapolateOutBC(label="OF_wall_06")
blk_8.bc_list[WEST] = ExtrapolateOutBC(label="OF_wall_07")
blk_10.bc_list[NORTH] = ExtrapolateOutBC(label="OF_wall_08")
blk_12.bc_list[EAST] = ExtrapolateOutBC(label="OF_wall_09")
blk_12.bc_list[NORTH] = ExtrapolateOutBC(label="OF_wall_10")
blk_12.bc_list[WEST] = ExtrapolateOutBC(label="OF_wall_11")
blk_13.bc_list[NORTH] = ExtrapolateOutBC(label="OF_wall_13")
blk_7.bc_list[EAST] = ExtrapolateOutBC(label="OF_outlet_00")# labelling
outlet B/C
blk_8.bc_list[EAST] = ExtrapolateOutBC(label="OF_outlet_00")
blk_9.bc_list[EAST] = ExtrapolateOutBC(label="OF_outlet_00")
# command to write BC labels
sketch.prefer_bc_labels_on_faces()
# plot .svg
sketch.xaxis(-0.05, 1.05, 0.2, -0.05)
sketch.yaxis(-0.05, 1.05, 0.2, -0.05)
sketch.window(-0.05, -0.05, 1.05, 1.05, 0.05, 0.05, 0.17, 0.17)
```

Appendix I: Parametric Study Graphs

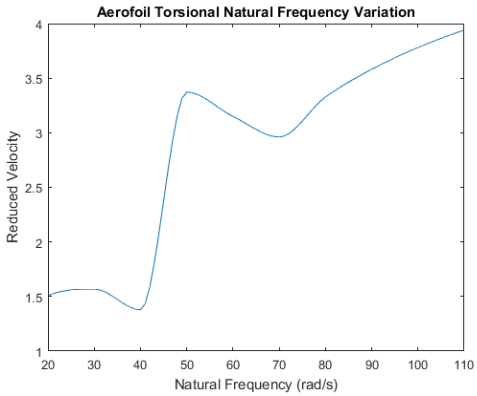

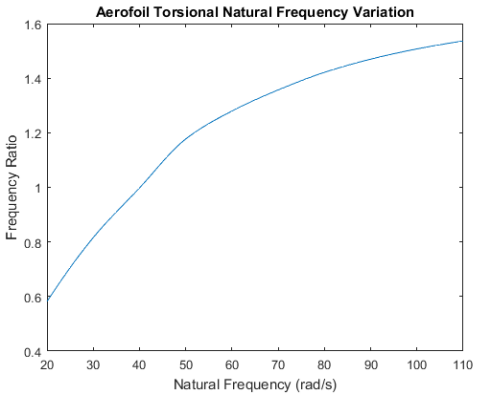

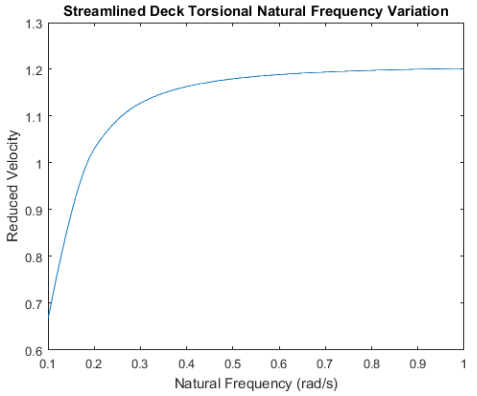

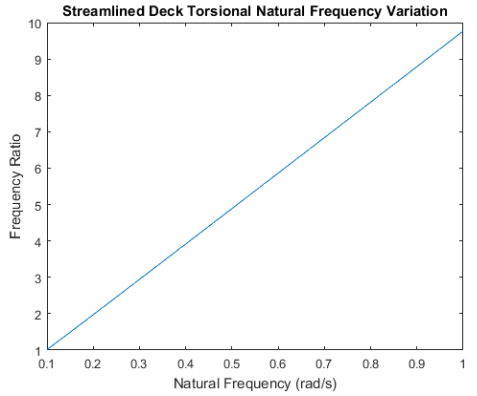

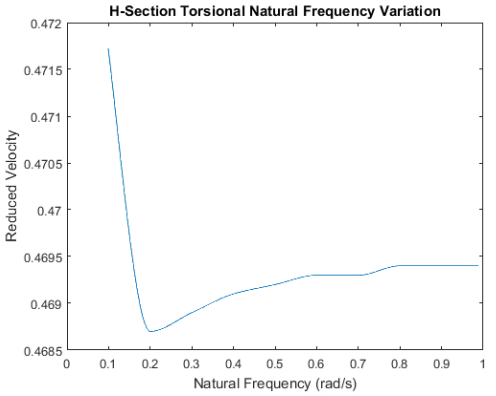

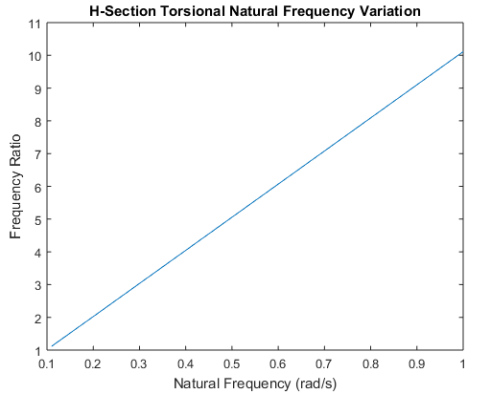

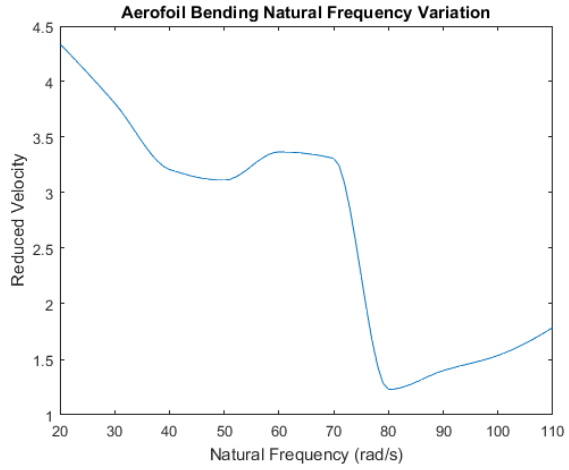
Aerofoil Bending Natural Frequency Variation
Reduced Velocity
Natural Frequency (rad/s)

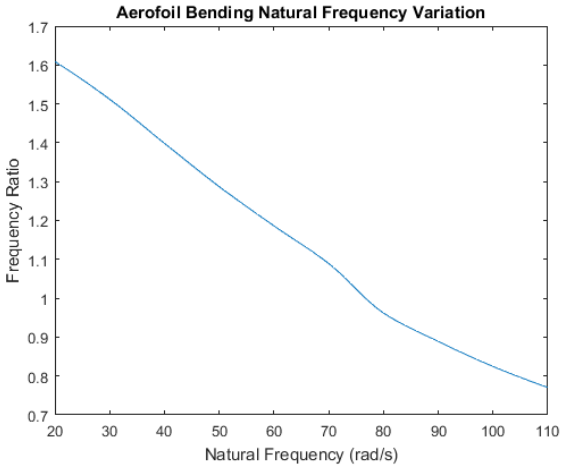
Aerofoil Bending Natural Frequency Variation
Frequency Ratio
Natural Frequency (rad/s)

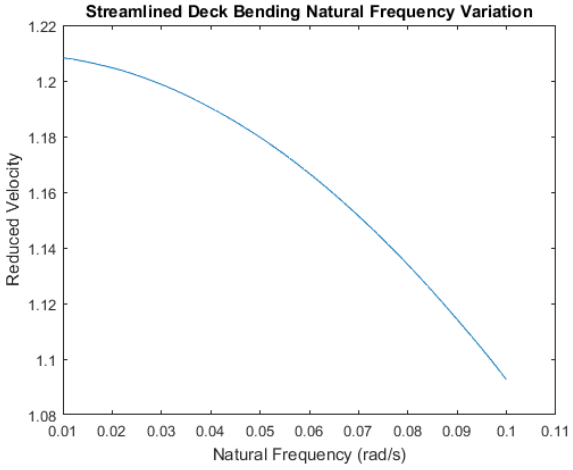
Streamlined Deck Bending Natural Frequency Variation
Reduced Velocity
Natural Frequency (rad/s)

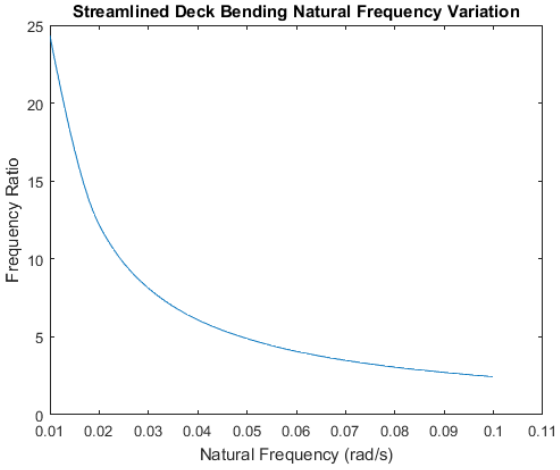
Streamlined Deck Bending Natural Frequency Variation
Frequency Ratio
Natural Frequency (rad/s)

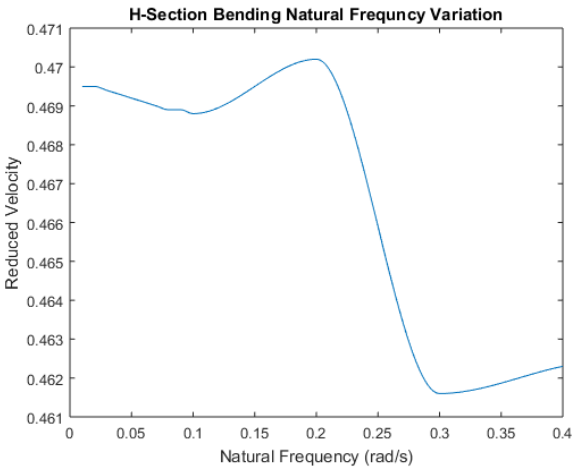
H-Section Bending Natural Frequncy Variation
Reduced Velocity
Natural Frequency (rad/s)

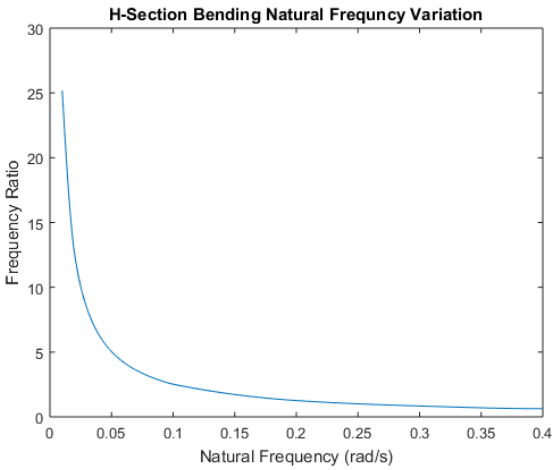
H-Section Bending Natural Frequncy Variation
Frequency Ratio
Natural Frequency (rad/s)

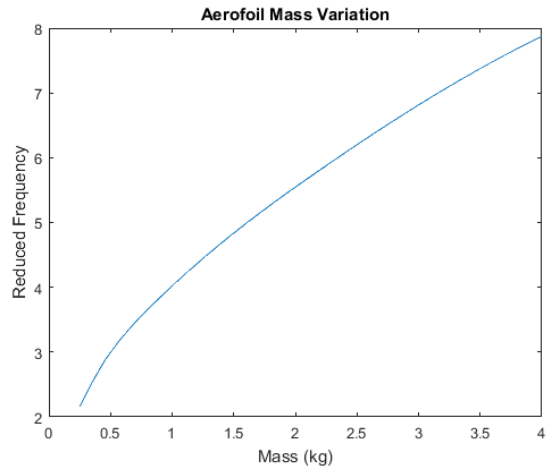
Aerofoil Mass Variation
Reduced Frequency
Mass (kg)

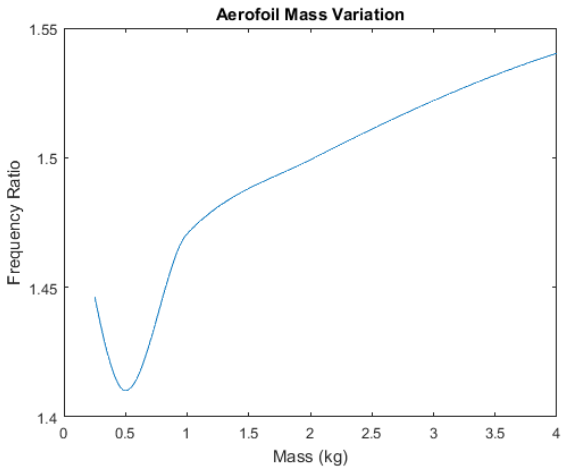
Aerofoil Mass Variation
Frequency Ratio
Mass (kg)

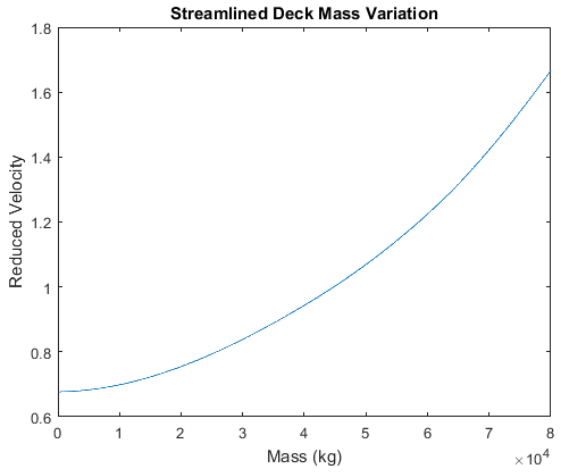
Streamlined Deck Mass Variation
Reduced Velocity
Mass (kg)
×10^4

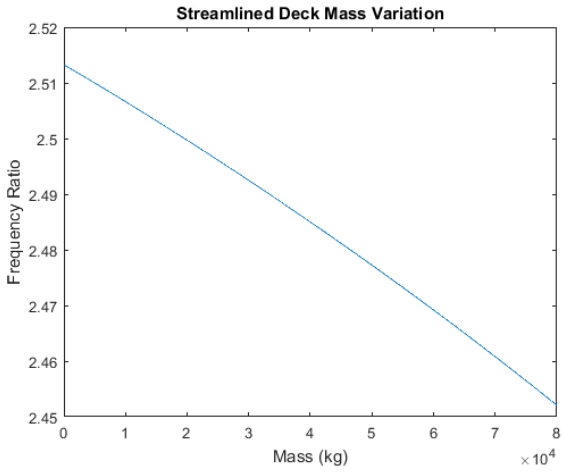
Streamlined Deck Mass Variation
Frequency Ratio
Mass (kg)
×10^4

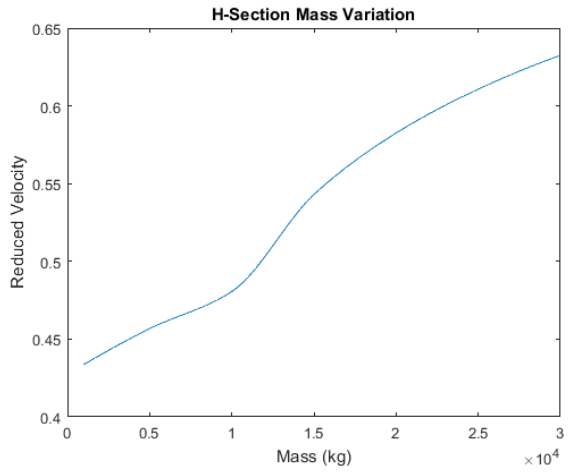
H-Section Mass Variation
Reduced Velocity
Mass (kg)
×10^4

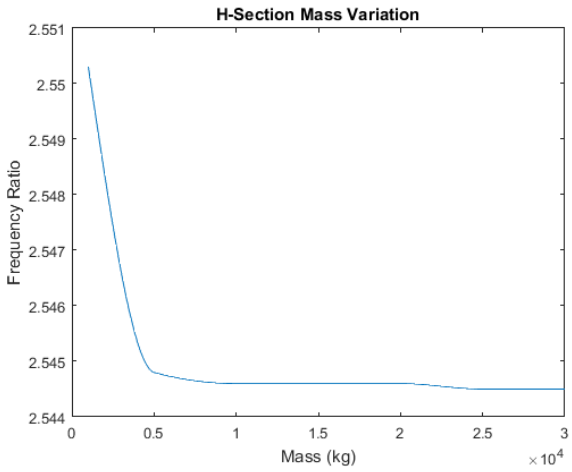
H-Section Mass Variation
Frequency Ratio
Mass (kg)
×10^4